COLLAGEN AND THEIR RELATIONSHIP

Thesis submitted for the degree of

Doctor of Philosophy

University of Leicester

By

Timothy John Green

April 2004

PREFACE

The content of this dissertation is original, except where specific reference is made to the work of others. No part of this dissertation has been submitted to any other University.

TIMOTHY JOHN GREEN
British School of Leather Technology,
University College Northampton

ABSTRACT

Mineralised collagen displays an improved hydrothermal stability compared to collagen that is unmineralised. The possibility of using *in-vitro* partial mineralisation of collagen as a method of increasing the hydrothermal stability was investigated. Remineralisation experiments using demineralised turkey leg tendon and chemically modified bovine hide collagen showed that although it was possible to grow hydroxyapatite mineral crystallites on the collagen substrate they were only present at the substrate-solution interface and as such did not give rise to an increase in hydrothermal stability. The morphology of the mineral crystallites produced *in-vitro* were compared with those in the naturally mineralised tendon using Scanning Electron Microscopy (SEM), Small Angle X-ray scattering (SAXS), X-ray Diffraction (XRD) and Fourier-Transform Infrared Spectroscopy (FT-IR).

Differential scanning calorimetry (DSC) studies on demineralised tendon identified a previously unknown high temperature endothermic transition to be present in the thermal scan of both mineralised and unmineralised collagen during denaturation. The position of this transition was found to be affected by hydration, presence of mineral, pH, and crosslinking similar to that of the first transition. Experiments using reagents known to selectively break various non-covalent interactions within collagen indicated that the transition was due to the breaking of covalent bonds via an endothermic chemical reaction, with the most likely candidate being the hydrolysis of peptide bonds within the polypeptide backbone. Optical microscopy of collagen after heating indicated that the fibrillar structure of the collagen was destroyed during the second transition, forming an amorphous gel.

Finally, the effect of the mineral phase on the hydrothermal stability of naturally mineralised collagen was discussed in context to its location within the collagen structure. It was postulated that the presence of mineral dehydrates the collagen structure, as well as decreasing the available space within the hole region.

ACKNOWLEDGEMENTS

I would firstly like to thank my supervisors, Dr Jifeng Ding, Prof. Geoff Attenburrow and Dr Matthew Collins for their guidance and encouragement during the course of my studies.

I am also indebted to all those who have allowed me access to their analytical facilities during the course of my research, especially Prof. Tim Wess at Cardiff University for SAXS analysis, Dr Elisa Capel-Lopez at the University of Newcastle for TGA and XRD, Mr David Dunbar of the Chemical Analytical Services Unit of the University of Newcastle for ICP-OES and FT-IR analysis and Dr Amanda Long and Mrs Amanda Michel of the British Leather Confederation for EDXA and SEM analysis and also the use of their cyro-microtome and freeze-drier.

I would also like to thank Miss Emma King for helping with the dissection of the turkey feet, and also Miss Hannah Koon for kindly allowing me to use a couple of her TEM images and for putting me up on my frequent visits to the University of Newcastle.

Also I would like to thank Prof. Tony Covington for his useful discussion on the subject of collagen hydrothermal stability.

Finally I'd like to thank all the staff of the British School of Leather Technology and the Graduate School for all the help I have received over the course of my studies and the submission of this thesis.

TABLE OF CONTENTS

CHAPTER TWO: AN INTRODUCTION TO BIOMINERALISATION

CHAPTER THREE: TURKEY TENDON DEMINERALISATION AND REMINERALISATION EXPERIMENTS

CHAPTER FOUR: CHEMICAL MODIFICATION OF COLLAGEN SUBSTRATES

CHAPTER FIVE: HYDROTHERMAL STABILITY STUDIES OF MINERALISED, DEMINERALISED AND REMINERALISED COLLAGEN

CHAPTER SIX: INVESTIGATION INTO THE NATURE OF THE 2ND ENDOTHERMIC TRANSITION

CHAPTER SEVEN: CONCLUSIONS AND FUTURE WORK

NOMENCLATURE AND ABBREVIATIONS

AFM	Atomic Force Microscopy
d	Lateral distance between collagen molecules in fibril
D	Longitudinal distance between collagen molecules in fibril
DSC	Differential Scanning Microscopy
EDC	1-ethyl-3-(3-dimrthylaminopropyl) carbodiimide
EDXA	Energy Dispersive X-ray Analysis
FT-IR	Fourier Transform Infrared Spectroscopy
Gly	Glycine
Hyp	4-Hydroxyproline
ICP-OES	Inductive Coupled Plasma Optical Emission Spectroscopy
mM^2	Molar product
NHS	N-hydroxysuccinimide
NMR	Nuclear Magnetic Resonance
Ppm	Parts per million
Pro	Proline
SAXS	Small Angle X-ray Scattering
SEM	Scanning Electron Microscopy
SF	Splitting factor
TEM	Transmission Electron Microscopy
TEOS	Tetraethyl orthosilane
TGA	Thermogravimetric Analysis
T_d	Temperature of denaturation
T_m	Temperature of melting
T_{max}	DSC peak maximum height
T_s	Temperature of shrinkage
XRD	X-ray Diffraction
ΔH_f	Enthalpy of fusion
γ-CGA	Gamma carboxyglutamic acid

Chapter 1

Type I collagen structure and stability

1.1 Structure of type I collagen

The structural proteins belonging to the collagen family are ubiquitous throughout the animal kingdom, there are known to be 27 genetically distinct types[1], of which type I is the most common, being present as the structural protein of skin, bone, and tendon[2]. Type I collagen is a stiff rod-shaped molecule about 300 nm long[3] and comprises of three chains of amino acids, each of 1052 amino acid residues long[4], giving a molecular mass of approximately 284000[5]. Each individual amino acid residue in the chains is separated by a distance of 0.29 nm[6] from its adjacent neighbours. Two chains are identical and denoted ($\alpha 1$) and the third is of a slightly different amino acid sequence and denoted ($\alpha 2$), the type I collagen molecule is denoted as $[\alpha 1(I)]_2\alpha 2$[7]. Each α-chain consists of three distinct domains, the largest of which is the 1011 residue long triple helical region which contains the repeating amino acid sequence –(Gly-X-Y)-, so that every third amino acid is glycine[4]. -X- is frequently the imino acid proline, and -Y- the imino acid hydroxyproline, so that the triplet –(Gly-Pro-Hyp)- is fairly common[8]. This -(Gly-X-Y)- repeat structure is shown diagrammatically in Figure 1.1.

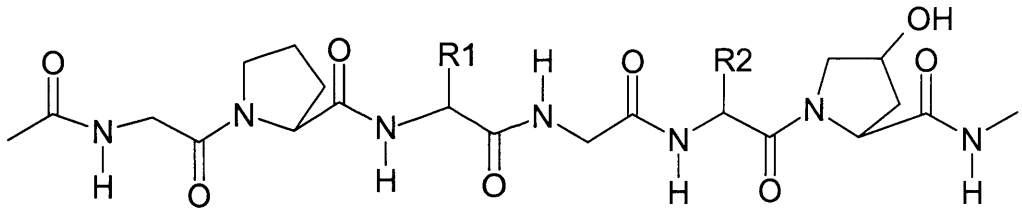

Gly - Pro - y - Gly - x - Hyp

Figure 1.1 Representation of chemical bonding of part of the α-chain.

The presence of these imino acid residues pulls the α-chain into a left-handed helix, which has been shown by X-ray diffraction studies[9] to be very similar to a polyproline II type structure in which the glycine residues are always near the helix axis and the residues X and Y always away from the axis. The helical structure is due to the steric restrictions placed on the amino acid chain caused by the presence of the imino acid rings. The α-chains also contain non-helical telopeptide regions at each end, the N-terminal telopeptide contains 16 amino acids and the C-terminal telopeptide contains 25 amino acids[4], these telopeptides do not contain glycine at

every third residue[4]. Three of these α-chains come together to form a right-handed triple helix as shown in Figure 1.2 below.

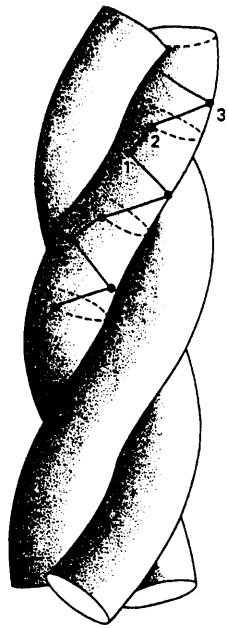

Figure 1.2 *diagram of a triple helix showing how the individual left handed α-chains coil together to make the right-handed super helix (taken from Woodhead-Galloway[10].*

The triple helix completes a full turn every ten residues, giving a 10/3 helix with an axial repeat between individual residues of 2.86 nm[11], however Okuyama et al[12] have proposed a model where collagen forms a 7/2 helix in which the helix makes a full turn every seven residues giving an axial repeat of 2.0 nm. However, it was found from a collagen model peptide[13] that the helical symmetry depends on the amino acid sequence, with those regions rich in imino acids having a 7/2 symmetry, and those deficient in these residues having a 10/3 symmetry. The presence of a glycine residue at every third position is essential for triple helix formation, model peptides in which glycine was substituted for different amino acids gave peptides that failed to form triple helices, also the non-helical domains of collagens, such as in types IV and VI, as well as the non-helical telopeptides in Type I collagen, are devoid of glycine.

The triple helix is prevented from unravelling into its constituent α-chains by the presence of hydrogen bonds which link the three α-chains together. Two rival models for the hydrogen bonding between α-chains have been proposed. Based on evidence from fibre x-ray diffraction studies, Ramachandran and Kartha[14] believed that two

hydrogen bonds were present within each Gly-X-Y tripeptide, one being between the NH group of glycine and the carbonyl group of the residue at position X in an adjacent α-chain, and the other between the carbonyl of glycine and the imino group of the residue at position -X- as long as this position is not occupied by an imino acid. Rich and Crick[11] however believed that only one hydrogen bond was present per tripeptide, situated between the imino group of the glycine residue and the carbonyl group of the residue at position X in an adjacent α-chain. They offered molecular modelling and x-ray diffraction data to support their view that two direct interchain hydrogen bonds originating from the amino acid backbone of the α-chains per tripeptide was stereochemically impossible, however didn't rule out the possibility that the amino acid side chains could be involved in interchain hydrogen bonding. The difference in hydrogen bonding for each of these two models is shown in Figure 1.3 below.

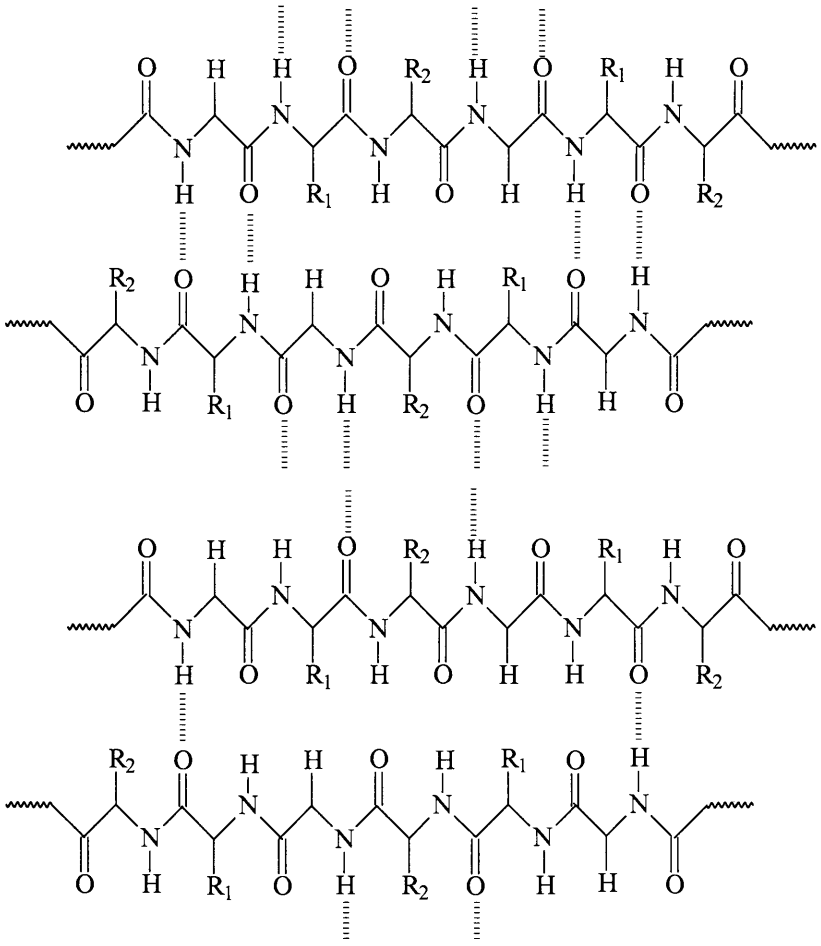

Figure 1.3 *Simplified diagram to show the difference in the location of the hydrogen bonds in the two-bonded Ramachandran (top) and one-bonded Rich and Crick (bottom) models of the collagen triple helical structure.*

Ramachandran and Chandrasekharan[15] later revised the two hydrogen bond per tripeptide model. Their new model was based on having one directly linked hydrogen bond per tripeptide, like in the model by Rich and Crick, but supplemented by hydrogen bonded water bridges that form a link between the backbone chain imino and carbonyl groups. Two such bridges could occur per triplet and the water molecules in these bridges could then become acceptors for further hydrogen bonds originating from C-H hydrogen atoms, thus forming an extensive network of hydrogen bonded water molecules. However, in Gly-Pro-Hyp tripeptides where there are no backbone imino groups at the X position these water bridges can't be formed, although the presence of hydroxyproline allows the formation of interchain water bridges between its hydroxyl group and the backbone chain of an adjacent α-chain[16], this thought to be the reason for the improved stability of tripeptides containing hydroxyproline at position –Y- compared to those containing proline at that position.
Bella et al[17] confirmed the existence of hydrogen bonded water bridges within the collagen like triple helical molecule $(Gly\text{-}Pro\text{-}Hyp)_4$-Ala-Pro-Hyp-$(Gly\text{-}Pro\text{-}Hyp)_5$. The triple helix formed by this peptide was surrounded by an extensive cylinder of hydration similar to that proposed by Ramachandran, in which the hydroxyproline residues act as "keystones" connecting the network of water molecules to the peptide chains. The hydration cylinder comprises of water molecules that are hydrogen bonded directly to the backbone carbonyl and hydroxyproline hydroxyl groups of the peptide chains, (these forming the first shell of hydration), water molecules that form bridges between these peptide bound water molecules (the second hydration shell), and also water molecules that are uni-pointly hydrogen bonded to the water molecules in the first and second shells (the third hydration shell). This is shown diagrammatically in Figure 1.4 overleaf.

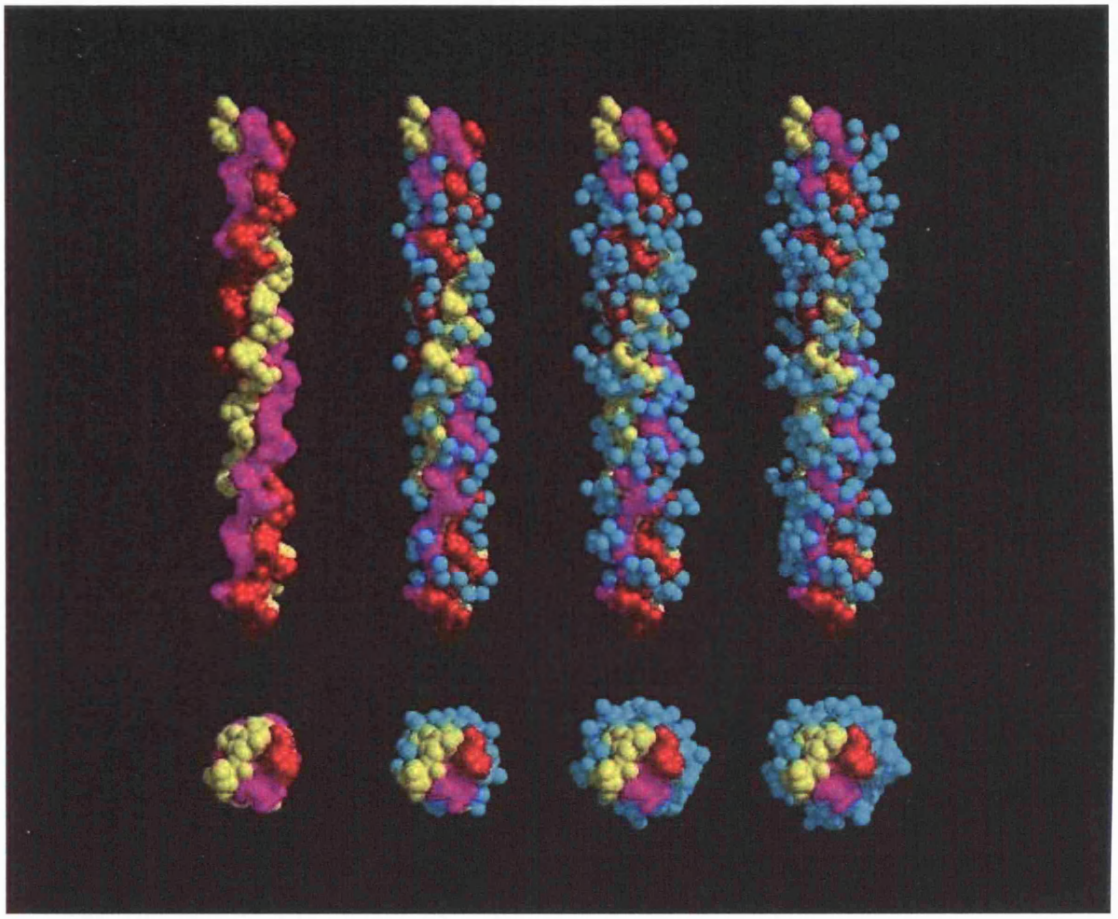

Figure 1.4 *Computer simulation of the hydration cylinder for the (Gly-Pro-Hyp)$_4$-Ala-Pro-Hyp-(Gly-Pro-Hyp)$_5$ peptide. On the left is the peptide without any associated water molecules, next to it is the peptide in which the first layer of water molecules (blue spheres) are directly hydrogen bonded to the peptide chains, the next peptide shows the addition of the second shell of water molecules which are hydrogen bonded to the water molecules of the first hydration shell. The peptide on the far right shows the addition of the third shell of water molecules. (From Bella et al[17])*

The specific amino acid sequence of the α-chains gives rise to alternating regions of polar and non-polar residues. These can be visualised using TEM by staining with phosphotungstic acid to show basic groups, and uranyl acetate to show acidic groups[18]. Staining shows that the positions of the acidic and basic groups precisely match each other so these charged side chains can form electrostatic inter-helical bonds between oppositely charged residues. Maximum interaction of these charged side chains gives rise to an array of triple helices with each one offset from its adjacent neighbours by a quarter of its length. Experiments carried out by Hodge and

Petruska[18] using the "segment long spacing" aggregated form of collagen fibrils showed that the normalised length of the collagen triple helical molecule is 4.4D, indicating that there is an end to end overlap of 0.4D, and each triple helix is separated from its immediate longitudinal neighbours by distance of 0.6D, where D = 67 nm. This gives rise to a quarter-staggered array of collagen molecules as shown in Figure 1.5 below. The space between longitudinal helices gives rise to holes in the array known as the hole, or gap region, which are important in mineralisation. It is the alternating gap and overlap region of collagen molecules that give collagen fibrils their characteristic banding pattern when stained with phosphotungstic acid. The structure is also further stabilised by hydrophobic interaction between aligned regions of non-polar residues on adjacent helices.

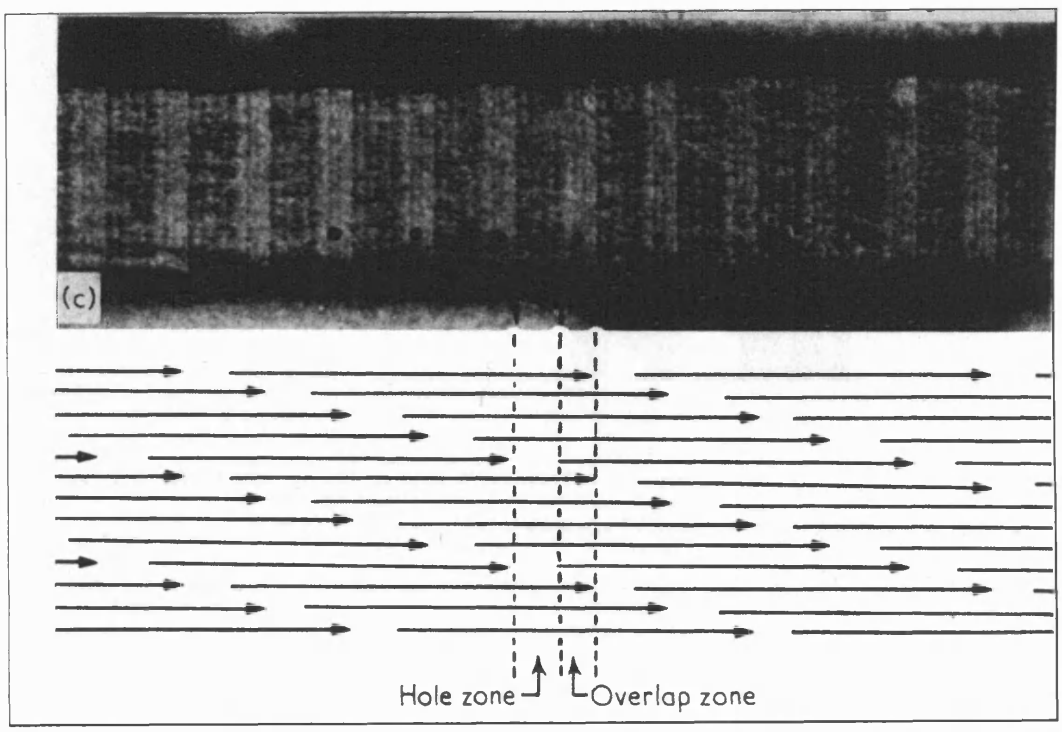

Figure 1.5 *Diagram showing how the banding pattern of a collagen fibril corresponds to the hole and overlap regions (shown in the TEM image at the top) formed by the quarter-staggered arrangement of the collagen molecules (taken from Hodge and Petruska[18].*

Collagen when it is packed into fibrils is composed of crystalline arrays of parallel collagen molecules[19]. The exact way in which the collagen molecules are packed into this array is unknown, however from analysis of the X-ray diffraction data several different packing schemes have been postulated. These are the quasi-hexagonal array of Hulmes and Miller[20], in which the cross section of the molecules are arranged in a pseudo-hexagonal array, and structures based on microfibrils such as the Smith pentafibril[21], as shown in Figure 1.6 below, and radially packed cylindrical structures[22].

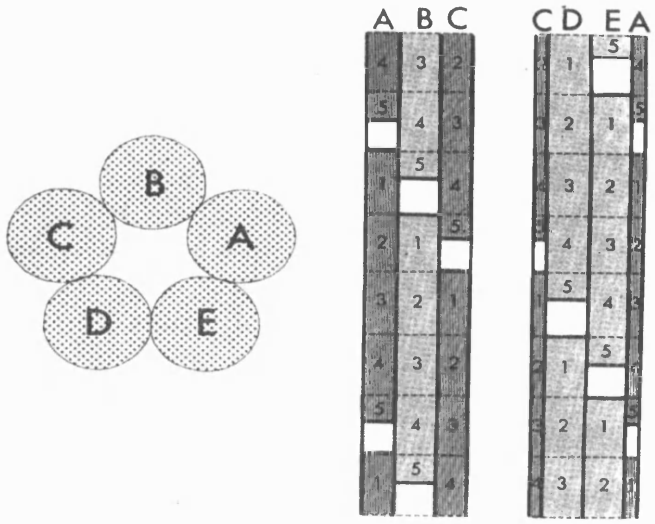

Figure 1.6 *Diagram of the Smith microfibril. Diagram (a) shows a cross section through the microfibril showing the 5 component helices, and (b) shows the view if (a) is bisected through C and A showing the alignment of the quarter stagger arrangement of the individual collagen molecules. (Taken from Smith[21])*

Such pentafibrils have a theoretical diameter of 3.5 nm, close to a value of 3.8nm observed in the x-ray diffraction spectra of rat tail tendon[19]. The five triple helices within the microfibril are coiled around each other so as to form another larger helical structure[23]. Fraser et al[24] suggested that the collagen fibrils are made up of a tetragonal repeating unit of four such microfibrils, forming a unit with a diameter of 8.5 nm in which a 1.6 nm channel occurs due to the packing of the microfibrils. Evidence for such structures was presented by Parry and Craig[25] who found from electron microscopy that the diameters of fibrils from tendon, skin, and cornea were

all multiples of about 8.0 nm. A model combining pentafibril structures arranged on a pseudo-hexagonal base in which the pentafibrils are compressed so as to fit a hexagonal array was proposed by Trus and Piez[26] and confirmed using x-ray scattering by Orgel et al[27]. The way in which the pentafibril is compressed is shown in Figure 1.7 below.

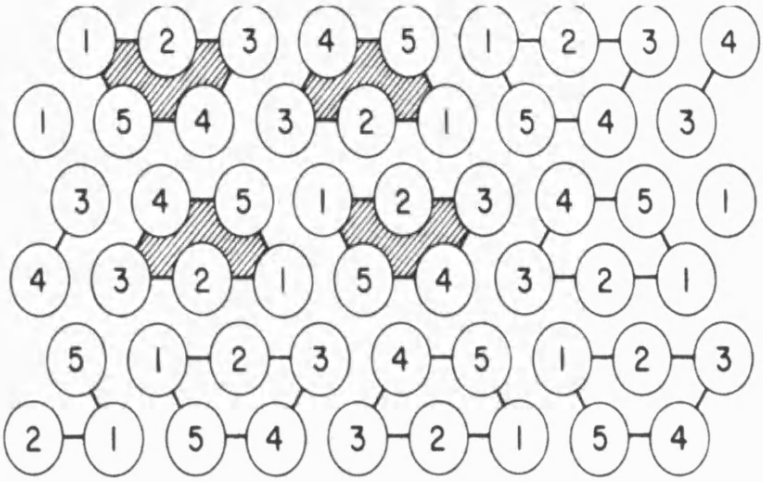

Figure 1.7 *Diagram of the molecular packing of collagen showing how the compressed pentafibrils fit onto a quasi-hexagonal packed array. The shaded pentafibrils are those involved in the formation of the four-member repeating unit. Taken from Trus and Piez[26]*

X-ray scattering patterns for collagen are not composed of sharp reflections as expected for a material with a crystalline structure, but of broad diffuse maxima, indicating a much lower degree of order. Woodhead-Galloway and Machin[28] have shown that the scattering due to the lateral arrangement of collagen molecules in tendon is better described using a two-dimensional liquid structure rather than a periodical arrangement. This model, known as the hard disc fluid model, was used by Fratzl[29] to explain the changes in the axial d-period, which measures intermolecular separation and hence the packing fraction of the collagen molecules within the fibril, with hydration level for tendon collagen. The model also explains how mineral crystallites are able to be present in the overlap regions even though the intermolecular distance is smaller than that for unmineralised tissue (4b in Figure 1.8).

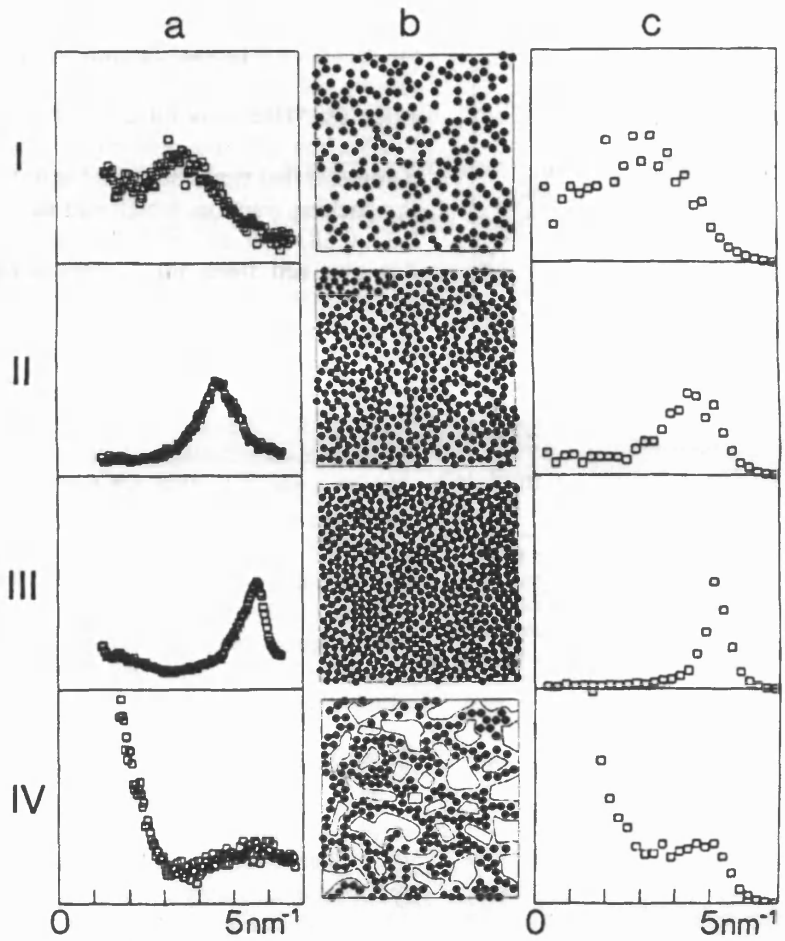

Figure 1.8 *(a) Diffuse equatorial x-ray spectra measured for fresh (I), dehydrated (II), and completely dry (III) unmineralised turkey leg tendon, as well as for mineralised (IV) tendon. (b) Computer model showing a possible configuration of the hard disc fluid with packing fraction 0.30 (I), 0.56 (II), and 0.70 (III), (IV) contains the same number of molecules as (I), but they are arranged so as to make space for the mineral crystals (shown as irregular white shapes). (c) Diffuse x-ray spectra calculated for the computer-simulated samples shown in (b). Diagram taken from Fratzl et al*[29].

These sub-fibrillar assemblies of collagen triple helices pack together to form collagen fibrils within which the individual triple helices are linked to their adjacent neighbours by covalent crosslinks. The formation of which is shown diagrammatically in Figure 1.9. The enzyme lysyl oxidase converts the amino group of lysine (i) and hydroxylysine residues in the telopeptide regions to aldehyde groups, forming allysine (ii) and hydroxyallysine respectively, these can then react with the

amino groups of lysine or hydroxylysine residues on an adjacent triple helix to form a dehydrolysinonorleucine crosslink (iii) if allysine and lysine are the residues involved. Similar crosslinks are formed between allysine and lysine, and also hydroxyallysine and hydroxylysine. These crosslinks are hydrolysable in acid but can be stabilised by maturation and also *in-vitro* by reduction with sodium borohydride to give the acid resistant crosslink lysinonorleucine (iv) or undergo reactions with other residues of adjacent chains to give other crosslinks.

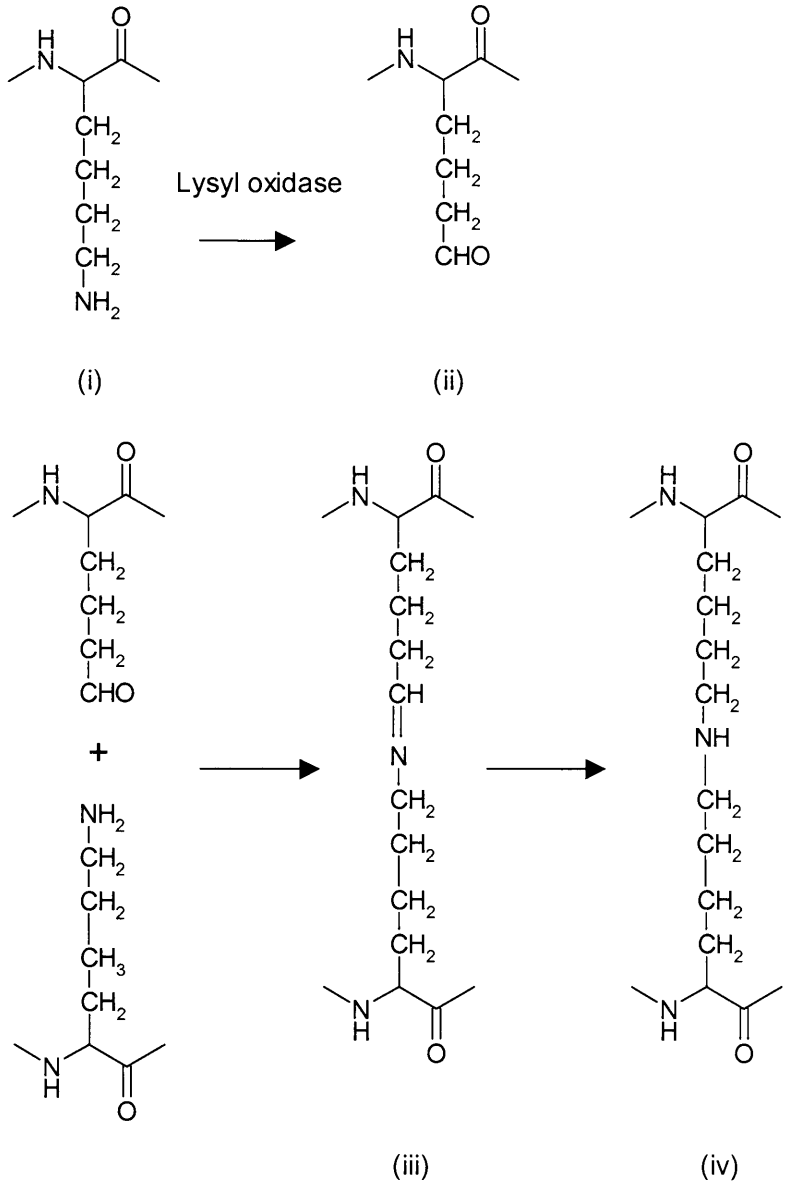

Figure 1.9 *Diagram showing the formation of the lysinonorleucine crosslink*

In the case of dried bovine hide these fibrils are about 100 nm in diameter and contain about 7000 individual collagen molecules[30]. The individual fibrillar units are woven together to form collagen fibres, which may be further woven into fibre bundles of

varying diameter. It is the diameter of the fibres and fibre bundles that causes the morphological differentiation between different collagenous tissues of the same collagen type, such as the ultrastructural differences between Type I collagen in tendon and skin.

1.2 Collagen swelling

Under certain conditions collagen undergoes a swelling of its structure at the intermolecular level. There are two types of swelling, osmotic swelling, and lyotropic swelling.

1.2.1 Osmotic swelling

Collagen, like all proteins, is a zwitterionic molecule; meaning that it contains both positively and negatively charged chemical groups. At a certain pH called the isoelectric point collagen displays no overall net charge with the oppositely charged forces exactly balancing out. In the case of native unmodified collagen this occurs at pH 7.88, modification of side chain functional groups (e.g. by deamidation) effects the pH at which the isoelectric point occurs. If we move the pH of the collagen away from its isoelectric point we cause the net overall charge of the molecule to become positive due to protonisation of the carboxyl groups in the case of adding acid, and more negative due to the neutralisation of protonated amino groups in the case of adding alkali, this is shown schematically in Figure 1.10 below.

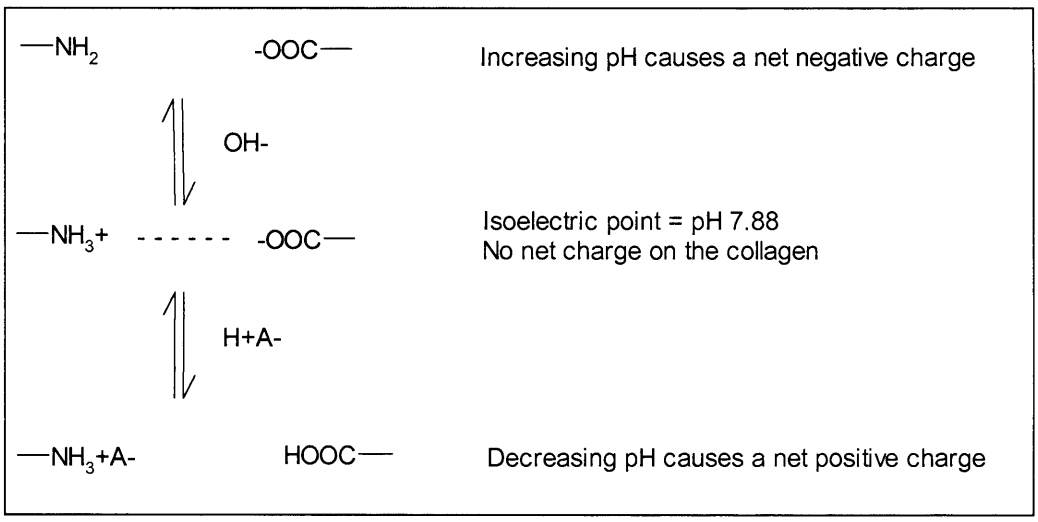

Figure 1.10 Diagram showing how the ionisation of the carboxyl and amino side chains vary with addition of acid and alkali.

The effect of providing the collagen molecule with an overall net charge causes two swelling effects: repulsion between similarly charged groups on adjacent molecules giving rise to a pushing apart of the molecules, which is seen as a swelling of the collagen fibrillar structure, and osmotic swelling. Collagen behaves as a semi-permeable membrane and at the isoelectric point contains equal amounts of charged ions within its structure. If acid is now added to the collagen the hydrogen ions bind to the ionised carboxylate groups, thus removing their negative charge. This leaves the collagen with a net positive charge due to the protonated amino groups. To retain electrical neutrality these positive charges must be balanced by negatively charged counter ions from the added acid, therefore the collagen contains more charged ions within its structure than in solution. This causes the influx of water into the collagen structure due to the osmotic effect trying to achieve equilibrium once more, which gives rise to swelling of the structure. This type of swelling can be suppressed at acidic pH by the addition of a relatively large concentration of neutral electrolyte, which swamps the difference in ionic strength between solution and within the collagen structure. The swelling of collagen with or without salt as a function of pH is shown in Figure 1.11 below[31].

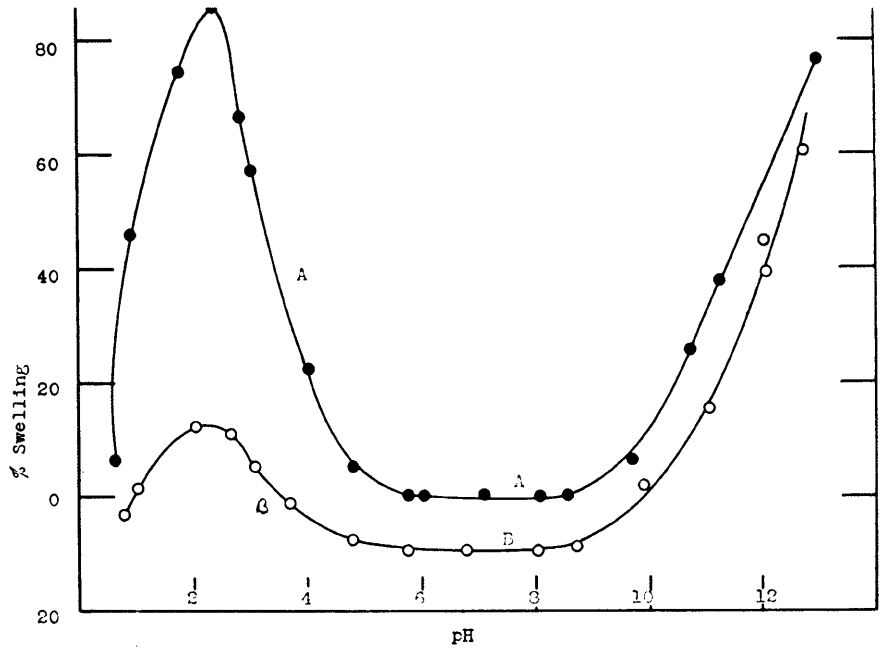

Figure 1.11 *Swelling curve of collagen as a function of pH (curve A). Curve B shows the swelling curve in the presence of salt. Taken from Theis and Steinhardt*[31]

1.2.2 Lyotropic swelling

Lyotropic swelling of proteins occurs in the presence of certain ions or small molecules that can either be adsorbed by or inserted within the collagen triple helical structure causing breaking of the interchain hydrogen bonds. This causing a reduction in the hydrothermal stability of the collagen until at a certain concentration of lyotropic agent the collagen becomes denatured. The relationship between the hydrothermal stability, measured as the denaturation temperature and the molar concentration of for various lyotropic agents was investigated by Lim[32], who found that as well as the denaturation temperature being reduced with increasing concentration for strong lyotropic agents, the enthalpy of denaturation was also reduced with increasing concentration. Some small organic molecules, such as urea and guanidine, have been shown to cause lyotropic swelling by out competing the individual collagen α-chains for hydrogen bonding sites within the triple helix[33]. These molecules insert themselves within the triple helix with which they then form hydrogen bonds; the swelling is a result of the molecules pushing the α-chains apart due to their larger size. The mechanism by which inorganic ions cause lyotropic swelling is less well understood, although the order in which ions show an increase in the ability to cause denaturation and swelling are arranged essentially in the Hofmeister series, e.g. for anions[34]:

Citrate > tartrate > sulphate > acetate > Cl^- > NO_3^- > Br^- >I^- > CNS^-

And for cations:

$Al^{3+} > H^+ > Ba^{2+} > Sr^{2+} > Ca^{2+} > K^+ > Na^+ > Li^{2+}$

It is thought that the order in which ions bring about swelling is due to the intensity of the electric field around the ions; small ions have a more intensive field than large ions of the same valency.

1.3 Collagen hydrothermal stability

Like all proteins, Type I collagen is denatured by heat, and lyotropic reagents such as urea and lithium bromide. Pauling[35] was the first to suggest that the denaturation of

proteins was due to the breaking of the hydrogen bonds that hold the individual protein chains in a certain configuration. In the case of collagen these hydrogen bonds link together the individual α-chains that form the triple helix and so breaking these hydrogen bonds brings about an unravelling of the triple helical structure to form randomly coiled α-chains. In tissues such as skin where the collagen fibres are highly interwoven a shrinking of the macro structure is observed upon denaturation, this is due to the swelling of the individual collagen fibrils, this presents the interwoven fibrils with a greater distance to travel around the fibre structure. As the collagen fibrils are of finite length this increased travelling through the structure causes an apparent observable shortening of the fibre structure. This shrinking of the fibre structure can occur to the extent of 50% of the initial length of a piece of skin collagen. Small angle x-ray scattering[36] has shown that the collagen molecule itself doesn't undergo any appreciable reduction in its length during the denaturation process. Early work on collagen hydrothermal stability was centred on the leather industry as tanning of hides and skins produces an increase in their hydrothermal stability. An improvement in this property was associated with the successful completion of the tanning reaction.

The denaturation of collagen occurs over a narrow temperature range, suggesting that the transition has a high degree of co-operativity[37]. A co-operative transition is one in which the state of the individual segments of the biopolymer chain are highly influenced by the state of the adjacent segments, favouring the chain to be in either the fully folded (native) or the fully unfolded (denatured) state rather than in any partially folded conformations. It is this "all or nothing" aspect of co-operative transitions that causes the transition to occur over a narrow temperature range as it gives rise to a situation in which a small change in the system can bring about a complete change in the conformation of the biopolymer.

The denaturation temperature of collagen in the form of individual triple helices has been found to be only a few °C above the physiological temperature of the parent organism. When the collagen molecules are incorporated into fibrils the denaturation temperature is increased by about 27°C[38], due to both the reduced number of possible conformations available to each collagen molecule now that it is arranged in a three dimensional quarter staggered array, and the formation of covalent and non-covalent forces between triple helices creating a more ordered structure. It was originally

thought that the increase in hydrothermal stability of the collagen for different species was correlated to the total amount of proline and hydroxyproline residues present within the collagen, with both residues contributing equally to the increase in hydrothermal stability[39][40]. Later studies showed that immature procollagen, which has not undergone post translational hydroxylation of its proline residues at the -Y-position, has a much lower hydrothermal stability than that of normal collagen, indicating that the hydroxyproline residues have a large affect on the increase in hydrothermal stability[41]. By analysing data in published literature on the hydrothermal stability of collagen from different organisms Burjanadze[42] established that the denaturation temperature was dependent on the hydroxyproline content of the collagen. Examples of the denaturation temperature of type I collagen obtained from different vertebrate sources, and their corresponding hydroxyproline contents are shown below in Table 1.1

Table 1.1 *denaturation temperature and hydroxyproline content for type I collagen from different vertebrate sources. (Taken from Burjanadze[40])*

Collagen source	T_d°C	Hydroxyproline/1000 residues
Antarctic ice fish skin	27	45
Cod skin	40	53
Shark skin	53	78
Carp swim bladder	54	81
Frog skin	58	65
Rat tail tendon	59	94
Calf skin	65	94
Rabbit skin	61	102

Gustavson[43] proposed that the amount of hydroxyproline present in the collagen determined its denaturation temperature long before the presence of hydroxyproline water bridges was postulated, suggesting that as the hydroxyl group of hydroxyproline is capable of forming hydrogen bonds, therefore any increase in the amount of hydroxyproline, and thus hydrogen bonds, must lead to an increase in the hydrothermal stability of the collagen. Burjanadze[42] later found that there was a correlation with hydroxyproline in the Y-position of the tripeptide with the

temperature at which denaturation occurred in collagens from different vertebrate species. These studies showed that as well as providing structural stability the interchain water bridges formed by the hydroxyproline residues also provide additional hydrothermal stability. The stabilising effect of imino acid residues in the –X and –Y positions has been verified using so called "guest-host" model triple helical polytripeptides of the type $(Gly\text{-}Pro\text{-}Hyp)_3\text{-}Gly\text{-}X\text{-}Y\text{-}(Gly\text{-}Pro\text{-}Hyp)_4$ where –X and –Y were altered, values for the T_m of some examples of these polytripeptides are shown in Table 1.2. The presence of a large number of Gly-Pro-Hyp repeats is necessary for the tripeptides to form a triple helix as tripeptides synthesised with other residues replacing glycine in the structure resulted in tripeptides that had difficulty in forming triple helices and had non-helical regions after the substituted glycine residue[44].

Table 1.2 *Effect of different guest triplets on the T_m of the $(Gly\text{-}Pro\text{-}Hyp)_3\text{-}Gly\text{-}X\text{-}Y\text{-}(Gly\text{-}Pro\text{-}Hyp)_4$ host peptide. Data taken from [a]Chan and Ramshaw[45], [b]Shah[46], and [c]Shah et al[47].*

Gly-X-Y guest tripeptide	T_m°C
Gly-Pro-Hyp	47.3[a]
Gly-Glu-Arg	40.4[a]
Gly-Asp-Arg	37.3[a]
Gly-Arg-Asp	35.0[a]
Gly-Arg-Glu	33.7[a]
Gly-Ala-Ala	32.9[b]
Gly-Asp-Lys	30.9[a]
Gly-Glu-Asp	29.7[a]
Gly-Gly-Ala	25.0[c]

As can be seen in Table 1.2 Gly-Pro-Hyp gives the most stable triple helical peptides due to the ability of the hydroxyproline residue to form hydrogen bonded water bridges. However the fact that the triple helical Polytripeptide made from $(Gly\text{-}Pro\text{-}Hyp)_{10}$ has a higher denaturation temperature than that from $(Gly\text{-}Pro\text{-}Pro)_{10}$ under the

anhydrous conditions achieved by dissolving in methanol or propane-1,2-diol,[48] under which water bridges between hydroxyproline residues cannot form suggest that a different mechanism may be responsible.

It has been proposed that the increase in denaturation temperature caused by hydroxyproline is because of the greater inductive effect of the hydroxyl group compared to that of the corresponding hydrogen atom in proline[49]. By replacing hydroxyproline in triple helical polytripeptides with fluoroproline, which gives an even larger inductive effect it was found that the denaturation temperature could be raised further, as can be seen in Table 1.3 below.

Table 1.3 *Denaturation temperatures as measured by circular dichroism of triple helical polytripeptides showing the effect of increasing the inductive effect of the imino acid ring*[49].

Polytripeptide	T_m (°C)
$(Gly\text{-}Pro\text{-}Pro)_{10}$	36
$(Gly\text{-}Pro\text{-}Hyp)_{10}$	67
$(Gly\text{-}Pro\text{-}Flp)_{10}$	87

Further evidence that the improved hydrothermal stability of peptides containing hydroxyproline may be due to the inductive effect rather than the formation of hydrogen bridges came from Okuyama et al[50] who found that for the polytripeptide $(Gly\text{-}Hyp\text{-}Pro)_{10}$ only three out of every seven hydroxyl groups of the hydroxyproline residues took part in the formation of hydrogen bonded water bridges.

1.3.1 Thermodynamics of denaturation

The overall denaturation process is endothermic, as energy has to be supplied to break the interchain hydrogen bonds that hold the triple helices together. The collagen denaturation reaction involves two steps:

$$\text{Native collagen} \leftrightarrow \text{Activated collagen} \rightarrow \text{Denatured collagen} \qquad (1)$$

The first reaction being reversible has two rate constants, one for the forward reaction, k_1 and one for the reverse reaction, k_{-1}. When collagen molecules undergo denaturation $k_1 >> k_{-1}$ and the reaction proceeds irreversibly.

The equilibrium constant, K, for the first reaction can be defined[51] in terms of the free energy of the reaction by the equation:

$$\Delta G^{\circ} = -RT\ln K = -RT\ln k_1/\ln k_{-1} \quad (2)$$

Where:

ΔG° = free energy of the reaction

R = universal gas constant

T = absolute temperature

K = equilibrium constant for the reaction

The following derivation can be used to relate equation (2) to the free energy of activation $\Delta G^{\ddagger}$ for denaturation:

$$\Delta G^{\ddagger} = \Delta H^{\ddagger} - T\Delta S^{\ddagger} \quad (3)$$

Where:

$\Delta H^{\ddagger}$ = activation energy of the reaction ($kJmol^{-1}$)

$\Delta S^{\ddagger}$ = activation entropy of the reaction ($JK^{-1}mol^{-1}$)

The Hammond postulate states that for an endothermic reaction the activated state is more like the products than the reactants[52] so the free energy of activation is similar in value to the free energy of the reaction, so:

$$\Delta G^{\ddagger} \approx \Delta G^{\circ} \quad (4)$$

And:

$$\Delta H^{\ddagger} - T\Delta S^{\ddagger} \approx -RT\ln k_1 + RT\ln k_{-1} \quad (5)$$

So when $k_1 >> k_{-1}$ as at denaturation:

$$\ln k_1 = \frac{\Delta S^*}{R} - \frac{\Delta H^*}{RT} \qquad (6)$$

Therefore the rate of denaturation depends on both the entropy of activation, which is the degree of disorder in the formation of the activated state, and the enthalpy of activation, which is the change in bond energy involved in the formation of the activated state. It shows from this that the rate of denaturation can be reduced, and hence the denaturation temperature increased by decreasing the activation entropy, increasing the activation enthalpy, or both.

1.3.2 The mechanism of collagen denaturation

1.3.2.1 Denaturation as a kinetic rate process

One of the first investigations into the mechanism of collagen denaturation was carried out by Weir[53] who measured the degree of collagen shrinkage with time at various temperatures. The results indicated that the shrinkage of collagen was a first order rate process and proceeded through the formation of an activated complex, i.e.

Collagen A	$\Leftrightarrow$	Collagen B	$\Rightarrow$	Collagen C
(inactive)		(activated complex)		(shrunk)

It is the breaking of hydrogen bonds that brings about the formation of the activated complex. When a hydrogen bond breaks it can reform if the conformation of the α-chains of the triple helix has not altered; however if enough hydrogen bonds are broken the α-chains are able to move about relative to one another. As the number of hydrogen bonds broken increases a point is reached where the triple helical structure will spontaneously unzip, this point is the activated complex. At this point the hydrogen bonds can reform to produce the original triple helical structure, or further bonds can break bringing about the denaturation of the whole molecule.

Miles and Bailey[54] have proposed that the denaturation of collagen is an irreversible rate process and that the stability of the collagen molecule against denaturation is not

constant along its length, there existing regions of the α-chains that are hydroxyproline poor and therefore have less hydroxyproline hydrogen bonded water bridges to further stabilise the structure, the largest of these regions is the 65 residue section between Gly877 and Pro941 (shown in Figure 1.12) located within the hole region[55]. The absence of these water bridges produces hydrothermally labile regions, known as the cooperative unit, which are less stable than the rest of the molecule. It is thought that the denaturation process starts at one such hydrothermally labile region allowing the unzipping of the entire molecule to occur.

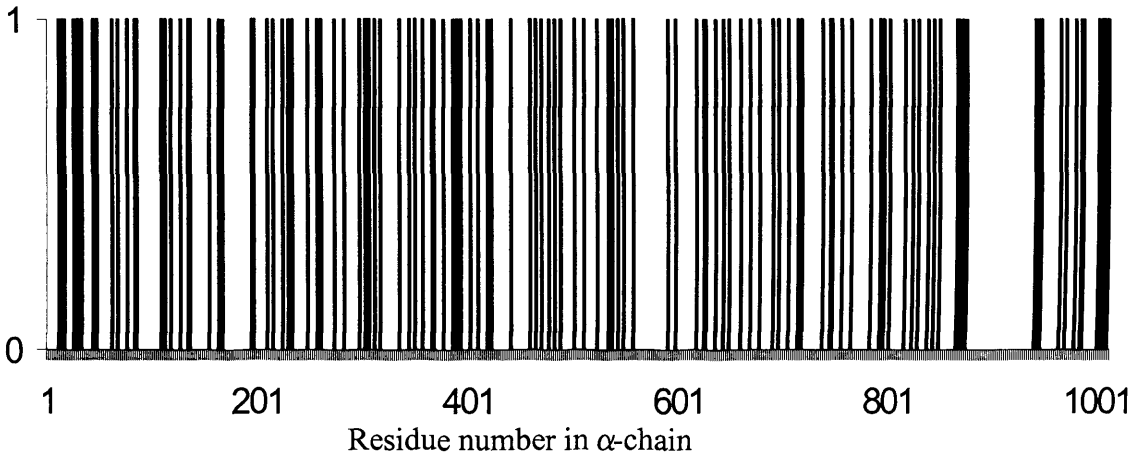

Figure 1.12 *Schematic diagram of the location of the hydroxyproline residues in the α-chain of bovine type I collagen showing the presence of a hydroxyproline poor region between residues 877-941. (Each bar represents the presence of a hydroxyproline residue.)*

1.3.2.2 Denaturation as an equilibrium melting process

A rival theory to that of the denaturation process being governed by a kinetic rate process is that it is due to an equilibrium melting process. This was first proposed by van Hook[56] who described the thermal denaturation of collagen as the fusion of a crystalline state of the organisation of orientated peptide chains. Flory and Garrett[57] used dilatometry to arrive at the same conclusion, suggesting that denaturation could be treated as a reversible phase transition with the presence of water acting as a diluent reducing the denaturation temperature of the collagen in an analogous way to the way the presence of a solute depresses the freezing point of a solvent. Privalov et al[58] developed a general theory of protein denaturation based on equilibrium thermodynamics in which the effect of temperature was to vary the effective

equilibrium constant between the native and the denatured states, from this the effective enthalpy, ΔH_{eff}, of denaturation for a protein can be determined. If the denaturation of the protein is a two-stage process then the calculated effective enthalpy of denaturation, ΔH_{eff}, should be equivalent to the ΔH_{cal} determined by calorimetry, as shown in the equation below.

$$\frac{\Delta H^{cal}}{\Delta H^{eff}} \approx 1 \qquad (7)$$

Some globular proteins conform to this rule, however collagen does not[59].

The denaturation of individual collagen triple helices in solution is partially reversible, the randomly uncoiled α-chains becoming renatured over time. Studies have shown that Type I procollagen can undergo renaturation, with the interchain disulphide crosslinks in the propeptide region acting as a refolding nucleus[60]. The same studies also showed that if the propeptides were removed then misfolded triple helices were obtained due to the refolding of chains not in their correct register. Misfolding forms aggregates of partially triple helical molecules that have a hydrothermal stability lower than that of the correctly folded helices[61], as shown in Figure 1.13. Reversibility of denaturation has also been observed in short sections of Type I collagen[62].

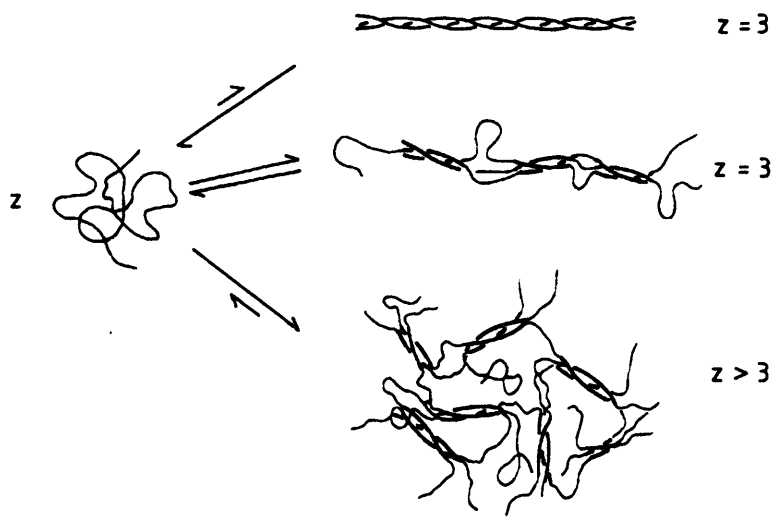

Figure 1.13 *Refolding of denatured collagen α-chains (left) to give mainly misfolded aggregates of partially triple helical molecules.*

1.3.3 The "Polymer in a box" hypothesis

The observation that the denaturation temperature of collagen increases with dehydration has been made by several workers[63][64][65][66]. Finch and Ledward[63] gave a value for T_m of 112°C for bovine achilles tendon collagen containing 13% water by mass compared with a T_m of 66°C for fully hydrated bovine achilles tendon collagen. Miles and Ghelashvili[67] made a quantitative study of the effect of collagen hydration on the denaturation temperature and found that by using the "polymer in a box" hypothesis of Doi and Edwards[68] a relationship between the denaturation temperature and the volume fraction of water in the fibre could be established. The individual collagen molecule when constrained within a fibre can be thought of as being confined within a box whose dimensions are governed by the intermolecular spacing of the individual collagen molecules. The "polymer in a box" theory relates the entropy of the polymer molecule within the box to the box dimensions and so decreasing the width of the box reduces the number of possible configurations of the three uncoupled α-chains within the activated state, thus reducing the configurational entropy of activation of the polymer and hence increases the Gibbs free energy of activation, consequently increasing the thermal stability. For a collagen molecule in solution there are no closely spaced molecules as in the fibre lattice and so the size of the box around the molecule is increased allowing higher configurational entropy, and hence a lower value for T_m. This is shown diagrammatically in Figure 1.14 below. The "polymer in a box" theory would also explain why fibrillar collagen that has been swollen in acid displays a lower T_m than for unswollen collagen, as the size of the box is increased due to the increased intermolecular separation of the collagen molecules bought about by the osmotic swelling at low pH.

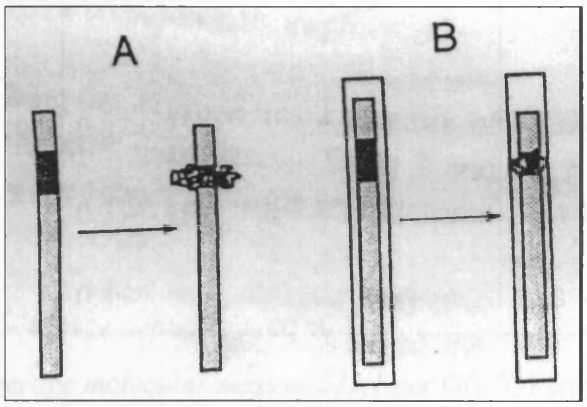

Figure 1.14 *Diagram to show the effect of reducing the size of the "box" on the space in which the collagen can denature into (taken from Miles and Ghelashvili[67]).*

1.4 Collagen hydration

1.4.1 Hydration levels of collagen

The level of hydration of the collagen fibrils has a large effect on the intermolecular separation of the collagen molecules within that fibril. The intermolecular distance, known as the d-spacing, can be found from small angle x-ray scattering (SAXS) from the first equatorial reflection of the collagen[69]. Pineri et al[70] postulated from dynamical mechanical thermal analysis (DMTA) investigations that collagen contains five levels of hydration within its fibrillar structure, a figure that has been also obtained by Cusack and Lees[71] from sonic velocity measurements of rat tail tendon at various hydration levels. Nomura et al[72] had previously presented results describing four levels of hydration, however this model had the two levels of structural water (level one and two in the Pineri model) combined. These five hydration levels from Pineri et al, and their corresponding mass fractions are shown below in Table 1.4

Table 1.4 *The levels of structural water in collagen as defined by Pineri et al[70] with their corresponding mass fractions and calculated ranges of molecules of water per tripeptide.*

Hydration level	Mass fraction (grams of H_2O/gram collagen)	Molecules of H_2O per triplet¶
1.) Structural water (Triply bonded)	0.00-0.01	0-0.15
2.) Structural water (doubly bonded)	0.01-0.07	0.15-1.14
3.) Bound water	0.07-0.25	1.14-5.04
4.) Absorbed water	0.25-0.45	5.04-12.37
5.) Free water	0.45-	12.37-

¶ = *assuming an average molecular mass of 272.1 per Gly-X-Y tripeptide repeat unit.*

The water in the first hydration level can only be removed by heating to 100°C in a high vacuum and its removal is irreversible. The water molecules here form three hydrogen bonds within the triple helix as part of a water bridge structure involving the hydroxyl group of hydroxyproline residues, such triple hydrogen bonded water molecules were proposed by Ramachandran and Chanrasekharan[15] as instrumental in stabilising the triple helical molecule. This is borne out by the fact that removal of the water in this hydration level results in a destruction of the triple helical structure. The fixation of one water molecule per three residues corresponds to 0.06 g of water per gram of collagen, however as the average hydroxyproline concentration in type I collagen corresponds to one hydroxyproline per ten residues then the amount of triply bonded water that can be fixed involving hydroxyproline hydroxyl groups is 0.018 g of water per gram of collagen[70]. The fact that only 0.01 g of water per gram of collagen is observed could be explained by the fact that not all of the hydroxyl groups of hydroxyproline in a model collagen tripeptide took part in water bridge formation[17], and this might also be the case in collagen. The other four hydration levels can be reversibly removed by vacuum drying at room temperature, suggesting that they are not bound so tightly within the collagen structure. The water involved with the second hydration level corresponds to one molecule of water per triplet of residues and was attributed to the doubly hydrogen bonded water molecule present in the intra helical water bridges formed in the structure as proposed by Ramachandran and Chandrasekharan[15]. The removal of the water in this hydration level does not have any effect on the helix integrity or on the equatorial spacing between individual collagen molecules. The third hydration level comprises of almost four molecules of water per triplet and has been attributed to the existence of doubly hydrogen bonded water molecules forming inter-helical water bridges between adjacent collagen molecules and between the microfibrils. Removal of water in this hydration level has a drastic effect on the equatorial spacing obtained from x-ray diffraction, which is a measure of the intermolecular distance[72]. The fourth level of hydration is believed to consist of water molecules that are bound to the collagen molecules by a single hydrogen bond and located between the individual molecules. The fifth hydration layer is made up of water molecules that have the properties of free water, these water molecules are not directly bound to the collagen but instead fill the spaces between molecules and microfibrils. The water molecules of this hydration layer can be frozen as ice within the collagen structure, although some workers have reported freezable

water present in the water molecules of the fourth hydration level, Nomura et al[72] observing freezable water to occur at 0.35 g/g collagen, and Haly and Snaith[73] observing ice formation at hydration levels as low as 0.26 g/g collagen in rat tail tendon collagen.

1.4.2 Effect of hydration on intermolecular spacing

It is well known that the intermolecular spacing between adjacent collagen triple helical molecules is highly dependent on the degree of hydration of those molecules. Fully hydrated collagen has a d-spacing of 1.6-1.5 nm which can be reduced to 1.16 nm by air drying at ambient temperature and 1.06 nm if dried at 60°C[36], this change in intermolecular spacing being attributed to the removal of free and absorbed water under drying at ambient temperature, and to the removal of bound water when heated to 60°C, continued heating at higher temperatures has no effect on the intermolecular spacing. There is also a decrease in the axial periodicity, D, during drying at ambient temperature from 67 nm to 64 nm attributed to the removal of free water, a decrease to 62 nm on heating to 100°C, attributed to the removal of bound and absorbed water and a further reduction to 57 nm for samples heated at 170°C when structural water corresponding to level two is lost. Both the reductions in intermolecular spacing and axial periodicity that occur on drying at temperatures below 170°C are completely reversible on rehydration of the collagen[36].

1.5 Mineralised collagen

Mineralised type I collagen is naturally present in bone, teeth, and the ankle tendons of some birds. Dry bone is composed of 65% inorganic mineral and 35% organic matrix (of which 90-95% is type I collagen)[74]. The remainder of the organic component is made up of lipid, including phospholipids[75], mucoproteins and sialoproteins[76]. Many studies of vertebrate hard tissue calcification have been carried out on naturally mineralised turkey leg tendon as this material is mineralised to about 70% dry weight of mineral in the adult bird and has a much simpler anatomical structure than bone, having the collagen fibres arranged in parallel rows[77].

1.5.1 Nature of the mineral phase

It was realised by the chemist Berzelius as early as 1845[78] that the mineral phase of bone was a calcium phosphate salt. The nature of the mineral phase was elucidated using wide angle x-ray diffraction, the diffractogram showing lines specific to hydroxyapatite[79]. The diffractogram for hydroxyapatite in naturally mineralised tissues is much more diffuse than that for synthetically produced mineral[78], suggesting that the hydroxyapatite is present in a poorly crystalline state. Studies on mineralised collagen using infra-red spectroscopy showed that some substitution of phosphate ions for carbonate occurs within the hydroxyapatite[78]. Other ions such as fluoride, citrate, magnesium, and sodium are also present within the crystal lattice of the hydroxyapatite concomitant with the role of bone as a reservoir for such ions within the organism[78].

1.5.2 Crystal size and shape

The dimensions of the mineral crystallites in calcified tissue have been investigated using electron microscopy[80][81] and both wide and small angle x-ray scattering[82][83][84] as well as inelastic neutron scattering studies. Scattering studies have the advantage over microscopy in that the average crystal dimensions within the sample are measured rather than just those in the microscopy image. Small angle x-ray scattering has advantages over wide angle scattering in that the scattering effect of the collagen can be ignored due to the much higher electron density of the mineral phase. From the small angle scattering profile the shape and thickness of the crystallites can be determined[83]. Using this technique Fratzl[84] determined the crystals in adult turkey leg tendon to be plate shaped with a thickness of approximately 2 nm, whereas those in bone were needle shaped with a thickness of 3-4 nm. Plate shaped mineral crystals have also been observed in tendon by electron microscopy, however for tendon that is just starting to mineralise needle shaped crystallites have been observed using stereo imaging electron microscopy[85].

1.5.3 Crystal location

Transmission electron microscopy studies of unstained native turkey leg tendon showed the presence of the initially formed mineral to be associated with the main banding pattern of the collagen fibrils[86]. This mineral was observed to be initially

nucleated within the hole zones formed by the quarter staggered arrangement of the collagen molecules[78], as shown diagrammatically in Figure 1.15.

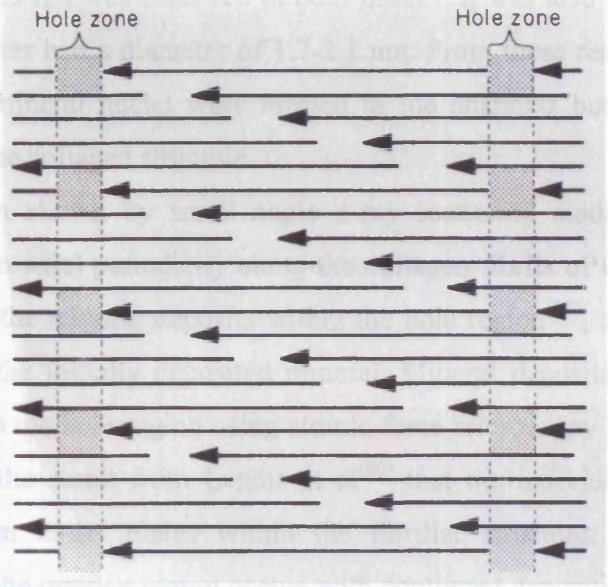

Figure 1.15 Diagram representing the position of initial mineral formation within the hole regions formed by the quarter stagger arrangement of the collagen molecules (arrows represent individual molecules, mineral represented by grey shading). Taken from Glimcher and Krane[78].

A transmission electron microscopy image of the location of the initially formed mineral deposits within the hole regions is shown below in Figure 1.16.

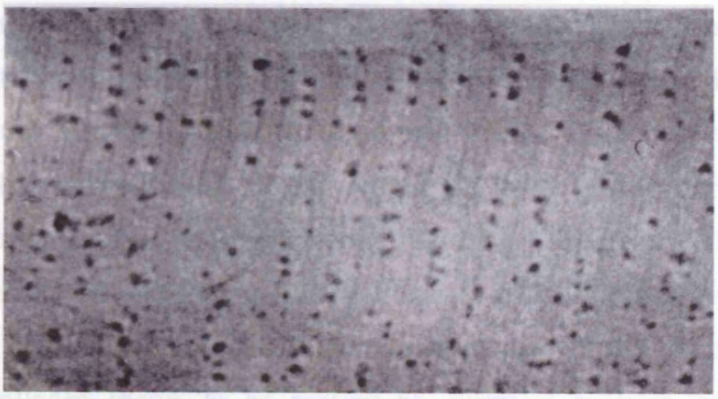

Figure 1.16 *TEM image of initially formed mineral deposits in turkey leg tendon (note the linear bands of mineral deposits due to the quarter stagger of the collagen molecules lining up the hole regions (x120000 magnification). Taken from Glimcher and Krane[78].*

From TEM images of mineralised bone and dentine, Hohling et al[87] measured the lateral spacing between the initially formed individual hydroxyapatite nuclei. A lateral separation of ~3.9 nm was observed in both tissues. It was also found that the initial mineral crystallites had a diameter of 1.7-2.1 nm. From these results it was proposed that the initial mineral nuclei were formed in the channels between the individual microfibrils of the collagen structure.

It has also been shown by small angle x-ray scattering studies that the mineral deposits show an axial periodicity along the collagen fibrils of 0.46D corresponding to the length of the mineral deposits within the hole region[88], confirming this to be the location of the initially deposited mineral. Mineral deposits have recently been visualised within the hole region using atomic force microscopy (AFM)[89]; this study also confirmed the result from Landis et al[90] that the individual mineral platelets coalesce to form larger plates within the fibrillar structure. Growth of mineral crystallites into the overlap region occurs with continued deposition of mineral within the fibril structure causing the complete encapsulation of the structure by the mineral phase[77]. The presence of mineral crystallites within the fibrillar structure has an impact on the intermolecular distance between adjacent collagen molecules, the equatorial spacing corresponding to the separation of the individual molecules reduces as the amount of mineral increases[91]. The presence of the mineral within the hole regions also has an effect on the axial periodicity of the collagen, which for mineralised tissue remains at 67 nm even when dry compared to unmineralised collagen fibrils where the D spacing shrinks to 64 nm.

In contrast to the findings that the initial mineral is nucleated in the hole region within the fibrillar structure Landis et al[92], using 3-dimensional computed tomography, found the initial mineral crystals to be formed on the surface of the individual collagen fibrils with very little mineral within the inside of the fibrils with more crystals appearing in the hole and overlap regions as the degree of calcification increases. From neutron scattering studies, Bonar et al[93] calculated that there is not enough space within the collagen fibrils to accommodate all of the mineral in fully mineralised collagen shown to be present by chemical analysis, suggesting that interfibrillar mineral must be present. Both these results suggesting the possibility that vesicle mediated mineralisation also occurs in mineralising turkey leg tendon[94]. However, in TEM studies of cross sections of herring bone, in which the collagen fibrils are naturally widely separated within the tissue, no interfibrillar mineral has

been observed even at the heaviest levels of mineralisation where the collagen banding pattern is totally obscured by mineral in both hole and overlap regions[95]. This result casts doubt on the proposed role of matrix vesicles in collagen mineralisation.

It was originally thought that collagen itself was responsible for initiating the nucleation of mineral clusters, the charged side chains of the collagen molecule interacting in some way with the hydroxyapatite mineral. However studies on the chemical blocking of side chain functional groups showed that this was not to be the case[78]. If collagen itself was responsible for the induction of mineral then a reason would be needed to explain why Type I collagen in bone undergoes mineralisation, while that in unmineralising tissue, such as skin doesn't. Glimcher et al[96] found that phosphoserine, phosphothreonine and γ-carboxyglutamic acid were present in turkey leg tendon that underwent mineralisation, but was absent in the unmineralising tendon, these three amino acids being associated with the mineral nucleating peptides. The proof that it wasn't the collagen itself inducing mineralisation came when Ennever, et al[97] showed that collagen that could previously be mineralised lost its ability to undergo mineralisation when subjected to solvent extraction with a mixture of chloroform and methanol. By separating the extracted mixture and subjecting the various fractions to mineralisation trials it was shown that the compound that induced mineralisation was a phospholipid-protein complex. Bone and other mineralised tissues contain such proteolipid compounds, whereas skin is relatively poor in them. These proteolipid complexes contain a large amount of anionic groups and are often highly phosphorylated.

Studies showed that the acidic protein associated with dentin mineralisation, phosphophoryn, binds to the collagen molecule in the gap region[98], this molecule is thought to initiate hydroxyapatite mineralisation in dentin. Similar acidic proteins are found in bone and mineralised tendon although the position at which they bind to collagen molecules is unknown. The length of the hole zone is approximately 40 nm[18], longer than the average crystal length, however the diameter of the hole zone is only 1-3 nm[18], much less than the width of the crystallites. It was proposed that the 3-dimensional alignment of collagen molecules gives rise to a situation where adjacent hole zones line up to form grooves or channels through the structure large enough to accommodate the crystals[90], (see Figure 1.17) evidence to support this was obtained using high voltage electron microscopic tomography.

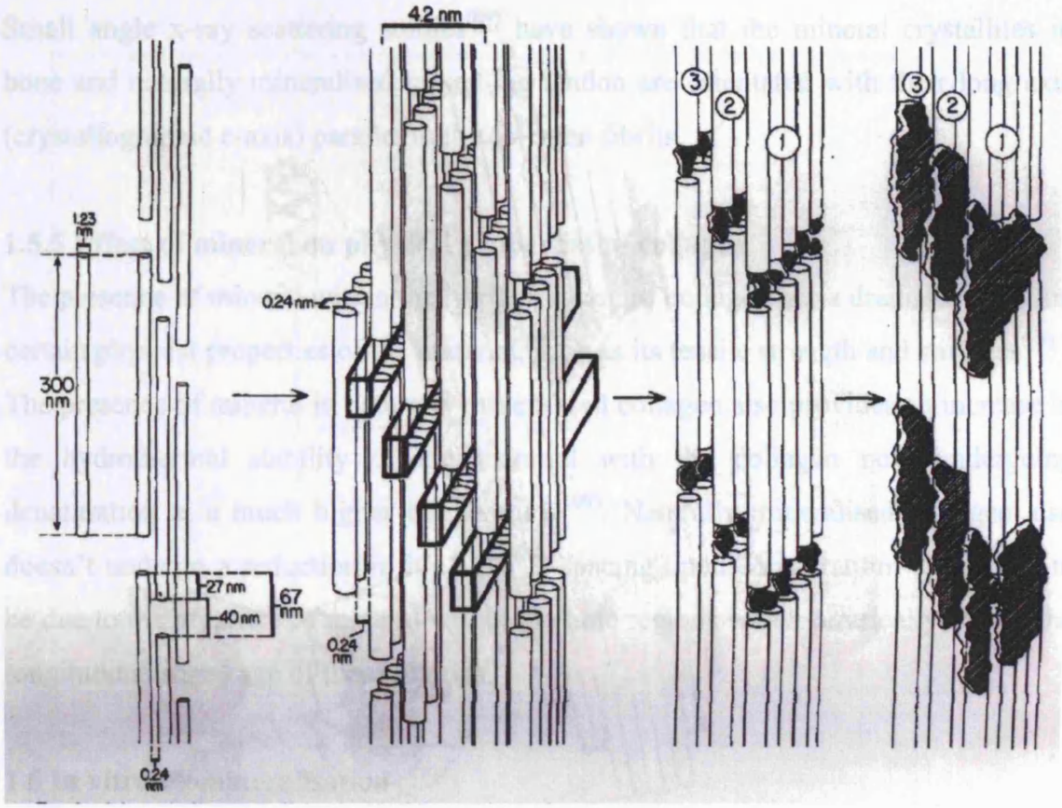

Figure 1.17 *Schematic diagram showing the mineralisation of a 3-dimensional array of collagen molecules. The far left image shows the dimensions of the quarter stagger arrangement of adjacent molecules which gives rise to the hole and overlap regions, this is then represented in 3-dimensions in the next diagram, showing the channels formed by the lining up of the hole regions (shown by the rectangular blocks). The 3rd diagram shows the initial mineral formed within the individual hole regions. The final image shows the formation of irregular shaped plates of mineral that have grown in width to occupy several adjacent hole zones, and in length to cover the overlap region as well. Fusing of platelets in adjacent holes also occurs leading to the formation of bands of mineral within the channels formed by the registration of hole regions, and ultimately to complete coverage of the molecules with mineral. (Diagram taken from Landis et al[90]).*

1.5.4 Crystal orientation

Small angle x-ray scattering studies[84] have shown that the mineral crystallites in bone and naturally mineralised turkey leg tendon are orientated with their long axis (crystallographic c-axis) parallel to the collagen fibrils.

1.5.5 Effect of mineral on physical properties of collagen

The presence of mineral within the fibril structure of collagen has a dramatic effect on certain physical properties of the material, such as its tensile strength and stiffness[99] The presence of mineral in naturally mineralised collagen also provides an increase in the hydrothermal stability of the material with the collagen now undergoing denaturation at a much higher temperature[100]. Naturally mineralised collagen also doesn't undergo a reduction in it's axial D-spacing upon denaturation[36], thought to be due to the presence of mineral within the hole regions which physically inhibit the longitudinal shrinkage of these regions.

1.6 In vitro biomineralisation

Much work has been carried out on the precipitation kinetics of calcium phosphates and also calcium carbonate from supersaturated solutions. The simplest method is known as the constant volume method and involves taking a supersaturated solution and adding seed crystals of the phase to be precipitated, which bring about the nucleation and growth of further mineral by heterogeneous nucleation. However, as new mineral is formed the concentration of the ions in solution falls until a level of supersaturation is reached where no more mineral will form, this is shown diagrammatically in Figure 1.18 overleaf.

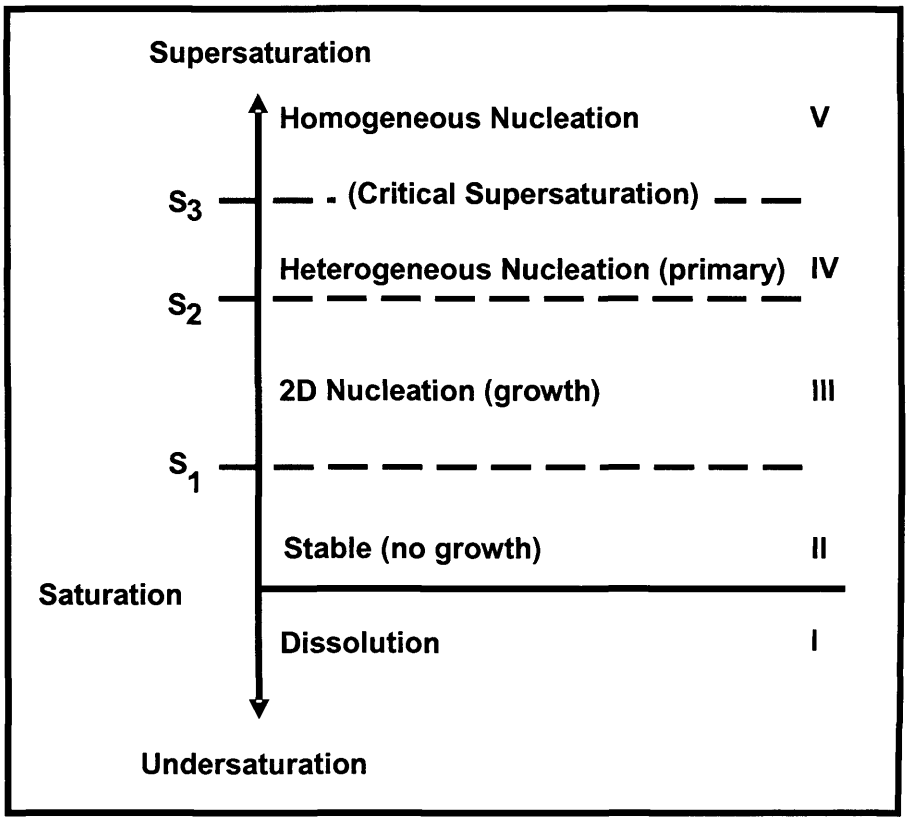

Figure 1.18 *Diagram showing the relative relationship of various nucleation processes with the degree of solution supersaturation.*

Another drawback when calcium phosphates are being precipitated is that the formation of calcium phosphates is accompanied by a change in solution pH as H^+ ions are produced. As a result the dynamics of the precipitation reaction change as the solubilities and hence supersaturations vary considerably with pH[101].

A way of avoiding the problems of the constant volume method is to use a technique known as the constant composition method[102]. This method maintains the concentration of the lattice ions of the mineral that is being precipitated, and also maintains the pH constant by the simultaneous addition of solutions containing the constituent ions. The addition of the solutions is triggered by a decrease in the solution pH, as measured by pH meter, (as H^+ ions are formed during mineral precipitation) so that those ions involved in the precipitation of mineral are replenished in solution by those added. These solutions also contain OH^- ions to bring the solution back to its starting pH. This method allows the precipitation of calcium phosphates to be investigated at various pH's as well as supersaturation levels.

Another use for the constant composition method is to investigate the inhibitory effect that certain biological substances have on crystal nucleation and growth. It has been shown that when free in solution, polyanionic proteins associated with mineralised tissues retard the formation and growth of mineral[103], this occurs through the binding of the anionic groups to certain preferred crystal faces resulting in altered crystal morphologies. Some smaller molecules, such as bisphosphonate compounds also show a powerful inhibitory effect on crystal growth[104]. These same growth inhibitors when bound to an insoluble matrix act as nucleators for mineral formation when immersed in a metastable solution[103] as the anionic groups bind mineral ions to form mineral clusters.

Robinson[105] was the first to propose a hypothesis as to what caused biological tissues to undergo mineralisation. He postulated that alkaline phosphatase was present in mineralising tissues and this enzyme raised local phosphate concentrations to metastable levels where mineral clusters could nucleate and grow. However this enzyme is also found in tissues that do not undergo mineralisation. This rationale however was used by Banks et al[106] to design an experiment that bought about the in vitro mineralisation of collagen fibres, which had been modified by covalently grafting the phosphate rich protein egg yolk phosvitin to them. Hydroxyapatite was deposited within the collagen fibres by allowing alkaline phosphatase to break down a solution of calcium β-glycerophoshate to elevate the local levels of calcium and phosphate ions. However due to the possibility of spontaneous precipitation of calcium phosphate due to the high concentration of ions produced by the alkaline phosphatase it was not known whether the mineral formation was induced by the modified collagen substrate or produced by direct precipitation. This experiment was repeated by Saito et al[107] using a metastable solution of calcium phosphate and it was found that phosvitin grafted collagen did indeed induce mineral formation, but only when the phosvitin was covalently bound to the collagen substrate. It was also found to be possible to induce mineral formation on agarose beads that had phosvitin grafted to them. *In-vitro* mineral formation within collagen fibres has also been achieved by Kronick and Cooke[108], using a decrease in atmospheric pressure to cause deposition of calcium phosphate within the collagen substrate. In this case though the mineral produced could be washed away from the collagen indicating that it was probably formed by deposition and not nucleated heterogeneously onto the collagen substrate.

Other biopolymers have been investigated as potential scaffolds for biomineral formation, various methods have allowed the growth of hydroxyapatite mineral on modified substrates such as cotton[109], bamboo[110] and chitin[111].

Remineralisation studies of demineralised collagen matrices such as bone[112], dentin[113], and turkey leg tendon[114] have been carried out to compare the *in-vitro* mineralisation of collagen with that which occurs *in-vivo*. In experiments on the *in-vitro* remineralisation of demineralised turkey leg tendon Bigi et al[115] found that mineral was nucleated on the surfaces rather than inside the collagen fibrils. X-ray scattering studies showed that there was no reduction in the intermolecular distance between the collagen molecules during this *in-vitro* mineralisation to levels found in naturally mineralised collagen further indicating that mineral formation was limited to the surface of the fibrils and not within the fibrils themselves.

1.7 Aims of the research

The work of Kronick on the improvement of the hydrothermal stability by partially mineralisation of collagen may offer the possibility of a type of stabilisation of collagen by incorporating a small amount of mineral within the gap region of the fibrillar structure, and thus offering a novel highly hydrothermally stable tanning agent. The key would be to incorporate enough of the mineral phase so as to increase the hydrothermal stability without affecting the desirable properties of the leather produced. The primary aim of the research was to investigate the hydrothermal stability of collagen that had been mineralised to varying levels of mineral content using demineralised turkey leg tendon as a model. Once a model of how the level of mineralisation affects the hydrothermal stability had been produced then chemical methods to modify skin collagen will be investigated to impart it with chemical groups capable of nucleating mineral. Using suitably modified skin collagen and information gained from the turkey leg tendon remineralisation model, the production of a hydrothermally stabilised collagen substrate by partial mineralisation will be investigated.

During the course of the research it was found that the remineralisation of demineralised turkey leg tendon did not give rise to an improvement in hydrothermal stability; however during trials to evaluate the effectiveness of the demineralisation process a second high temperature endothermic peak was observed in the DSC thermogram of demineralised tendon. From this observation new aims were added to

the research, these being to determine the cause of the second high temperature endothermic transition and to determine how the position of this transition is affected by different experimental conditions.

Chapter 2

An introduction to biomineralisation

2.1 Introduction

The search for new biomaterials for hard tissue rebuilding and repair is an ongoing area of research as the currently used materials for repairing bone fractures all suffer from drawbacks as none have the physical properties to match those of the bone itself. Bone has a unique set of properties that makes it ideally suited to its role as a structural support material, it can be thought of as a composite material made up of a mineral phase incorporated within a matrix of collagen fibres. It is this combination of the hard, brittle mineral phase with the soft viscoelastic collagen fibres that gives bone its unique mechanical and biological properties.

It is not surprising then that the *in-vitro* mineralisation of collagen is such an appealing area of research, as not only would such biomaterials have uses in orthopaedic surgery, but they could also be used in other applications where a biodegradable material which is strong yet not brittle is required, especially as large quantities of waste skin collagen are produced by the meat and leather industries.

Unwanted mineralisation in soft biological tissues also occurs in some pathological diseases, such as kidney and gall stones, dental calculus[(116)] and also in the calcification of replacement heart valves made from bovine pericardium[(117)]. A better understanding of the mechanisms of mineralisation and how they can be controlled would be beneficial in providing treatment for the prevention of these diseases.

2.2 Naturally biomineralised materials.

Biomineralisation is best described as the process by which living organisms produce mineral deposits. Biomineralisation is a diverse, widespread, and common phenomenon throughout the natural world, all five biological kingdoms contain organisms that carry out biomineralisation, these are distributed across some 55 phyla which produce over 60 different biominerals, although the majority of examples of biomineralisation utilise either calcium carbonate, calcium phosphate, or silica. Analysis of the fossil record shows that biomineralisation has certainly been around at least since the time of the Cambrian explosion around 525 million years ago[(118)] and may have been around long before then, occurring within single celled primitive life forms similar to the mineralising bacteria of today, indeed it is quite possible that the process of biomineralisation may be as old as the process of life itself.

Biomineralisation can be split into two types, the first is uncontrolled biomineralisation, which was named "biologically induced mineralisation" by

Lowenstam[119], where the organism exerts no control over the biomineralisation process and in its simplest sense there is no interaction between the mineral and the structural matrix of the organism; an example of this is the deposition of mineral within cells, formed by the coming together of ions produced by cellular metabolic processes, such as the formation of calcium carbonate within algae from the carbonate ions (CO_3^{2-}) produced during photosynthesis reacting with calcium ions in the intracellular fluids. This allows the algae to avoid a build up of carbonate ions within their cellular fluids. The second type is controlled biomineralisation which was given the name "biologically controlled mineralisation" by Mann et al[120], where the organism controls all aspects of the mineral formation, such as the mineral phase laid down, the crystal size, shape, and orientation to the organic matrix. This high level of control allows complicated and intricate shapes to be produced such as in the shells of marine gastropods and in coccoliths. Such intricate crystal shapes are not seen in any other branch of inorganic chemistry. However the distinction between the two biomineralisation mechanisms is not so clear-cut in nature and there is a gradual progression between these two extremes.

Although the scope of biomineralisation is large and involves many different minerals, the underlying principles of controlled biomineralisation are the same. A biomineralisation system consists of three distinct components, an insoluble organic matrix that is to be mineralised (i.e. collagen in bone, chitin in shell), which is known as the framework macromolecule, a mineral phase, and a polyanionic acidic component, which binds to the insoluble matrix and brings about the nucleation of the mineral phase. This polyanionic component can be either a protein or a polysaccharide.

2.2.1 Nucleation

Nucleation is the first step in the formation of the mineral phase, it is a chain of collision events that lead to the formation of a stable cluster of ions capable of survival and growth to form a crystal of the precipitated mineral phase. Classical nucleation theory[121] states that the energy changes that occur during nucleation are given by the equation:

$$\Delta G_l = \alpha l^3 \Delta G_v + \beta l^2 \sigma \qquad (8)$$

α and β are both constants that depend on the shape of the ion cluster, l is the mean cluster diameter, σ is the energy expended in creating a unit area of cluster surface (i.e. the interfacial energy), and ΔG_v is the free energy change resulting in the ion binding within the cluster. ΔG_v can also be expressed as:

$$\Delta G_v = \frac{-RT}{v}(\ln S) \tag{9}$$

Here v is the number of ions in the formula unit (e.g. 9 for hydroxyapatite) and lnS is the natural logarithm of the ratio of the ionic product in the supersaturated solution (IP) over the thermodynamic solubility product (SP) for the phase precipitated, therefore S is equal to IP/SP. As σ is always positive then for nucleation to occur ΔG_v must be negative, for this to occur the supersaturation ratio S must be greater than 1 otherwise ΔG_l becomes an increasingly positive energy barrier with increasing size of the cluster, l, so clusters formed would rapidly dissolve[101]. The formation of mineral nuclei is not instantaneous but occurs after an induction time, τ, which is inversely proportional to the supersaturation[102]. The induction time reflects the time taken for the formation of critical nuclei and has been used as a measure of the nucleation rate[122].

During the initial stages of nucleation the interfacial energy still exceeds the energy released by ion binding within the nuclei, the growth of the nuclei only becomes thermodynamically favourable once the energy released from ion binding becomes larger than the interfacial energy[101]. This occurs when the ion cluster reaches a certain size called the critical diameter l^* as shown in Figure 2.1 overleaf.

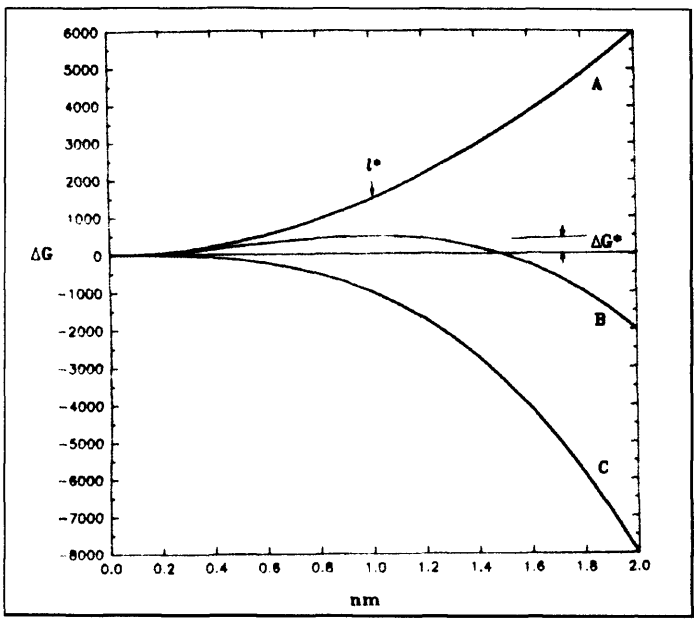

Figure 2.1. *The relationship between net particle free energy and mean particle diameter (curve B). The change in this with size results from the opposing effects of surface (interfacial, curve A) and volume (bonding, curve C) energies. The critical nuclei here occur at 1.0 nm and so the region to the right of this represents stable post nuclear mineral growth.*

The energy needed to reach this critical state is called the activation energy barrier (ΔG^*) and is related to the solution saturation by the equation:

$$\Delta G^* = \frac{C\sigma^3}{T^2}(\ln S)^2 \tag{10}$$

Where C is a constant and T is the absolute temperature.

It is the size of this activation energy barrier that is the critical factor for how fast nucleation from a supersaturated solution occurs, the rate of nucleation is given by:

$$J = D\exp\frac{-\Delta G^*}{kT} \tag{11}$$

Where D is a constant and k the Boltzmann constant.

From this equation it can be seen that there are two ways in which the nucleation rate can be increased at a given temperature: (1) by increasing the supersaturation of the solution, and (2) by lowering the interfacial energy (σ).

The supersaturation level where the critical nuclei form is called the critical supersaturation and at levels above this precipitation occurs rapidly by homogeneous nucleation. Nucleation can occur at supersaturations below this level if a suitable substrate is present, such nucleation is called heterogeneous nucleation. For this to occur the substrate surface must have an affinity for the ions that form the nucleus, and also a structural and electrical topography that allows the adsorbed ions to arrange themselves into a stable cluster, the net effect is a lowering of the interfacial energy (σ) as part of the structure of the forming ion cluster is provided by the substrate. This is how the bound polyanionic macromolecules associated with biomineralised tissue bring about the nucleation of mineral crystals, as the ionic groups involved in the formation of the nucleation site are arranged in such a shape so as they provide part of the unit cell of the crystal so that less energy is required to form that crystal. The interfacial tension of a substrate can be found by using the following formula[123]:

$$\sigma = k\mathrm{T}\ln[10(5\alpha/2\beta\nu_{\mathrm{m}}^{2})^{1/3}] \qquad (12)$$

Where:

k = Boltzmann constant

T = absolute temperature

β = a shape factor, 16/3 for spherical nuclei

ν = molar volume of the crystalline phase

α = The slope of a plot of log(induction time) vs log(supersaturation)$^{-2}$

Some values of σ found in the literature for various substrates known to nucleate hydroxyapatite *in-vitro* are shown in Table 1.1 overleaf.

Table 2.1 *examples of interfacial tension of various substrates known to induce mineral nucleation in vitro. DCPD = dicalcium phosphate dihydrate, $CaHPO_4.2H_20$. (1 erg cm^{-2} = 10^{-3} J M^2)*

Substrate	Interfacial tension (σ)/erg cm^{-2}	Reference
Synthetic liposomes	295	Kraus and Crenshaw[124]
DCPD crystals	152	Koutsoukos and Nancollas[123]
Agarose bound phosvitin	300	Kraus and Crenshaw[124]
Calcium fluoride crystals	167.3	Koutsoukos and Nancollas[123]

The interfacial tension gives a measure of the mineral induction potential of a surface, it is the measure of the free energy required to form a critical nucleus, therefore the lower the interfacial tension of a surface the easier it is to form mineral nuclei on that surface. If the chemical groups of a surface are in total alignment with those of the mineral phase that is to be nucleated then the crystal growth is termed epitaxy, or orientated overgrowth. This is a special case of heterogeneous nucleation in which the growth of the nuclei on the substrate follows a specific orientation, for this to occur the surface must have a low interfacial tension. This occurs with the growing of mineral on seed crystals of the same substance but its occurrence in the biomineralisation of biopolymer substrates is open to speculation.

The mechanism by which a surface directs orientated crystal growth from a metastable solution has been investigated by Addadi et al[125], who based on findings that mineralised tissues, such as shell[126] and bone[127] contain large amounts of bound sulphate, used a model for shell mineralisation consisting of poly(aspartate) adsorbed onto sulphonated polystyrene to mimic the nucleating surface. They found that a cooperative process occurred between the sulphonate groups and the carboxylate groups. In a similar experiment using a sulphate containing acidic matrix glycoprotein from mollusc shell bound to the polystyrene sheet the cooperative effect was also observed. Addadi et al[125] postulated that the bound sulphate ions show an ionotropic effect in attracting the oppositely charged cations such as calcium ions, drawing them to the area of the nucleation site but not binding them to specific groups on the substrate. Once the calcium ions have been attracted to the vicinity of the nucleation

site the bound carboxylate groups in the case of shell, or phosphate groups in the case of bone, can bind the calcium ions into an ordered array forming the crystal nuclei due to their high cation binding capacity. A schematic diagram of this cooperative process is shown in Figure 2.2 below.

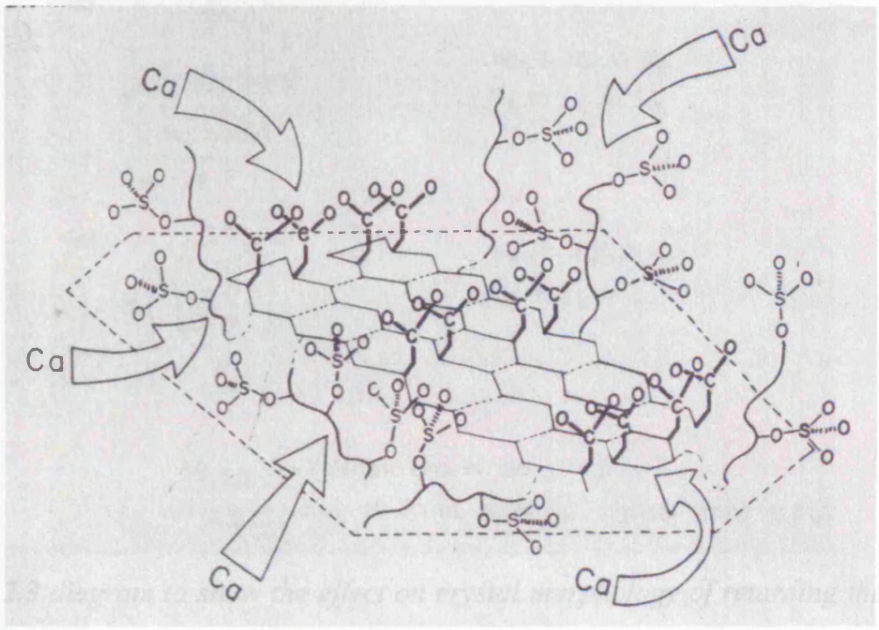

Figure 2.2 *diagram showing the interaction between bound sulphate and carboxylate groups in the formation of mineral nuclei in the mineralising matrix of shell (taken from Addadi et al[125]).*

2.2.2 Crystal growth

Once crystal nuclei of larger than the critical size are formed they can undergo crystal growth as long as the solution remains supersaturated with respect to the mineral being deposited. Crystal growth can take place by one of two mechanisms, screw dislocation propagation, and two dimensional (2D) surface nucleation[121]. In the case of hydroxyapatite formation the crystals appear to grow by the 2D surface nucleation mechanism[121]. With this mechanism the crystal grows by a successive layering of the reactant ions, with each layer initiated by a nucleation event on the surface of the previously deposited layer.

Certain molecules can bind to one or more faces of growing crystals and alter the size and shape of the crystal by stopping or retarding the uptake of ions by that crystal face, examples of the way in which retarding the growth of crystal faces has on the shape of the crystals are shown in Figure 2.3 overleaf.

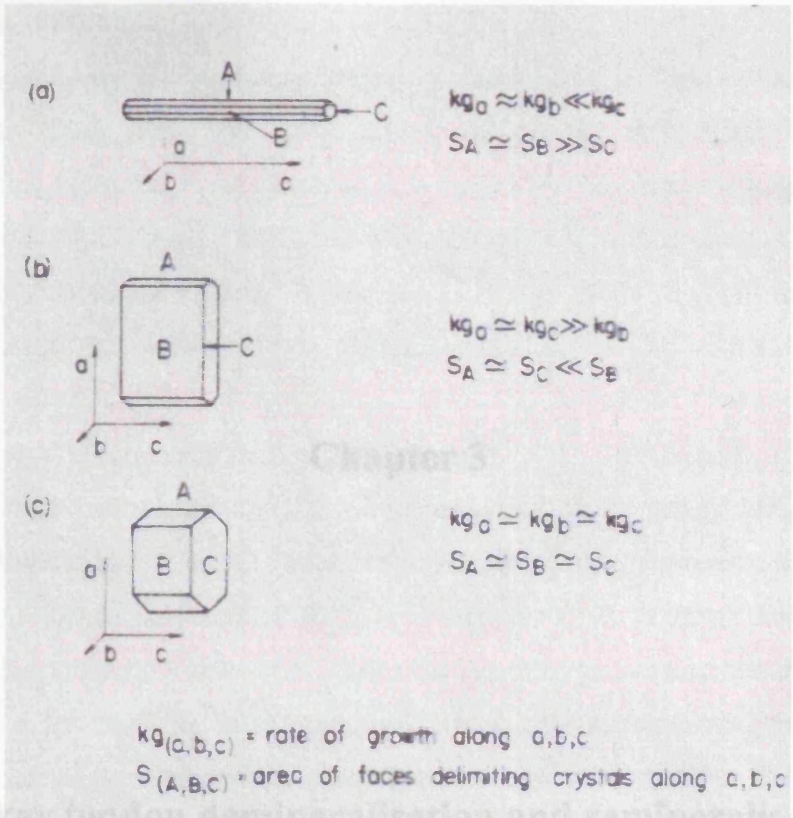

Figure 2.3 *diagram to show the effect on crystal morphology of retarding the crystal growth of different crystal faces.*

Figure 2.3 is explained as follows; c) depicts a crystal in which growth is not limited on any of its faces which yields crystals that are roughly isotropic. In b) growth is retarded on face B and so the crystal shows rapid growth on the other faces relative to this face, giving rise to crystals that are plate shaped. The situation in a) represents a crystal where growth is retarded on both the A and B faces so that rapid growth along the c-axis is observed giving rise to needle shaped crystals. Compounds that retard growth on certain crystal faces so that the crystal morphology is altered are termed crystal growth modifiers, many examples of these are known, for example phosphoserine, extracted shell proteins[128] and synthetic polymers[129]. If the agent that retards crystal growth binds to all crystal faces then crystal growth stops, such a compound is termed a crystal poison and will inhibit the dissolution of the mineral phase. This property of crystal poisons is taken advantage of in the treatment of certain medical conditions where bisphosphonate compounds are used to stop abnormal bone growth or dissolution[104].

Chapter 3

Turkey tendon demineralisation and remineralisation experiments

3.1 Introduction

The ankle tendons of the domestic turkey (*Meleagris gallopavo*) are naturally mineralised. Much work has been carried out on the mechanism of collagen mineralisation using turkey leg tendons as a model for hard tissue mineralisation as these provide a good model for bone calcification, but with a simpler anatomical organization than that of bone[114], and also because of the high degree of fibril alignment in tendon[77].

3.2 Removal of mineralised turkey leg tendons

Feet from adult domestic turkeys were obtained from a local turkey farm and frozen straight after slaughter. The feet were then defrosted and the mineralised tendons were removed as outlined by Knott et al[130] by cutting away the skin of the ankle, then separating the tendon compartment before cutting through the unmineralised part of the tendons at the ankle joint. The removed tendon compartment was then washed in distilled water to remove blood, synovial fluid and other debris. The individual tendons were then separated from the synovial membrane and scraped free of the collagenous sheath, which covers them. The unmineralised tendon from the ankle joint was also removed. The clean tendons were then washed in distilled water and stored frozen at -20°C until required.

3.3 Partial demineralisation studies

To obtain samples of partially mineralised collagen with a mineral content lower than that of naturally mineralised turkey tendon the method of Kronick and Cooke[108] was used. Clean, naturally mineralised turkey tendons from section 3.2 were frozen under liquid nitrogen and snapped into smaller pieces, these pieces were then ground into a coarse powder using a liquid nitrogen cooled stainless steel pestle and mortar. This tendon powder was then soaked in a large excess (50 mg tendon powder in 100 ml) of 0.5 mol dm^{-3} sodium citrate adjusted with 0.2 mol dm^{-3} hydrochloric acid to pH 5.20, the solution was then agitated for 17 hours at room temperature. The partially demineralised tendon powder was then washed twice in deionised water. The powder was split into two roughly equal parts, one part being freeze-dried ready for chemical analysis and the other immersed for 24 hours in pH 7.0 phosphate buffer ready for DSC studies.

3.4 Remineralisation of turkey tendons

3.4.1 Preparation of demineralised tendon slices

To remove the mineral phase of the naturally mineralised collagen, ethylenediamine tetra-acetic acid (EDTA) is normally usually used[130], however this reagent also removes the non-collagenous phosphoproteins associated with the nucleation of the mineral phase, in fact the use of EDTA is actually used as a method to remove and isolate mineral associated proteins from biomineralised tissues.[128] Therefore the use of EDTA in demineralisation could cause problems in the subsequent remineralisation of the turkey tendon slices. Dilute acids can also be used to remove mineral from mineralised tissue, acids bring about demineralisation much faster and so avoid the need for incorporating protease inhibitors in the demineralisation solution. Therefore 0.1 mol dm^{-3} hydrochloric acid was chosen for the demineralisation, and the tendons were totally demineralised if excess hydrochloric acid was present according to the formula:

$$Ca_{10}(PO_4)_6(OH)_2 + 20HCl \rightarrow 10CaCl_2 + 6H_3PO_4 + 2H_2O \qquad (13)$$

Dissected turkey tendons were defrosted and soaked in several changes of 0.1 mol dm^{-3} hydrochloric acid at 4°C for 48 hours, after which the tendons took on a translucent appearance. The demineralised tendons were then washed in distilled water and cut into pieces roughly 2 cm long. The cut tendon pieces were then embedded onto stubs using a polyvinyl alcohol (PVA) based embedding medium (Tissue Tek 4583, Sakura-Finetek, Netherlands), frozen, and cut into 60 μm thick transverse sections on a cryo-microtome (Cryocut 1800, Reichert-Jung) at -14°C. The tendon sections were then washed twice in distilled water to remove the residual embedding agent, and then soaked in 0.1 mol dm^{-3} hydrochloric acid for 24 hours at 4°C to remove any residual mineral. The tendon slices were then soaked in several changes in distilled water to remove any free acid and the pH of the washed tendon slices was then adjusted to pH 7.0 as measured by pH electrode, using ammonium bicarbonate to neutralise any free acid within the structure as well as the acid bound as the hydrochloride to the basic groups of the collagen, this being necessary to avoid possible acid damage of the collagen during freeze-drying. The neutralised tendon slices were then washed with several changes of distilled water to remove the

ammonium chloride formed from the neutralisation of the bound hydrochloric acid. The tendon slices were then freeze-dried overnight and kept until required for remineralisation in a dessicator over phosphorus pentoxide.

3.5 Formulation of mineralisation solutions.

Two different mineralisation solutions were evaluated for their suitability for the remineralisation of the turkey tendon slices. These were;

1) The metastable calcium phosphate solution used by Saito et al[107], which has a molar [Ca]x[P] product of 3.31 mM^2.
2) A less concentrated version of Saito's solution, which has a molar [Ca]x[P] product of 1.77 mM^2.

3.5.1 Method 1

The 3.31 mM^2 [Ca]x[P] Saito solution was made up using doubly de-ionised distilled water in glassware that had been acid washed with a 2% ammonium persulphate in concentrated sulphuric acid cleaning solution. This was followed by then washing in a 2% solution of phosphate free detergent (Micron 90, international products corporation, London, UK) in warm de-ionised water, then rinsing in de-ionised water and soaking overnight in 2M hydrochloric acid, finally rinsing twice with doubly de-ionised distilled water, and then oven drying. The mineralisation solution had the following composition per litre; 2.35 mM $CaCl_2$ (99.99% purity, Sigma), 1.41 mM K_3PO_4 (99% purity, Sigma), 150 mM KCl (99% purity, Sigma), 10 mM [4-(2-hydroxyethyl)-1-piperazine ethanesulphonic acid (HEPES) (98% purity, Sigma), and 3.08 mM NaN_3 (95% purity, Sigma), sufficient 0.1 mol dm^{-3} sodium hydroxide solution was added to the HEPES to give a final solution pH of 7.40 at 37°C. The solution was made up as follows in order to avoid precipitation; the HEPES was dissolved in 200 cm^3 of de-ionised water and 0.1 mol dm^{-3} NaOH was added whilst stirring with a magnetic stirrer until the pH was 7.40 as measured by pH electrode. The HEPES solution was then made up to 1000 cm^3. The $CaCl_2$ and KCl were then dissolved and made up to 2000 cm^3, and the K_3PO_4 and NaN_3 were made up into another 2000 cm^3 volumetric flask. The contents of all three flasks were filtered through a 0.45 μm filter (Oxoid Ltd) under vacuum and then filtered again through a fast filter paper. All three volumetric flasks were heated in a water bath at 37°C and

then their contents added to a 5000 cm^3 volumetric flask with vigorous mixing. The final mineralisation solution was then vacuum filtered through a 0.45 μm filter and then again through a fast filter paper. The final solution had a saturation {log(ion activity product)-log(activity product at saturation)} of 7.74 with respect to hydroxyapatite at 37°C[107] and a [Ca]:[P] ratio of 1.67, this ratio being the same for the mineral hydroxyapatite. 1000 cm^3 of the solution was then put into one litre capacity screw cap bottles that each contained 50 slices of freeze-dried demineralised turkey tendon. 1000 cm^{-3} bottles were used so as to give a high solution to tendon ratio thus enabling higher levels of potential for mineralisation as the solution only contains enough calcium and phosphate ions to form 233.33 mg of hydroxyapatite per litre. The bottles were then placed in a shaking incubator at 37°C for 21 days.
Hydroxyapatite was formed on the collagen slices from the ions in solution by the equation:

$$2OH^- + 10Ca^{2+} + 6PO_4^{3-} \rightarrow Ca_{10}(PO_4)_6(OH)_2 \qquad (14)$$

The mineralisation reaction was stopped by decanting most of the mineralisation solution from the bottle and then pouring the remaining contents into approximately ten times the amount of distilled water. The tendon slices were then washed well in several changes of distilled water to remove the mineralisation solution, as it was found that if it was not totally washed out, potassium chloride crystals were formed on the tendon slices during freeze drying. The tendon slices were then freeze-dried and stored in a dessicator over phosphorus pentoxide before being taken for analysis.

3.5.2 Method 2

The 1.77 mM^2 [Ca]x[P] Saito's solution was made up the same way except that 1.67mM $CaCl_2$ and 1.06 mM K_3PO_4 was used, still keeping the [Ca]:[P] ratio of the solution at approximately 1.67.

These preliminary mineralisation trials identified the 3.31 mM^2 solution to be the only one of the two mineralisation solutions to be effective in forming mineral deposits on the demineralised turkey leg tendon collagen substrate, therefore this solution was used for all subsequent mineralisation trials in which demineralised

turkey leg tendon slices were incubated in the mineralisation solution for periods up to 28 days.

3.6 Chemical analysis of remineralised tendon

Samples of the naturally mineralised, partially citrate demineralised, acid demineralised, and remineralised turkey leg tendon were digested in sealed glass tubes containing 1 ml of 6 mol dm^{-3} HCl at 105°C for 18 hours, after which time they had completely dissolved. The acid digest was then rinsed into a 4 ml volumetric flask and made up to the mark with deionised water. This solution was then filtered through a fast filter paper to remove any undissolved particles and then used for the chemical analysis of the tendons.

3.6.1 Determination of calcium and phosphate content

The amounts of both calcium and phosphate (as phosphorus) in each sample were determined by inductive coupled plasma optical emission spectroscopy (ICP-OES) at the chemical analytical services unit of the University of Newcastle, using a Unicam 701 ICP-OES. As the acid digestion process can leach ions from the glass tubes used, a blank digest containing no tendon was taken as a control and the values for this subtracted from the values obtained for each sample.

3.6.1.1 Results

The results for both the calcium and phosphate contents of the tendon substrates are shown below in Table 3.1.

Table 3.1. *Comparison of calcium and phosphate concentrations for native, demineralised, and remineralised tendon (remineralised for 21 days in Saito solution).*

Collagen substrate	$[Ca^{2+}]$ (ppm)	$[PO_4^{3-}]$ (ppm)
Naturally mineralised tendon	216950	102590
Demineralised tendon	904	245
1.77 mM^2 remineralised	1043	297
3.31 mM^2 remineralised	224540	107456

As can be seen from the table the 3.31 mM^2 solution gives a level of mineralisation similar to that occurring in the naturally mineralised turkey leg tendon, however the 1.77 mM^2 solution produces a substrate with similar calcium and phosphate levels to the demineralised tendon used, indicating that the solution doesn't facilitate the formation of calcium phosphate mineral on the demineralised tendon substrate used.

3.7 Scanning Electron Microscopy (SEM) of remineralised turkey tendon.

Three sections of turkey tendon were taken from each day's remineralisation trial, these samples were freeze-dried and two small pieces roughly 2 mm long cut off from each section. These 2 mm pieces were then mounted onto an SEM stub with the long axis of the sample flat to the stub. The samples were then gold coated using a PS3 coating unit (Biorad, U.K.) and kept in a dessicator until required for imaging. The sections were viewed using either a S2500 or a S3000N (Hitachi Science Systems Ltd) Scanning Electron Microscope at magnifications from x100 to x30000 in order to observe the appearance of mineral crystal formation, and the images recorded electronically. Images of both naturally mineralised and acid demineralised turkey leg tendons were taken as controls for comparison.

3.7.1 Results

3.7.1.1 Naturally mineralised turkey leg tendon

The SEM images of the naturally mineralised turkey leg tendon displayed a jagged appearance of the individual collagen fibrils, especially where the fibrils had been broken (as in Figure 3.2). Individual mineral crystallites could not be visualised due to their extreme small size and their location within the collagen fibrils. Mineral deposits were not visualised between the individual collagen fibrils, although in most cases jagged processes were observed pointing out from fibrils perpendicular to the fibril direction, the nature of these processes was uncertain although they did appear continuous with the collagen fibrils themselves. Examples of SEM images of naturally mineralised turkey leg tendon are shown below in Figures 3.1 and 3.2 overleaf.

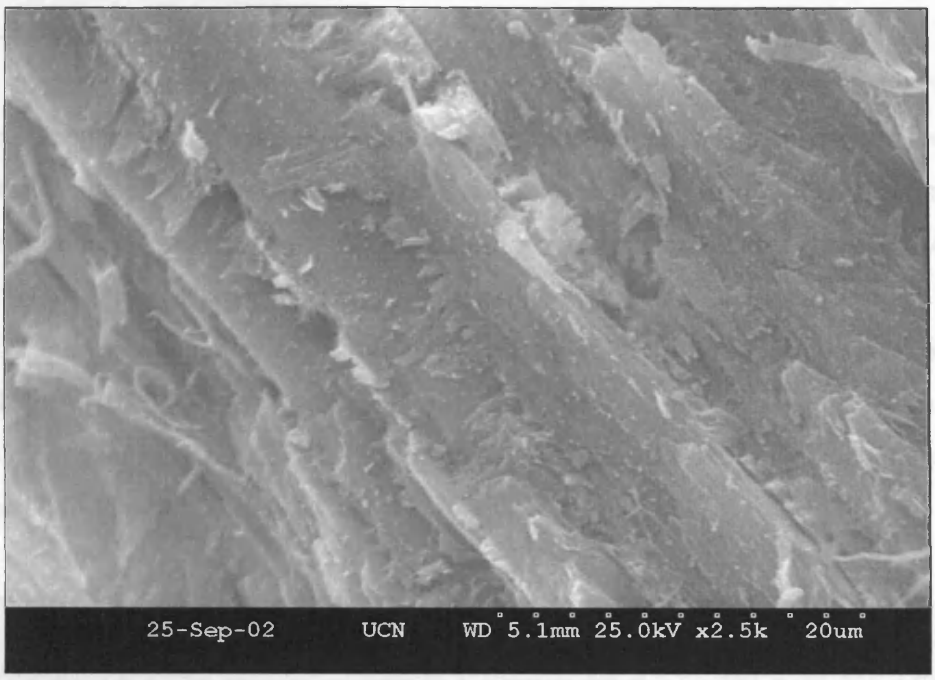

Figure 3.1 *SEM image of collagen fibrils in naturally mineralised turkey leg tendon. The platy appearance of the mineralised fibrils can clearly be seen (x2500 magnification).*

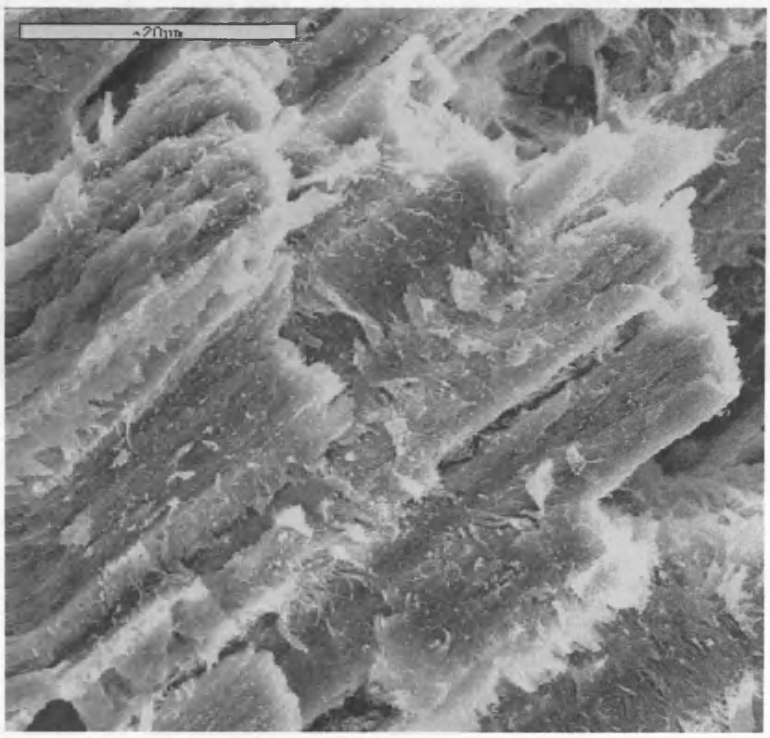

Figure 3.2 *SEM image of fractured collagen fibrils within naturally mineralised turkey leg tendon showing the platy nature of the fractured surface due to the presence of mineral within the fibril (x2000 magnification, scale bar = 20 μm).*

3.7.1.2 Demineralised tendon

SEM images of samples of demineralised turkey leg tendon showed a much less cluttered appearance of the collagen fibrils than those of naturally mineralised tendon. In the absence of mineral both the jagged appearance of the fractured fibrils, and the perpendicular processes observed in naturally mineralised tendon was no longer apparent, and the collagen fibrils were shown having a smooth appearance. In some cases (especially apparent in Figure 3.4) cracking of the fibrils had occurred due to shrinkage of the collagen structure during the freeze-drying technique used in the sample preparation. Typical SEM images of demineralised turkey leg tendon are presented in Figures 3.3 and 3.4.

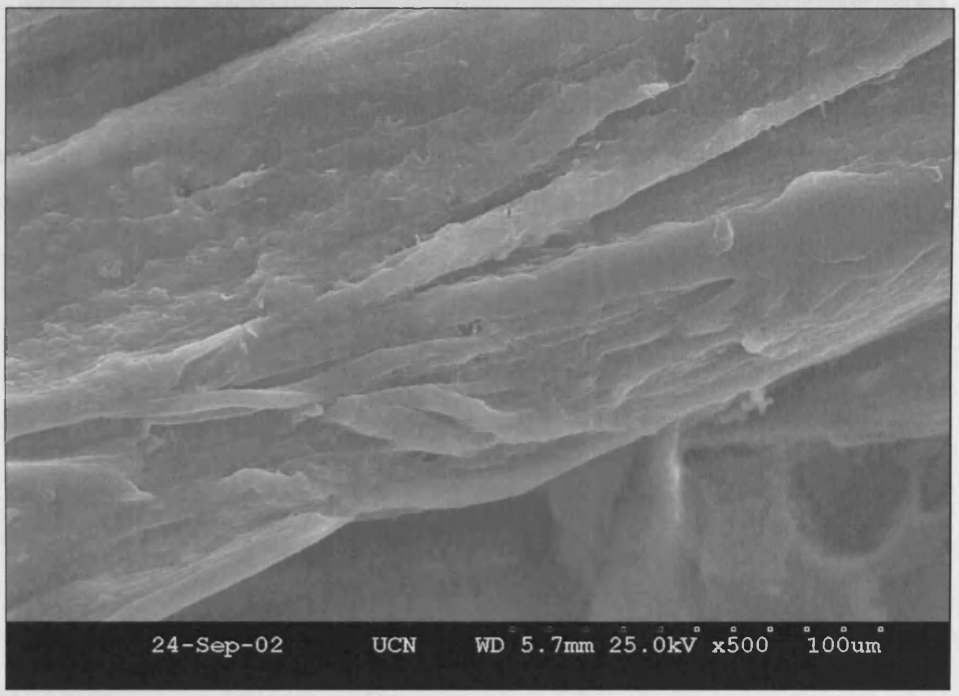

Figure 3.3 *SEM image of acid demineralised turkey leg tendon showing the smooth appearance of the collagen fibrils in the absence of mineral (x500 magnification).*

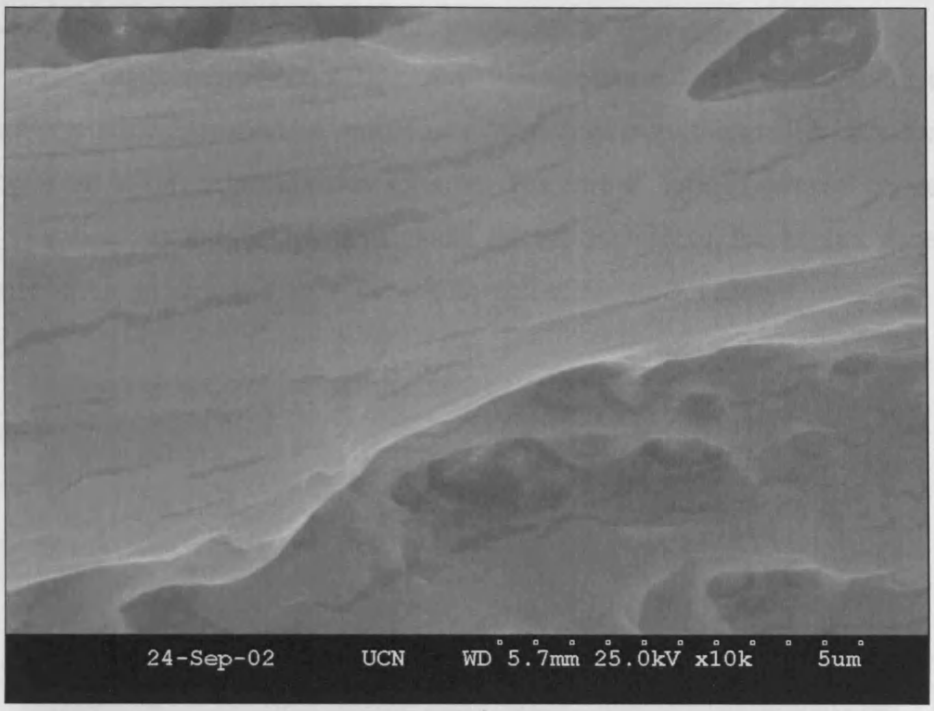

Figure 3.4 *SEM image of acid demineralised turkey leg tendon showing cracking of the collagen fibrils due to freeze-drying (x10000 magnification).*

3.7.1.3 Remineralised tendon

Only tendon remineralised using 3.31 mM^2 Saito solution displayed any evidence of mineral crystallite formation, in some cases crystallites were found after only six days of incubation in this mineralisation solution. The earliest formed mineral crystallites were visualised as a speckled appearance on the surface of the tendon slices, an example of this speckling is shown in the top left of Figure 3.5 shown below.

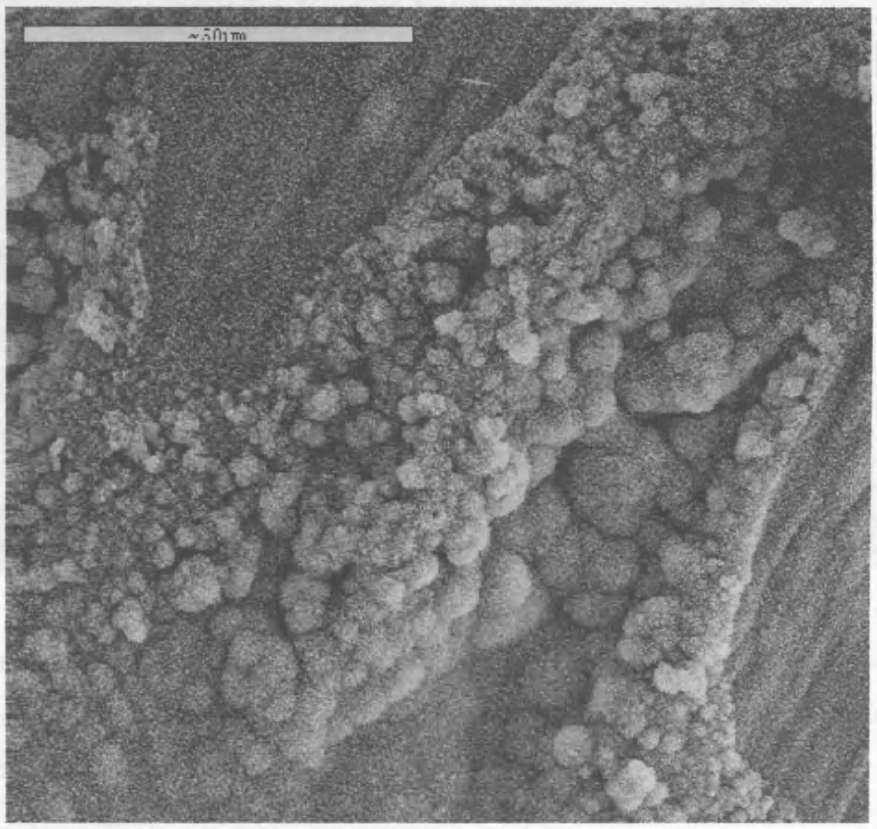

Figure 3.5 *SEM image of the surface of a piece of heavily remineralised turkey leg tendon showing the progressive growth of the mineral specks (top left hand corner) to form larger spherulites of mineral crystals (centre of image). The direction of the underlying fibrils can just be made out in the top left and bottom right of the image. Scale bar = 50 μm (x1000 magnification).*

These speck-like crystal deposits would then grow in size to form a deep layer of spherulitic clusters of randomly orientated, rectangular, plate shaped mineral crystals that cover the entire surface of the turkey tendon as the time of incubation was increased. This progressive growth from specks to spherulites can also be seen in the same image (Figure 3.5). The mineral spherulites would grow to sizes large enough so

as to be easily seen under fairly low magnification and would form a dense layer that covered the surface of the fibrils. An example of the visibility of the spherulites at low magnification is shown in Figure 3.6, which shows the surface of a very heavily remineralised piece of turkey leg tendon.

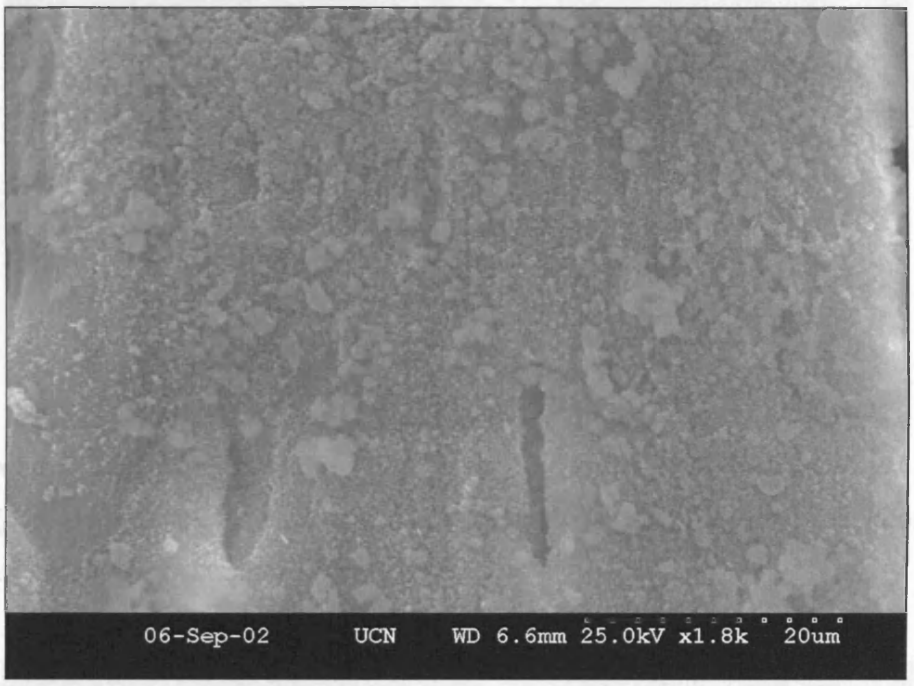

Figure 3.6 *SEM image of a sample of in-vitro remineralised turkey leg tendon after 24 days incubation in 3.31 mM^2 mineralisation solution (x1800 magnification). Note the speckled appearance of the surface due to the presence of mineral spherulites obscuring the underlying fibrils.*

The mineral plates covering the fibrils were larger than those found in naturally mineralised tendon, having dimensions of up to 1000 nm x 600 nm. The thickness of the plates is difficult to establish from the images but is considerably more than the 2 nm quoted from studies using small angle x-ray scattering of naturally mineralised turkey leg tendon[83]. An idea of the size of these plates is shown in Figures 3.7, 3.8, and 3.9. At the magnification used in Figure 3.9 it can be seen that the plates have an irregular surface associated with their width and that fragmentation of the plates occurs perpendicular to this face in the direction of the long axis.

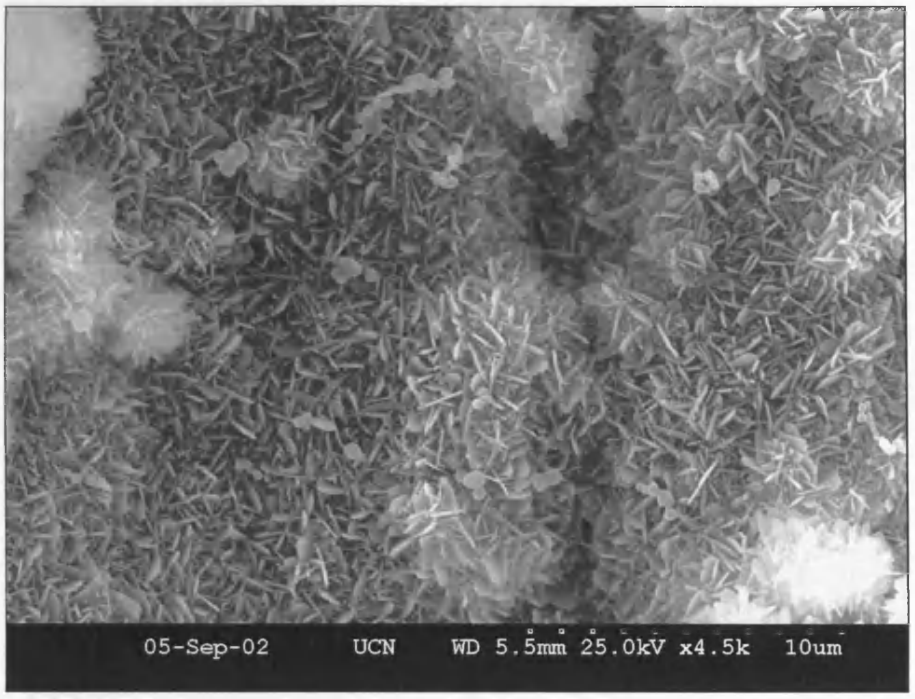

Figure 3.7 *SEM image of the surface of the remineralised tendon at higher magnification showing the surface to be covered in plates of calcium phosphate mineral (x4500 magnification).*

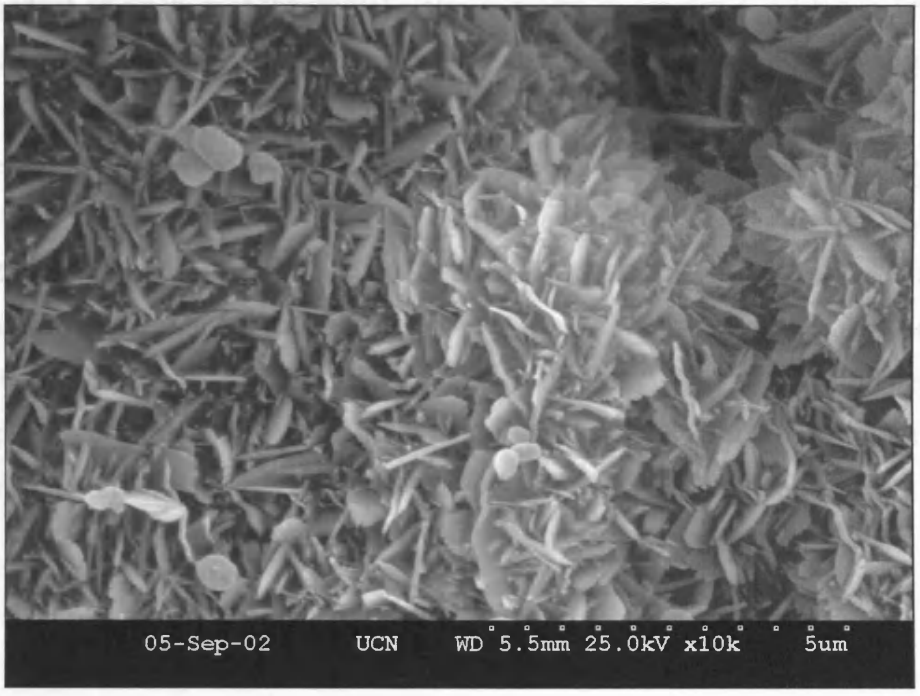

Figure 3.8 *SEM image of Figure 3.6 at still greater magnification showing the random orientation of the mineral plates on the surface of the fibrils (x10000 magnification).*

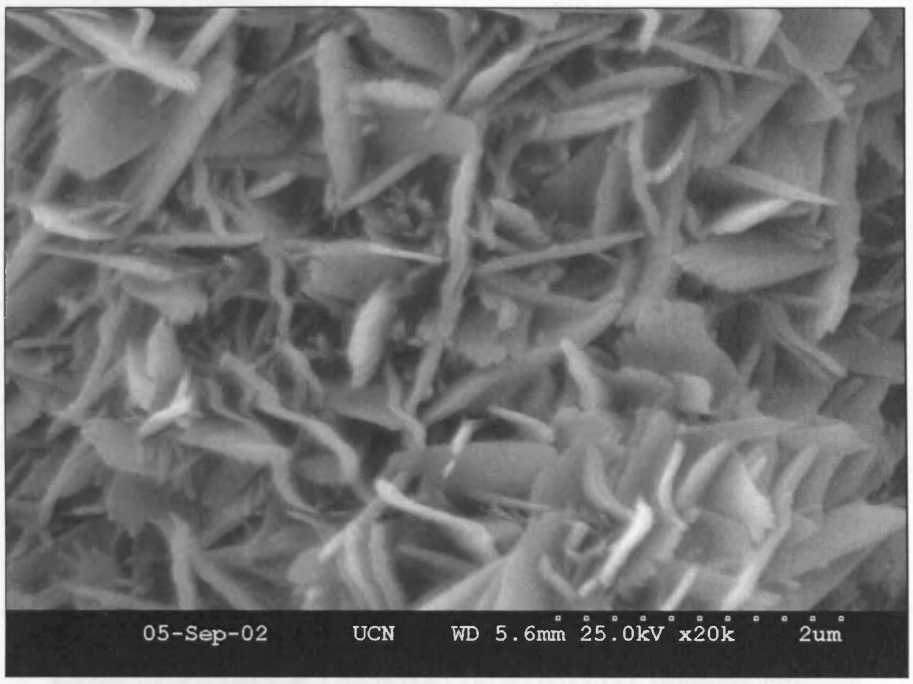

Figure 3.9 *Magnified image of figure 3.7 showing the irregular edges of the crystal plates and also the fragmentation of the plates in the direction perpendicular to the irregular edges.*

The random orientation of the crystal plates is shown in Figures 3.7, 3.8 and 3.9. The crystals appear to be randomly orientated about their long (c-) axis but do appear to grow with their long axis perpendicular to the underlying collagen fibrils. In the case of the very heavily mineralised samples it appeared that secondary nucleation of crystallites had occurred on the surface of those crystallites already present resulting in a dense layer of spherulites. In such cases the crystal plates are seen to radiate outwards from a point, similar in shape to the petals of a flower. This petal-like growth of the crystallites can be clearly seen in Figures 3.7 and 3.8. In the heaviest examples of crystallite growth observed the entire surface was covered in a multiple layer of spherulites as shown in Figure 3.10 overleaf.

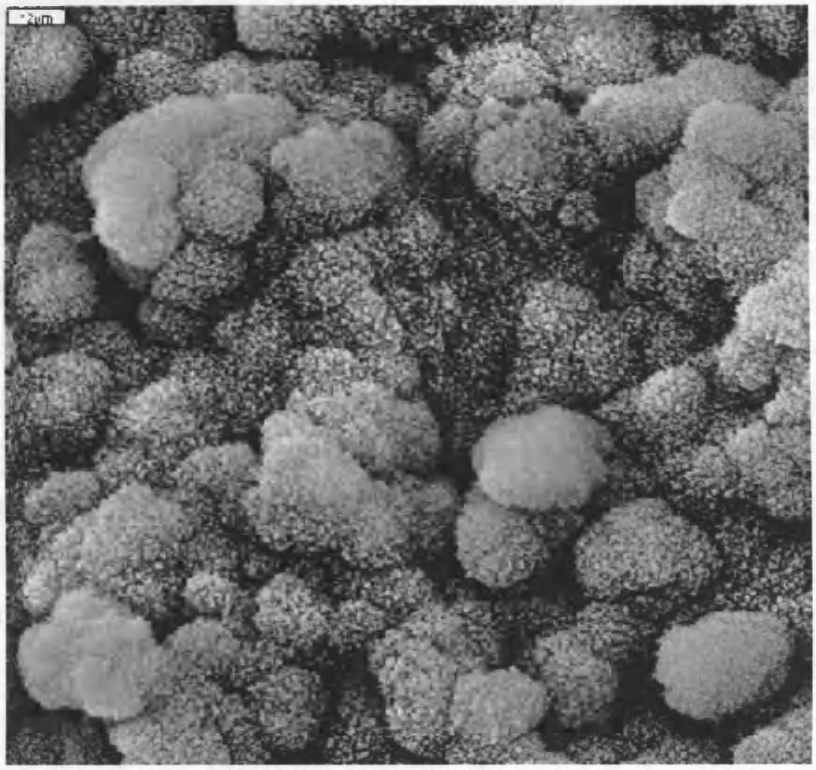

Figure 3.10 *SEM image of the heaviest levels of mineralisation, the surface of the tendon is covered in a dense layer of spherulites each made up of hundreds of individual crystal plates that appear to radiate outwards from the centre of the spherulite. (x4000 magnification, scale bar = 2 μm).*

3.8 Energy Dispersive X-ray Analysis of remineralised turkey tendon

Samples of the remineralised tendon sections for each day's trial were mounted on SEM stubs with the long axis of the sample flat against the stub, and carbon coated using a K450 carbon coater (Emitech Ltd, UK). The sections were then subjected to Energy Dispersive X-ray Analysis (EDXA) to determine the elements present in the section and also their location. Elemental mapping was carried out for phosphorus and calcium for the bulk sample (at a magnification of approximately x100) and then at the level of the tendon fibres (at a magnification of approximately x1000-3000). The elemental composition of anything that resembled mineral deposits was also determined. Samples of naturally mineralised and acid demineralised tendons were used as controls for comparison.

3.8.1 Results

The x-ray emission spectrum from a sample of naturally mineralised turkey leg tendon displayed two major peaks, one at 2.0 keV corresponding to the presence of

phosphorus, and another at approximately 3.8 keV corresponding to calcium. A typical emission spectrum for a sample of naturally mineralised turkey leg tendon is shown in Figure 3.11. Elemental mapping of this sample showed a high concentration of calcium and phosphorus associated with the collagen fibrils as shown in Figure 3.12.

Demineralised tendon samples gave an emission spectrum that was devoid of the peak associated with calcium and only displayed a tiny peak for phosphorus, probably due to the phosphorus present in the phosphoproteins associated with mineral nucleation. A typical example is shown in Figure 3.13. Elemental mapping of demineralised samples showed almost a total absence of both calcium and phosphorus indicating the successful removal of mineral during the demineralisation process as shown in Figure 3.14. Samples of demineralised tendon that had been incubated in 3.31 mM^2 Saito solution for 24 days gave an emission spectrum similar to that of the naturally mineralised turkey leg tendon, as shown in Figure 3.15, showing the presence of calcium and phosphorus. Elemental mapping showed that the mineral was present covering the entire surface of the tendon. Typical results are shown in Figure 3.16.

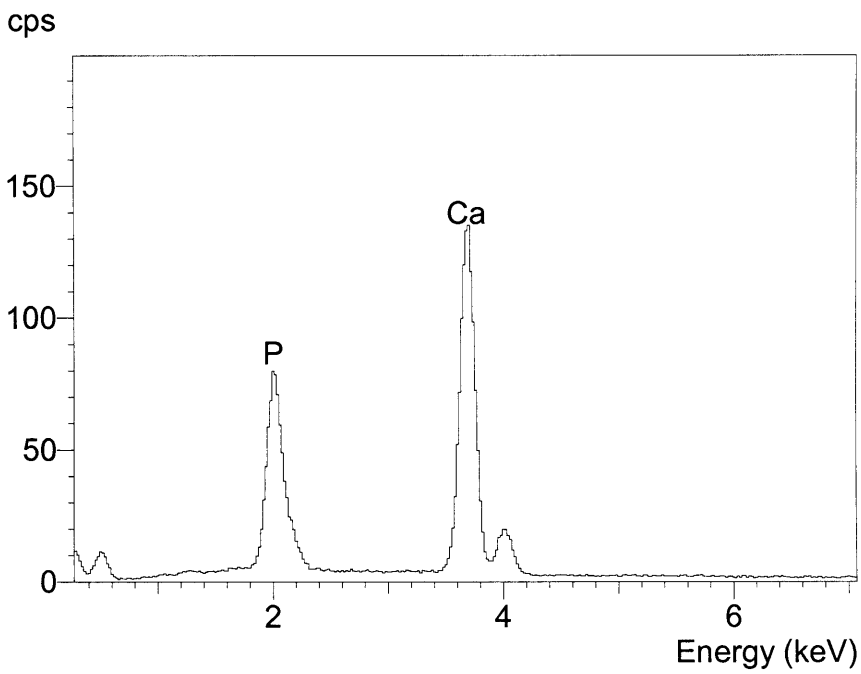

Figure 3.11 *X-ray emission spectrum for naturally mineralised turkey leg tendon showing the presence of peaks due to calcium and phosphorus.*

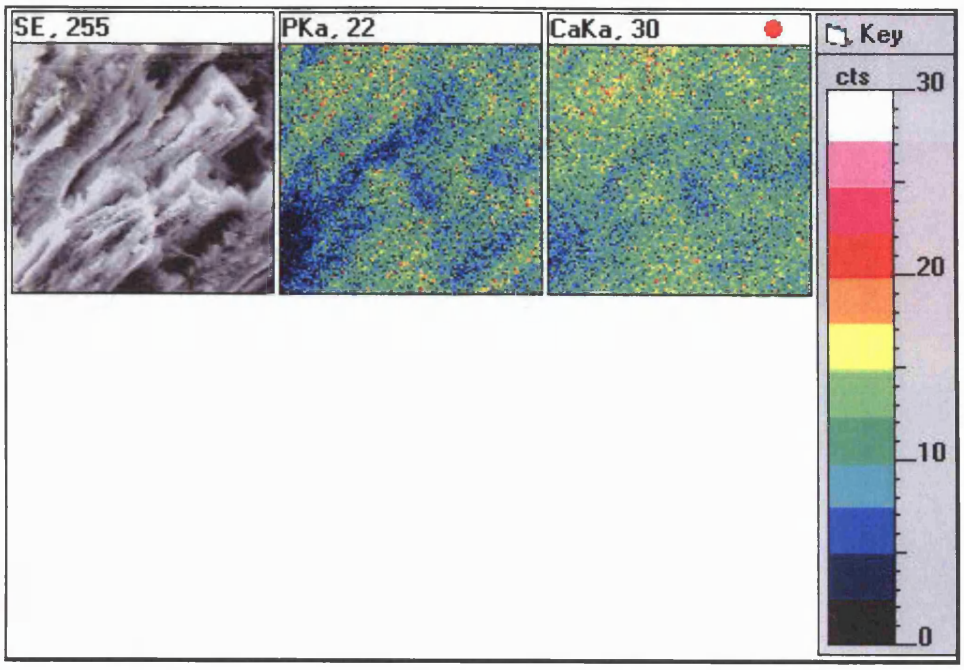

Figure 3.12 *Elemental maps for phosphorus (central image) and calcium (right hand image) from a typical sample of naturally mineralised turkey leg tendon. The left hand image is a SEM image of the area taken for mapping (x2200 magnification).*

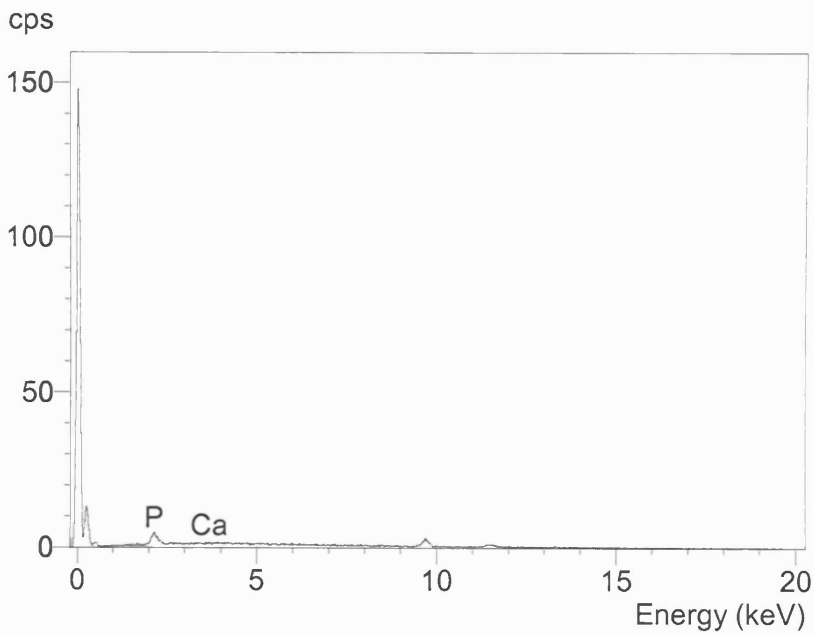

Figure 3.13 *X-ray emission spectrum of demineralised turkey leg tendon showing the absence of peaks corresponding to calcium and phosphorus indicating the successful completion of the demineralisation process.*

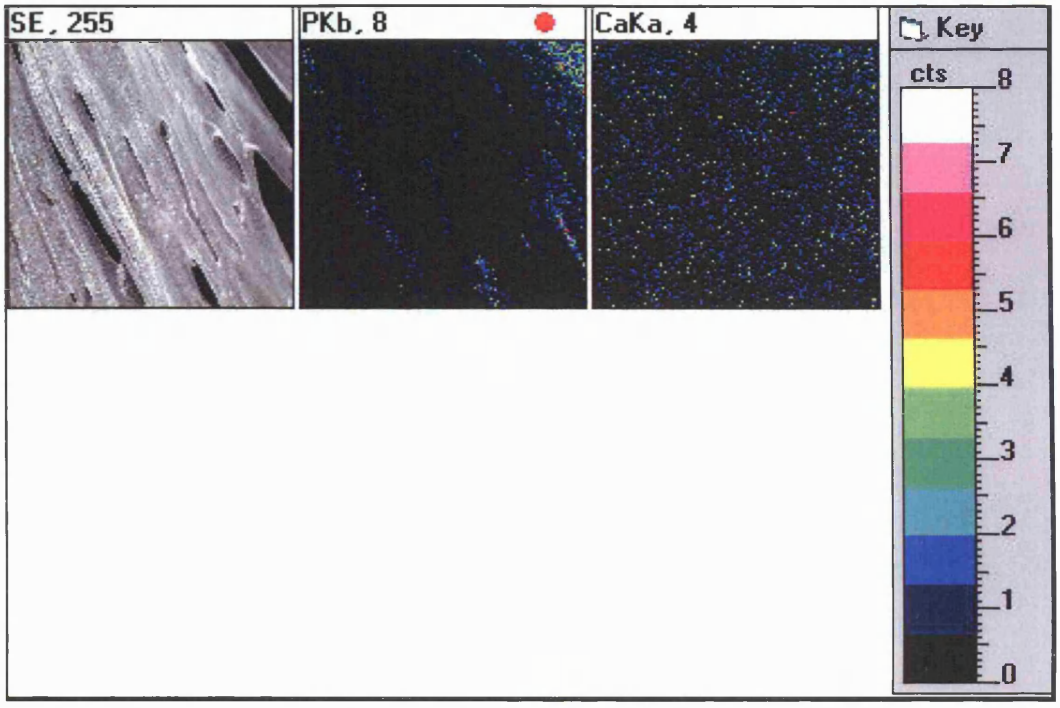

Figure 3.14 *Elemental maps for phosphorus and calcium for a sample of demineralised turkey leg tendon (x110 magnification).*

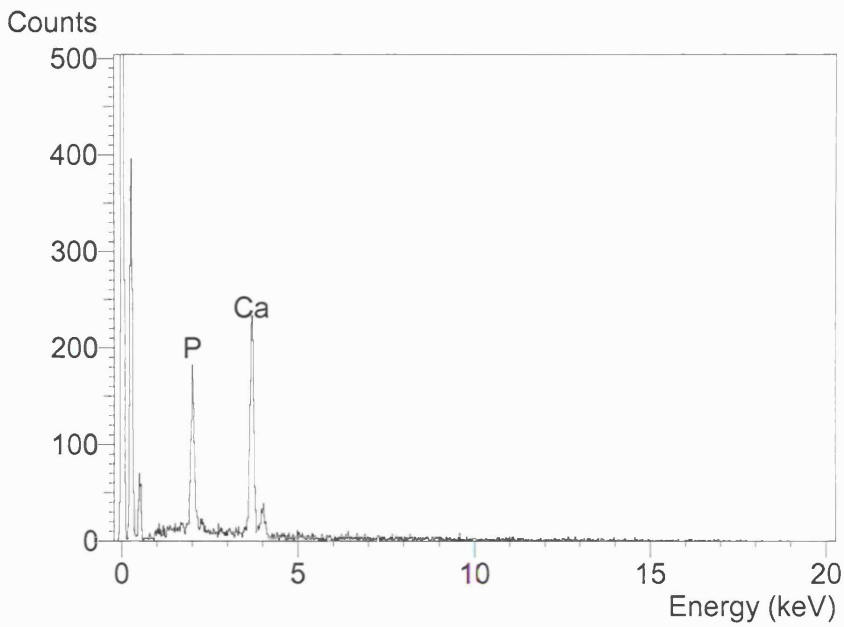

Figure 3.15 *X-ray emission spectrum of a sample of demineralised turkey leg tendon that had been remineralised by incubation in 3.31 mM[2] Saito solution for 24 days showing the presence of peaks corresponding to calcium and phosphorus indicating that mineral crystallite formation had occurred.*

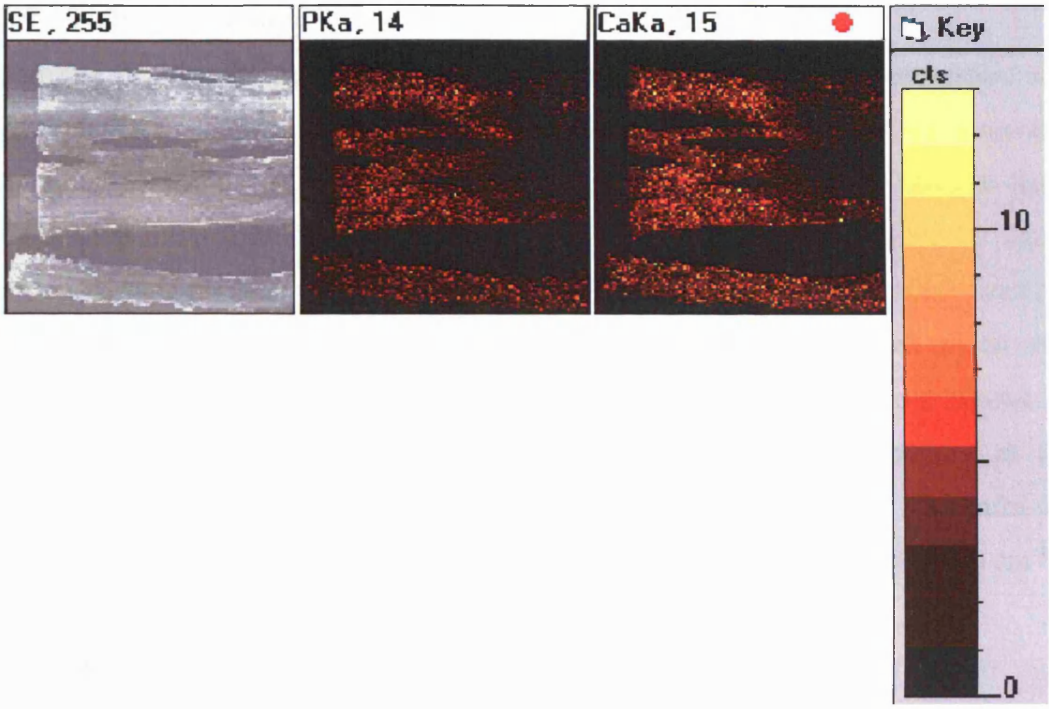

Figure 3.16 *Elemental maps of phosphorus and calcium for a sample of tendon remineralised for 24 days in 3.31 mM[2] Saito solution, showing the total coverage of the sample with mineral crystallites. (x30 magnification.)*

3.9 FT-IR spectroscopy

Samples of naturally mineralised turkey leg tendon, acid demineralised tendon, and remineralised turkey leg tendon were subjected to analysis by infra-red spectroscopy. Samples of tendon in each case were ground into a fine powder using a Spex Centriprep 6750 freezer mill, (Glen Creston Ltd, Stanmore, UK) cooled by liquid nitrogen. Samples were ground for two minutes following two minutes of pre-cooling, this giving a fine powder in each case. The powdered samples were then mixed with potassium bromide and pressed into discs which were then inserted into a Nicolet 20 PC-IR (Thermo Electron Corporation, Stone, UK.) FT-IR spectrometer at the Chemical Analytical Services Unit of the University of Newcastle. The infra-red spectrum of each sample was measured in absorbance mode between 4000-400 cm^{-1}.

3.9.1 Results

Typical results for naturally mineralised turkey leg tendon are shown below in Figure 3.17 and those for demineralised and remineralised tendon shown in Figures 3.18 and 3.19 overleaf.

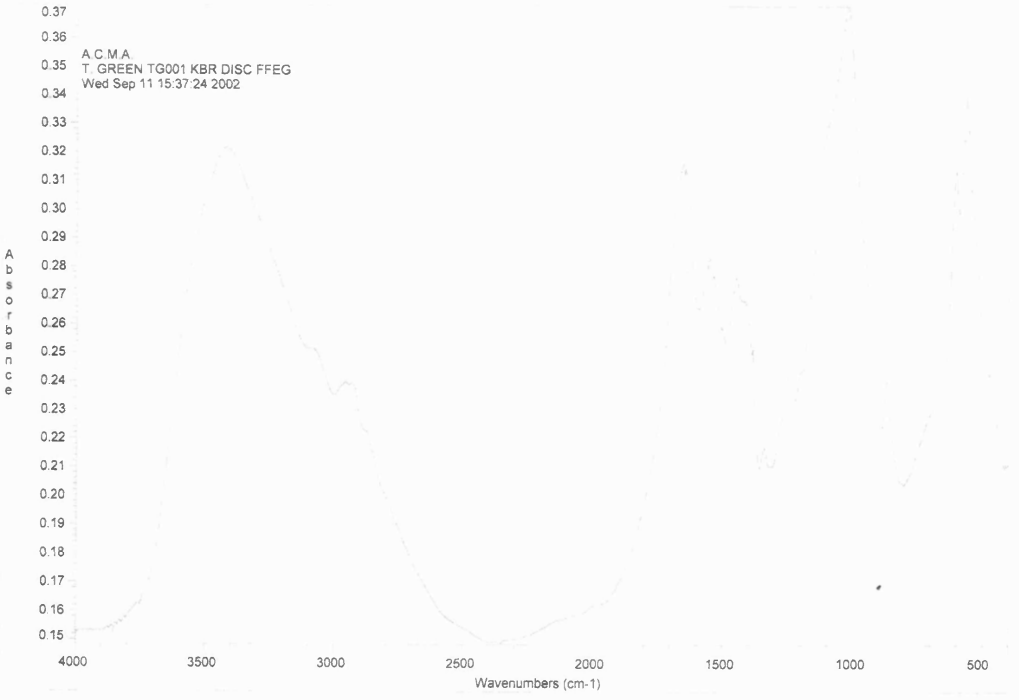

Figure 3.17 *FT-IR spectrum of naturally mineralised turkey leg tendon powder.*

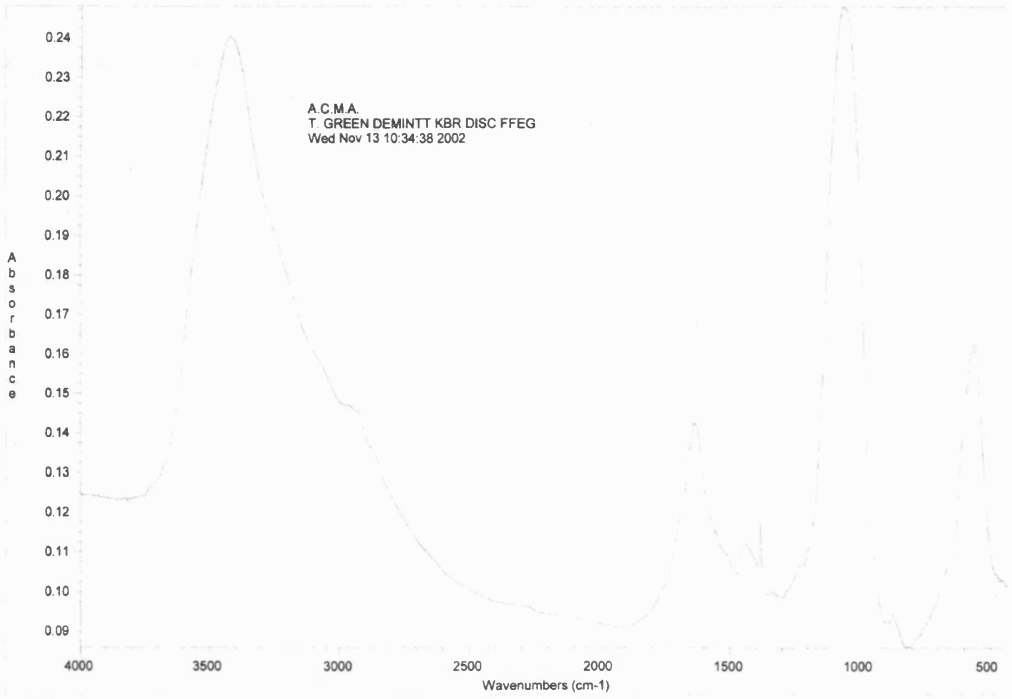

Figure 3.18 *FT-IR spectrum of acid demineralised turkey leg tendon.*

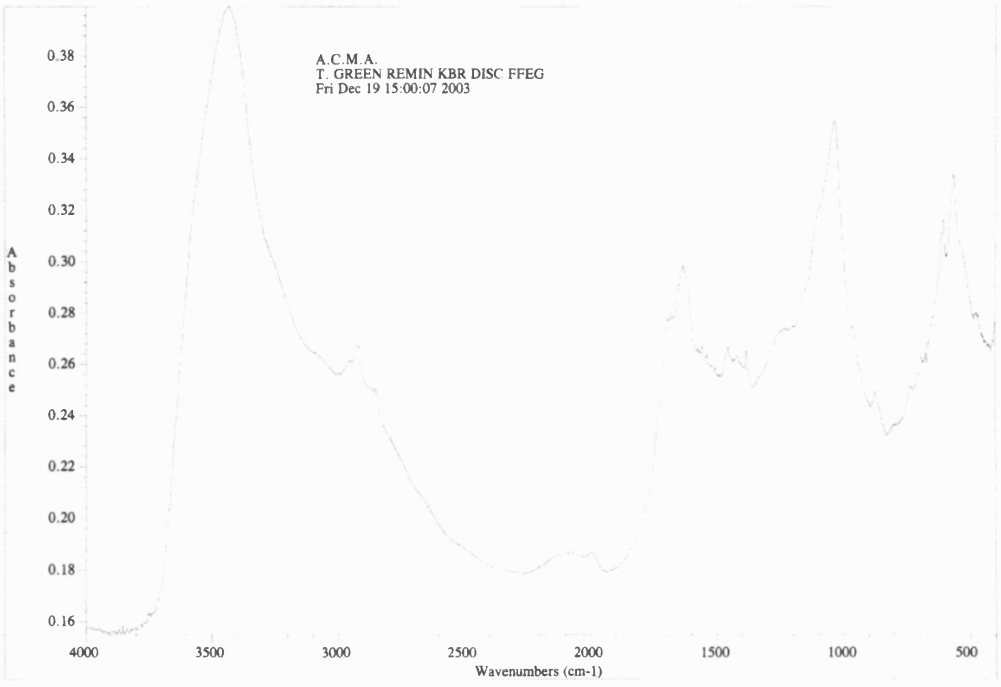

Figure 3.19 *FT-IR spectrum of demineralised turkey leg tendon that had been remineralised by incubation for 24 days in 3.31 mM^2 Saito solution.*

The FT-IR spectra of naturally mineralised turkey leg tendon were similar to those obtained by Gadaleta et al[131] for mineralised turkey leg tendon and displayed several peaks that can be attributed to the presence of the hydroxyapatite mineral phase, the most prominent being the shouldered peak of the phosphate ν_1, ν_3 region between 900-1200 cm^{-1}, and those of the phosphate ν_4 doublet at 565 cm^{-1} and 603 cm^{-1}. Removal of the mineral phase from the tendon by acid demineralisation results in an FT-IR spectrum that is a lot simpler in appearance, with the spectrum in the regions corresponding to phosphate group vibrations being markedly altered. FT-IR spectra of samples of *in-vitro* remineralised tendon were very similar to those of the naturally mineralised samples, suggesting that the two were very similar chemically.

3.9.2 Determination of splitting factor

From the obtained FT-IR spectra an indication of the crystal perfection of the hydroxyapatite within the sample can be gained by determining the value for the extent of the splitting of the two absorptions of the phosphate ν_4 doublet at 565 cm^{-1} and 603 cm^{-1}, this splitting factor is calculated from the formula of Termine and Posner[132];

$$SF = \frac{a+b}{c} \qquad (15)$$

Where:

a is the height of the peak at 603 cm^{-1}

b is the height of the peak at 565 cm^{-1}

c is the height of the trough between them.

This is represented diagrammatically in Figure 3.20 overleaf.

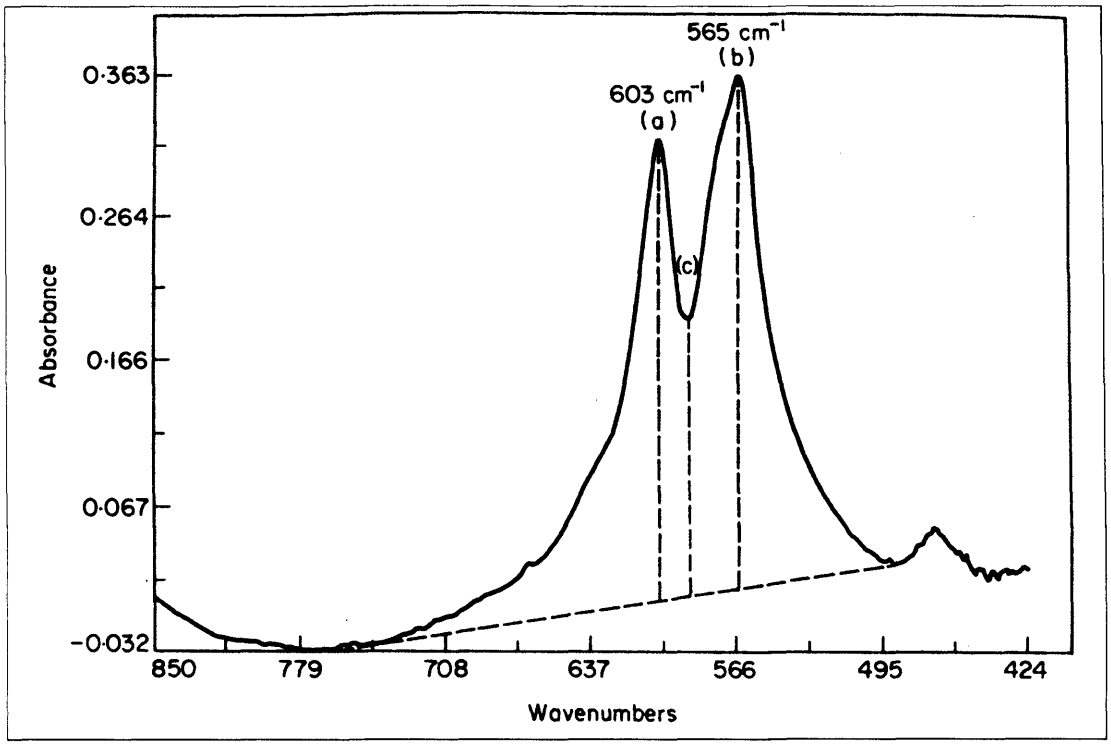

Figure 3.20 *Diagram to show how the splitting factor for calcified tissue is calculated from the phosphate v_4 doublet at 565 cm^{-1} and 603 cm^{-1} (taken from Weiner and Bar-Joseph[133])*

The higher the value of the splitting factor, the larger or more highly ordered the crystals are[132]. A comparison between the splitting factors found for naturally mineralised turkey leg tendon, and that of the in-vitro remineralised tendon is shown in Table 3.2 below.

Table 3.2 *Comparison of splitting factors for naturally mineralised turkey leg tendon, and in-vitro remineralised turkey leg tendon.*

Source	Splitting factor
Naturally mineralised turkey leg tendon	2.566
Remineralised turkey leg tendon	2.895

3.10 X-ray diffraction

The powdered samples of both naturally mineralised, and remineralised turkey leg tendon used for FT-IR analysis were also subjected to wide angle x-ray diffraction to identify the nature of the mineral present. The powdered samples were analysed at the Chemical Analytical Services Unit at the University of Newcastle on a Phillips binary x-ray diffractometer using a beam of nickel filtered Cuk_α radiation with a wavelength of 0.154 nm. The scattered x-rays were detected between 7-70° with a step size of 0.03°. The mineral crystallites scatter the x-rays much more strongly than the collagen matrix as they are more electron dense, and so the diffraction pattern produced by the collagen is swamped by that produced by the mineral and so can't be identified in the diffractogram. The diffractogram for the naturally mineralised turkey leg tendon powder is shown in Figure 3.21 below.

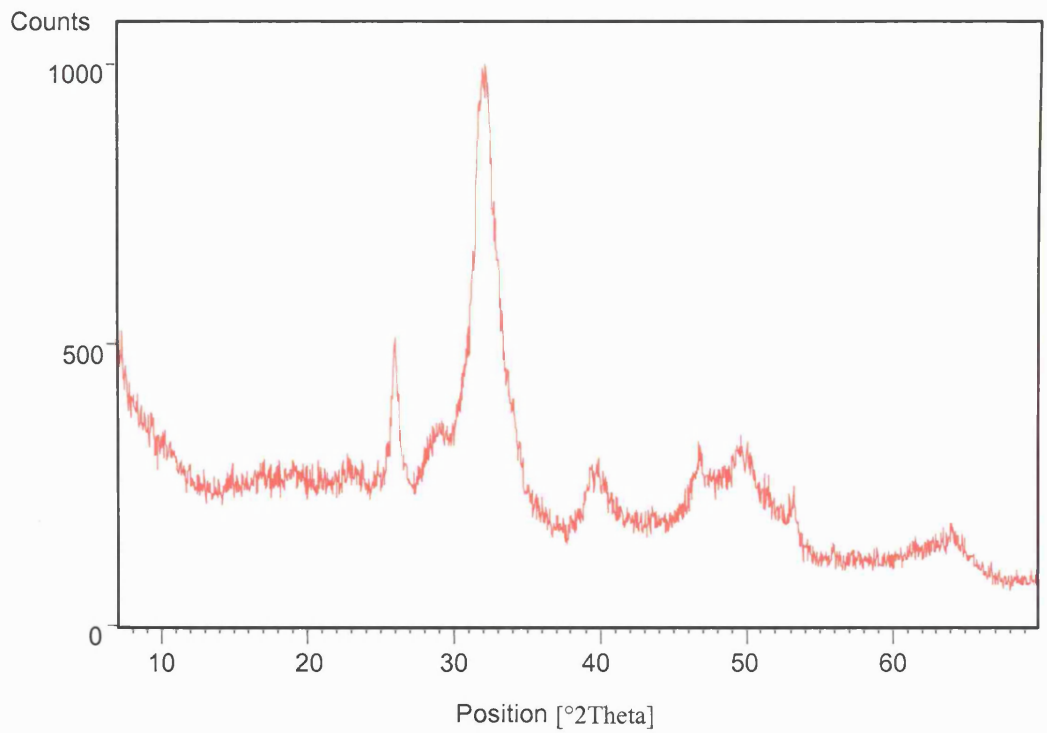

Figure 3.21 *Wide angle x-ray diffractogram of naturally mineralised turkey leg tendon powder.*

Two major peaks are prominent in the above spectrum, a large peak at about 32° corresponding to the 211 plane, and a smaller peak at 26° corresponding to the reflection of the 002 plane of hydroxyapatite[134]. Several small diffuse peaks are also present in the diffractogram that are also characteristic for hydroxyapatite mineral.

The diffractogram obtained for a sample of the *in-vitro* remineralised tendon displayed peaks in the same locations as those obtained from the naturally mineralised samples, although all the peaks were much sharper than those occurring in the naturally mineralised sample. A typical diffractogram of the *in-vitro* remineralised tendon is shown in Figure 3.22 below.

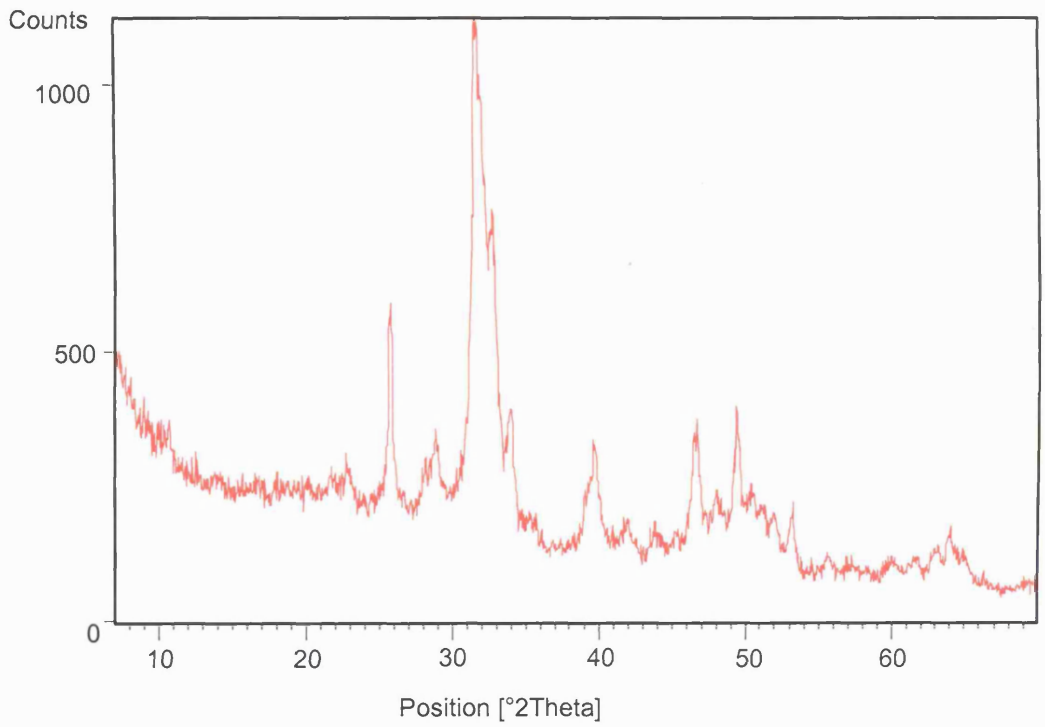

Figure 3.22 *Wide angle x-ray diffractogram of in-vitro remineralised turkey leg tendon.*

To confirm that the mineral in the remineralised samples was hydroxyapatite the positions of the peaks obtained from the diffractogram of the remineralised turkey leg tendon were compared with those of synthetic hydroxyapatite crystals (as shown in Figure 3.23 overleaf). The positions and intensities of the peaks from the remineralised tendon corresponded to those of the synthetic hydroxyapatite confirming that the mineral present was hydroxyapatite in both the naturally mineralised and the remineralised tendon samples.

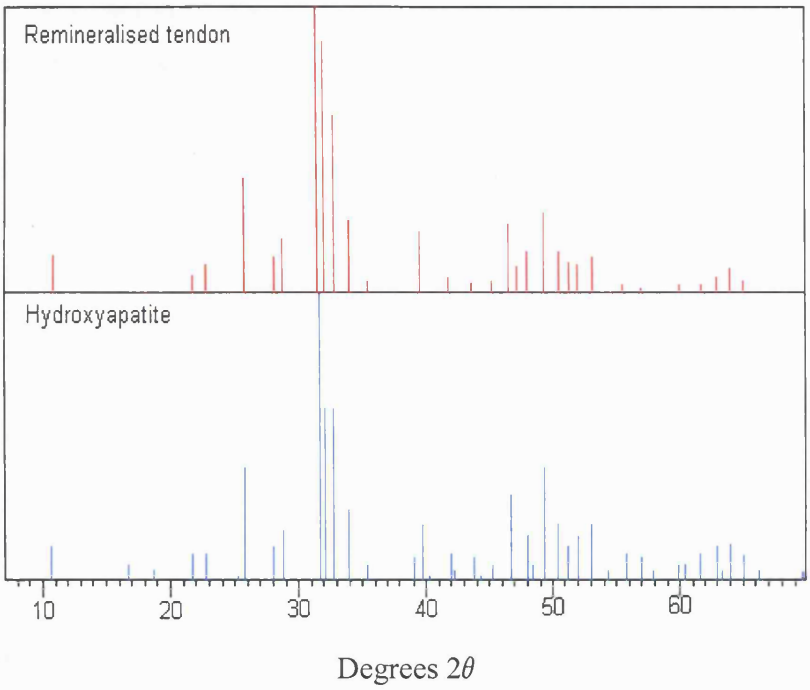

Figure 3.23 *Comparison of the diffraction peak positions from a sample of in vitro remineralised turkey leg tendon (top diagram), with those of synthetic hydroxyapatite crystals (bottom diagram).*

3.11 Small angle X-ray scattering

3.11.1 Experimental method

Samples of remineralised tendon, naturally mineralised turkey leg tendon, and demineralised turkey leg tendon were subjected to analysis by small angle x-ray scattering (SAXS) using a nanoSTAR (Bruker AXS, Karlshruhe, Germany) X-ray facility at the Biological Sciences Department of the University of Stirling. SAXS allows information on the average crystal size, shape, location, and orientation compared to the collagen fibrils to be elucidated from the intensity of the scattering data[(135)(83)(84)]. This technique has been used previously on naturally mineralised turkey leg tendon[(84)], as well as bone[(83)].

Thin slices of remineralised or demineralised tendon were placed on top of each other to create a pile of four or five slices so that a thick enough layer of sample was present to obtain a diffraction pattern. The pile of tendon slices was then clamped into the sample holding carriage, which was then positioned inside the vacuum chamber of the instrument so that the x-ray beam would strike the sample perpendicularly to the axial

direction of the collagen fibrils. In the case of native mineralised turkey leg tendon a thin piece of tendon was mounted into the frame, as this was thick enough to provide a diffraction pattern. The samples were each subjected to 9 hours exposure to the x-ray beam, which comprised of monochromated Cuk_α radiation with a wavelength of 0.154 nm, so as to produce a scattering spectrum. The detector distance was set at 1.00 m for small angle scattering and to 0.04 m for wide angle scattering. To obtain information about the crystal thickness and morphology the two-dimensional detector output was converted into spherically averaged one-dimensional profiles using the built in software of the instrument. Details of the procedures used to calculate crystal thickness and to determine the crystal shape have been presented in published literature[136].

3.11.2 Results

Wide angle x-ray scattering profiles of the remineralised tendon were obtained to verify the presence and nature of mineral within the collagen structure as the presence of hydroxyapatite crystals gives rise to rings and arcs in the scattering profile. Examples of pairs of scattering profiles for demineralised and remineralised turkey leg tendon are shown in Figure 3.24 below.

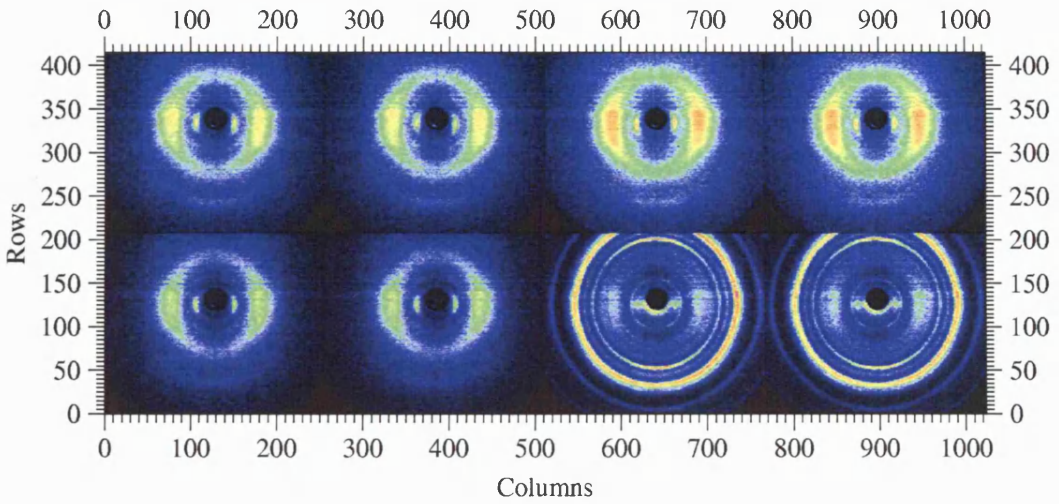

Figure 3.24 *Wide angle x-ray scattering profiles of demineralised turkey leg tendon (top left and right and bottom left pairs of images), and in-vitro remineralised turkey leg tendon (bottom right pair).*

An example of the small angle x-ray scattering profile of a sample of the remineralised tendon is shown in Figure 3.25 below.

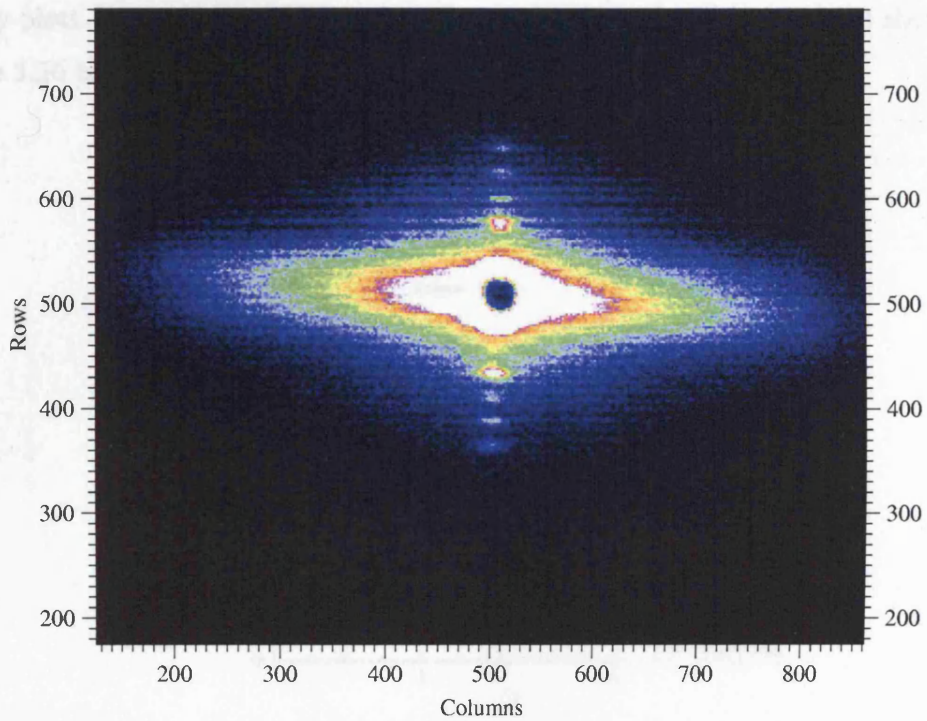

Figure 3.25 *Small angle x-ray scattering profile of in-vitro remineralised turkey leg tendon. Note the vertical line of dot-like reflections due to the 67 nm axial repeat of the collagen fibrils.*

Spherically averaging the intensity data from these small angle x-ray scattering profiles allows the determination of the mean thickness of the crystals within the collagenous matrix. Data obtained from the scattering profiles of naturally mineralised, and remineralised turkey leg tendon is shown in Table 3.3 below.

Table 3.3 *Mean crystal thickness of naturally mineralised and remineralised turkey leg tendon.*

Mineralised tissue	Mean crystal thickness (nm)
Native turkey leg tendon	2.4
Remineralised turkey tendon	7.0

Information on the shape of the crystals can also be obtained from the spherically averaged intensity data by plotting "form factor" plots, which are also known as Kratky plots and are found by integrating the spherically averaged intensity data[136]. Kratky plots for the three different crystal morphologies found in bone are shown in Figure 3.26 below.

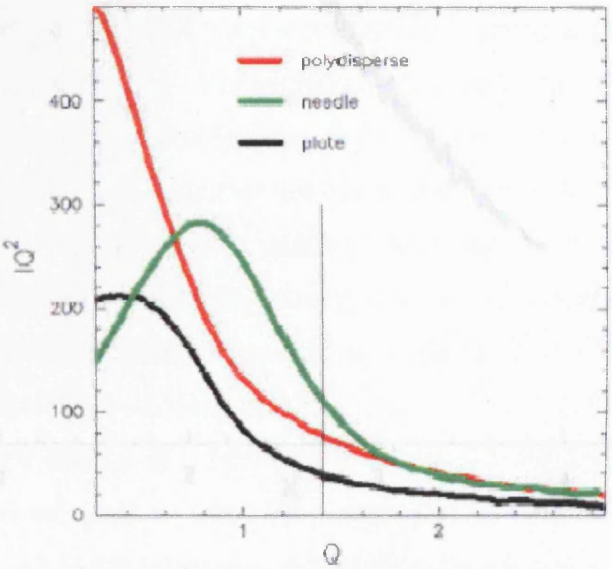

Figure 3.26 *Kratky plots of the three different crystal morphologies found in bone. (After Wess et al[137])*

Kratky plots were calculated for the samples of remineralised tendon to determine the shape of the crystals within the collagen; a typical plot is shown in Figure 3.27 overleaf.

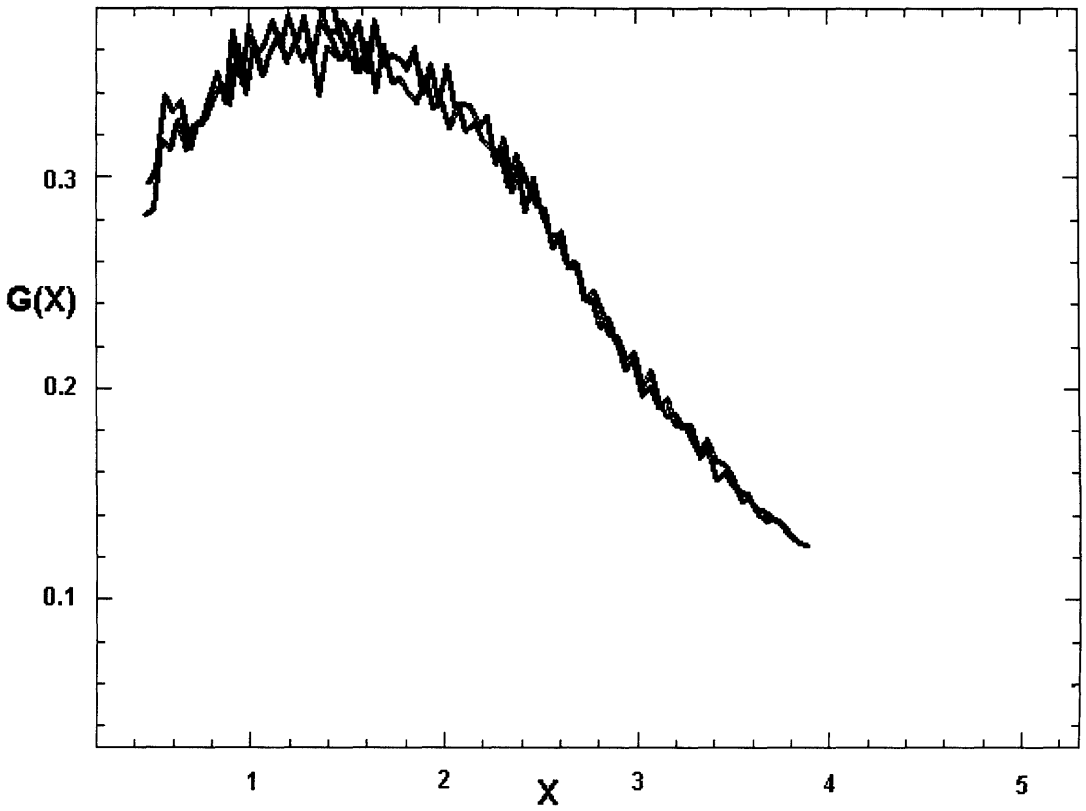

Figure 3.27 Kratky plot of a sample of in-vitro remineralised tendon.

3.12 Discussion of results

3.12.1 Demineralisation of turkey leg tendon

Demineralisation of the turkey leg tendon pieces was complete within 48 hours when 0.1 mol dm^{-3} hydrochloric acid was used. The presence of mineral was not detected by EDXA or SEM, and ICP analysis gave values for the calcium and phosphorus contents of the demineralised tendon similar to those of the controls. Partial demineralisation using citrate gave samples of tendon powder that had a translucent demineralised surface, but an opaque central area highlighting the point at which the demineralisation front had reached. The fact that the demineralisation reaction using citrate relies on diffusion to transport the citrate to the areas of the tendon in which the mineral is still present, and also that it is a powerful chelating agent and so quickly demineralises the tissue when it comes into contact with mineral, gives rise to a situation in which tissue is completely demineralised before the demineralisation front moves on. This produces a situation in which a front of demineralisation moves through the tissue, the presence of which can be seen as a boundary between the

translucent demineralised tissue and the opaque mineralised tissue. This makes it difficult to produce a partially demineralised sample of turkey leg tendon in which the remaining mineral is distributed evenly throughout the tissue, although areas of partially demineralised tendon might exist at the demineralisation front.

3.12.2 Remineralisation of demineralised turkey leg tendon

It was found that using the constant volume method for creating a metastable solution resulted in difficulty in obtaining consistently reproducible levels of mineralisation of the tendon slices. This was a consequence of the difficulties in keeping the initial supersaturation level of the solution constant due to the inevitable slight precipitation of calcium phosphate formed during mixing. Also the supersaturation level is constantly falling as the formation of hydroxyapatite mineral brings about a lowering of the levels of calcium and phosphorus in solution. As the level of supersaturation is the driving force behind the formation of mineral, continued lowering of this will eventually result in the halting of the mineral formation. Despite these failings of the constant volume method used, it was still possible to produce large quantities of mineral after periods of 24 days using the 3.31 mM^2 Saito mineralisation solution. No mineral formation was ever observed using the 1.77 mM^2 Saito mineralisation solution, suggesting that this solution had a molar product below that of the critical supersaturation required for the formation of mineral nuclei. The mineral crystallites formed were not removed by washing in deionised water, indicating that they were not loosely bound to the surface of the tendon, as would be the case if they had been formed by chemical deposition due to homogeneous nucleation of mineral from solution. If homogeneous nucleation of mineral had occurred in solution and the mineral deposits formed had then deposited onto the surface of the tendon slices, some mineral deposits would also be seen on the bottom of the vessels used in the mineralisation experiments. As no such deposits were observed, and the mineral formed on the tendon surface was not removed during extensive washing, it can be concluded that the mineral formed on the surface of the tendon slices was produced by heterogeneous nucleation on the tendon itself. The initial mineral deposits were observed by SEM to be in the form of small spheroids of individual crystallites that appeared to grow larger with time until a dense layer of crystal platelets covered the surface of the tendon. Similar spheroidal shaped clusters of crystal platelets have been

observed on the surface of the substrate in previous biomineralisation experiments using titanium metal[138], silica gel[139], and other biopolymers[109][110][111].

3.12.3 Nature of the mineral crystallites

EDXA spectra show that the mineral crystallites in both the naturally mineralised and *in-vitro* remineralised turkey leg tendon are composed of calcium and phosphorus as expected. However, this technique gives no information on whether the mineral formed *in-vitro* is hydroxyapatite, as is the case in naturally mineralised turkey tendon. The results from wide-angle x-ray diffraction studies of the native and remineralised tendon in section 3.10 show that the mineral phase present in naturally mineralised turkey leg tendon, and in tendon remineralised using 3.31 mM^2 Saito solution are identical. Comparison of the diffractogram peaks with those of synthetic hydroxyapatite identified that in both cases the mineral phase present was hydroxyapatite.

3.12.4 location of the mineral crystallites

From the results in section 3.7 of SEM imaging of the remineralised turkey tendon, it can be seen that the mineral crystallites formed during remineralisation are located on the surface of the tendon slices as a layer several crystals deep, and often as spherical clusters of crystals. The mineral crystallites in naturally mineralised turkey leg tendon are located within the hole and overlap regions of the fibrils in a repeating pattern and can be shown to be present in the hole region using small angle x-ray scattering[136]. The prominence of the different order axial scattering maxima is different between mineralised and unmineralised collagen. Unmineralised collagen displays visible maxima in its meridional scattering profile at higher orders of D than does mineralised collagen, which only displays prominent maxima for the first six orders of the meridional 67 nm D-axial spacing of the collagen fibrils[114], these maxima corresponding to highly scattering material being present at repeating intervals along the collagen molecule[140]. Small angle x-ray scattering profiles, such as that shown in Figure 3.25, from tendon samples that had been remineralised for 24 days in 3.31 mM^2 Saito solution showed scattering orders greater than D = 6 to be present. This is similar to that of the scattering profile of unmineralised tendon, indicating that the mineral present was not contained within the hole regions of the quarter staggered structure. Both the SEM results showing crystal formation on the surface of the

collagen fibrils, and the SAXS results showing the mineral to be not located in the hole region indicate that the mineral formation in the *in-vitro* remineralised collagen is different to that that occurs *in-vivo*.

3.12.5 Size and shape of the crystallites

An approximate estimate of the average size of the hydroxyapatite crystals in the sample of *in-vitro* remineralised tendon can be determined by visual measurement from the SEM images, using a ruler to measure the crystal dimensions of the magnified image and then converting these to absolute values using the scale bar of the image. Using this technique it was found that the plate-like crystallites on the surface of the *in-vitro* remineralised tendon had a long axis of between 600-1000 nm and a width of between 200-800 nm. The thickness of the crystallites however could not be determined with any accuracy using this method. Despite the uncertainties in the measurements of the crystal lengths and widths it is obvious that the crystallites are very much larger than the crystals found in naturally mineralised turkey leg tendon and bone, crystallites in these tissues have lengths of approximately 40 nm and widths of 25 nm[(90)]. The thickness of the crystallites was obtained from the SAXS data in section 2.11, and a figure of 7.0 nm was obtained, again this is much larger than the value of 2 nm stated for naturally mineralised turkey leg tendon[(83)(84)]. The shape of the crystallites for the *in-vitro* remineralised tendon could also be ascertained from the SEM images. From these it could be observed that the crystallites were in the form of elongated plates that were roughly rectangular in shape. These crystallites appeared to have an irregular face corresponding to the width of the plate, which displayed a fractured-like appearance, almost as if the plate was made up of many long needles fused together. The mineral crystallites found in naturally mineralised turkey leg tendon are too small to be visualised using SEM, however, the shape of the crystallites can be elucidated from Kratky plots obtained from SAXS data. Previous studies[(83)] have found that hydroxyapatite crystals in tendon have a plate like morphology, whereas those in bone are more needle like. Samples of remineralised tendon produced Kratky plots that appeared midway between those observed for plate-like and needle-like crystals suggesting that the crystals are in the form of elongated plates. A comparison of the FT-IR splitting factors from samples of the *in-vitro* remineralised tendon with those from naturally mineralised turkey leg tendon shows that the crystallites in the remineralised tendon are larger and/or more perfect

than those in the naturally mineralised tendon. This is further substantiated by comparing the results from the XRD analysis of the two substrates. The XRD diffractogram of the remineralised tendon shows much sharper peaks corresponding to hydroxyapatite than in the case of the naturally mineralised tendon, indicating that the crystals in the remineralised tendon are larger and/or more crystalline than those in the naturally mineralised samples, as the smaller or less perfect the crystals are, the more diffuse the diffraction patterns they give[141].

3.12.6 Orientation of the mineral crystallites

The orientation of the long axis of the crystallites with respect to the collagen long axis can be found from both wide angle and small angle x-ray scattering results, due to the uniform collagen fibril direction found in turkey leg tendon. Orientation of the long axis of the crystallites in a non-random direction causes the rings in the wide angle x-ray diffraction profile that are due to the hydroxyapatite to be observed as arcs. The position in which these arcs appear relative to the position of the tendon sample gives information on the orientation of the crystallographic long axis with respect to the direction of the fibrils[83][84]. In the case of the wide angle x-ray scattering profiles for the *in-vitro* remineralised tendon samples, shown in Figure 3.24, the scattering intensities corresponding to the hydroxyapatite mineral were present as a faint ring with stronger arcs in the horizontal axis of the diffractogram. This indicates that the mineral crystallites had a preferred orientation with respect to the long axis of the collagen fibrils. The position of the arcs along the horizontal axis indicates that the crystallites are orientated parallel to the collagen fibrils, as is the case in naturally mineralised collagen. Information on the crystal orientation can also be obtained from the small angle scattering profiles, randomly orientated crystallites giving rise to a spherical scattering profile whereas orientated crystals give rise to profiles that are in the form of a flattened ellipse[136]. The remineralised samples gave rise to flattened elliptical small angle scattering profiles, as shown in Figure 3.25, in which the ellipse was perpendicular to the fibril direction, again indicating that the crystallites were orientated with their long axis parallel to the fibril axis. The fact that the mineral crystallites show a preferred orientation with the collagen fibrils further confirms that the mineral crystallites are formed by heterogeneous nucleation, and not by the deposition of homogeneously nucleated mineral on the substrate surface, as crystallites deposited in this way would display a random orientation.

3.12.7 Comparison between naturally mineralised and remineralised tendon

A comparison of the morphological properties of the crystallites found in naturally mineralised and in the *in-vitro* remineralised turkey leg tendon is shown in Table 3.4 below.

Table 3.4 Comparison of mineral crystallites in naturally mineralised turkey leg tendon and remineralised turkey leg tendon.

	Naturally mineralised	*In-vitro mineralised*
Mineral phase	*Hydroxyapatite*	*Hydroxyapatite*
Crystal size	*40 nm x 25 nm x 2.4 nm*	*1000 nm x 600 nm x 7 nm*
Crystal shape	*Irregular rectangular plates*	*Irregular rectangular plates*
Crystal location	*Hole/overlap region*	*Fibril surface*
Crystal orientation	*Parallel to fibril*	*Parallel to fibril*

From these results it can be seen that in both cases the mineral crystallites are irregularly shaped rectangular plates of hydroxyapatite orientated with their long axis parallel to the fibril direction. The mineral crystallites in the naturally mineralised tendon are located throughout the width of the collagen fibrils and are present within the hole regions of the fibrillar structure. For this to occur and give uniformly sized crystallites across the substrate, some control of the nucleation and growth of the mineral crystallites must be in action. Such spatial and temporal control over these processes is carried out by the cellular processes of the organism, which in some way provides the materials for mineral formation at the nucleation centres prior to their requirement. This in turn allows temporally synchronised nucleation across the whole substrate. For tendon collagen remineralised *in-vitro* the nucleation centres are still present, being a function of the stereochemistry of the amino acid sequence of the substrate, and so mineral nucleation can occur. In this case however, there are now no cellular processes to control the growth of mineral at these nucleation sites, and so the crystal growth will be governed by the physico-chemical laws of crystallisation. As the mineral ions in solution come into contact with the tendon collagen substrate they form crystal nuclei at the nucleation sites on the surface of the fibrils, such nuclei then grow to form crystallites. Not only do these crystallites formed impede the diffusion of the mineral ions from solution into the collagen fibrils, but they also provide a

substrate for their continued growth and formation of new crystallites by secondary nucleation. This results in the observed covering of crystallites on the surface of the substrate and the presence of spheroidal clusters of crystallites.

Chapter 4

Chemical modification of collagen substrates

4.1 Introduction

For the mineralisation process to be useful in the preparation of *in-vitro* mineralised collagen biomaterials some way of chemically modifying non-mineralised collagen must be considered, as this collagen from these tissues can be dissolved under acid conditions and then reconstituted into gels, foams, and sponges which would offer potentially useful substrates for making mineralised biomaterials. For non-mineralising collagen to undergo mineralisation some way of providing the substrate with the ionisable acidic groups that form the nucleation sites involved in mineral nucleation must be utilised. The grafting of polyanionic phosphoproteins, such as phosvitin, to non-mineralising collagen using reagents such as divinyl sulphone[142] or a combination of 1-ethyl-3-(3-dimethylaminopropyl) carbodiimide and N-hydroxysuccinimide (EDC/NHS)[143] have been previously reported. However, these phosphoproteins are expensive. For mineralised collagen matrices to be a commercially viable material an inexpensive way of modifying the substrate is required. Two potential methods of chemical modification that are simple and inexpensive are to utilise the reaction of proteins with formaldehyde to covalently link amino group containing compounds such as phosphoserine to the collagen, and the direct silation of freeze-dried collagen. In both cases the starting material for chemical modification would be freeze-dried collagen foam obtained from the acid soluble component of rat-tail tendon collagen.

4.2 Experimental methods and materials

4.2.1 Production of acid soluble rat-tail tendon collagen

Rat-tail tendon was chosen to produce the collagen foams that would be used to evaluate the two different methods for collagen modification. The reasons for this choice were two-fold; rat tail tendon is almost totally all type I collagen[144], and it gives relatively good yields of acid soluble collagen compared to skin collagen. The tendons were removed from the tails of adult rats and washed in distilled water to remove any blood and debris. The tendons were then immersed in cold 0.5 mol dm^{-3} acetic acid to dissolve the acid soluble collagen component of the tendons. The tendons were left in the acid overnight and the resulting solution was then filtered through mineral wool to remove any insoluble material. The acetic acid solution of collagen was then stored at -20°C until required.

4.3 Formation of collagen gels and foams.

The frozen acid soluble collagen solution was defrosted and the pH was raised to 7.4 by the slow addition with stirring of 1.0 mol dm^{-3} sodium hydroxide solution, using a pH meter. The solution was then carefully poured into plastic petri dishes to a depth of approximately 8 mm and placed in an oven at 37°C and left for 24 hours for fibrilogenesis to occur. The collagen gels formed were then freeze-dried to form a collagen foam. The freeze-dried foams contained a large amount of sodium acetate carried over from the neutralisation step and so the collagen foams were each washed in a large excess of distilled water three times and then freeze-dried again.

4.4 Collagen modification

4.4.1 Grafting of amino group containing compounds using formaldehyde

4.4.1.1 Introduction

The reaction between protein and formaldehyde is used commercially in the tanning of hides and skins, and also as a method of grafting amino acids such as glycine to collagen in leather making to improve the uptake of chromium sulphate tanning salts[145]. The reaction involves the formation of an N-methylol group by the formaldehyde with the ϵ-amino group of lysine residues within the collagen. These N-methylol groups can then react via a condensation reaction with amide groups from either asparagine and glutamine residues, or guanidine groups from arginine residues,

to form a stable methylene bridge crosslink[146]. The formation of the N-methylol group and the condensation reaction are both slower at acidic pH than neutral or slightly alkaline values. The grafting experiment differed slightly from this as the compounds chosen as potential nucleation sites contained the amino group for formation of an N-methylol group, which could then react with the amide or guanidinyl groups of the collagen as outlined in Figure 4.1 below.

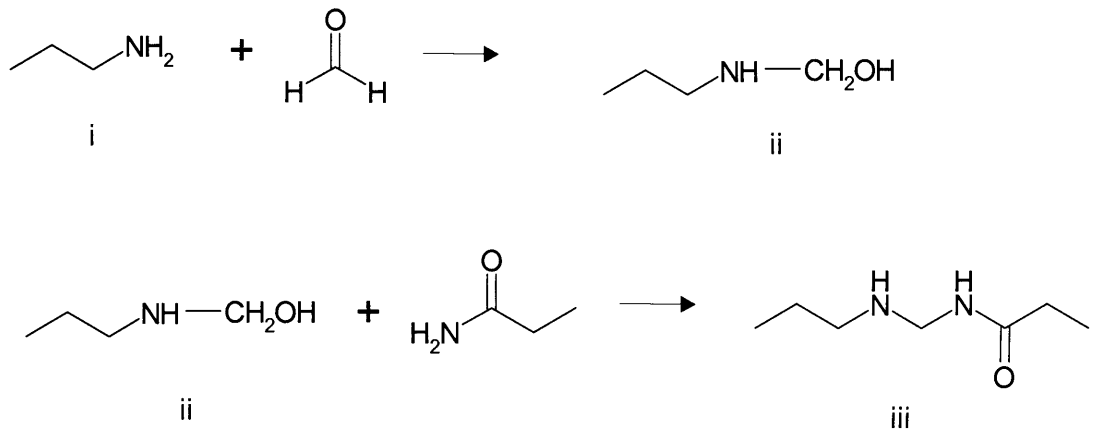

Figure 4.1 *Diagram to show the reaction of the amino group of a compound (i) with formaldehyde to form an N-methylol compound (ii) and then the condensation of this with an adjacent side chain amide group to form a methylene bridge crosslink (iii).*

4.4.1.2 Experimental method

About 30 mg of the freeze-dried collagen foam was taken and placed inside a screw capped glass tube, along with enough 0.1% formaldehyde solution to give a 2% offer of formaldehyde on the mass of collagen in the tube. The compounds used for grafting were phosphoethanolamine, which contains a covalently bound phosphate group, taurine, which contains a covalently bound sulphonate group, and the amino acid γ-carboxyglutamic acid, which is found in some mineral associated bone proteins thought to be involved in the nucleation of mineral[147]. A sufficient quantity of the compound to be grafted was then added to the tube as a 0.1% aqueous solution so as to give a 0.3:1 ratio with the formaldehyde present. Finally 7 ml of deionised water was added to each tube and the solution pH measured by pH meter. The initial pH for each of the grafting experiments are shown below in Table 4.1. The tubes containing

the grafting solutions were then incubated at 30°C overnight in order to allow the reagents to permeate into the collagen samples.

Table 4.1 *Initial solution pH for each formaldehyde grafting experiment.*

Grafted compound	Initial pH
Phosphoethanolamine	3.78
Taurine	3.81
γ-CGA	3.26

The contents of each tube were then poured into a 25 ml beaker and the pH slowly increased to pH 8.0 by the addition of 0.1 mol dm^{-3} sodium bicarbonate solution. The contents of each beaker were then returned to the original tubes and heated at 40°C for 6 hours for the reactions to occur. The modified collagens were then washed with several changes of deionised water and freeze-dried. Mineralisation experiments were then carried out on the modified collagens using the same method as for demineralised tendon in section 3.5. After 28 days in the mineralisation solution the collagen was removed and washed well with deionised water and freeze-dried. Samples were taken for analysis by SEM and EDXA as in sections 3.7 and 3.8 to determine the presence, if any, of mineral formation.

4.4.2 Silation of collagen

4.4.2.1 Introduction

It is well known that the silanol group –(Si-OH) can act as a nucleation site for hydroxyapatite mineral formation[148]. Mucalo et al[149] found that by silating cotton fibres using tetraethyl orthosilane (TEOS) and then incubating these silated fibres in 1.5 times concentration simulated body fluid gave rise to the formation of hydroxyapatite clusters on the modified cotton substrate. Silation by TEOS followed by immersion in metastable calcium phosphate solution to initiate hydroxyapatite formation has also been carried out successfully on silicone substrates[150]. Due to the simple nature of the process silation could offer a convenient method of producing modified collagen substrates for mineralisation. The silation method used a temperature of 125°C for the silation reaction, this is above the denaturation temperature for fully hydrated collagen but is still achievable if the collagen used has been freeze-dried and thus has a denaturation temperature higher than the 125°C

required in the silation step. The collagen also needs to be dehydrated, as the TEOS will react with any free water present in the substrate.

4.4.2.2 Experimental method

20 mg of freeze-dried rat tail tendon collagen foam was placed inside an oven dried screw capped glass digestion tube along with 10 ml of tetraethyl orthosilane, the tube was then heated in an oil bath at 125°C for 2 hours with occasional shaking. The pieces of freeze-dried collagen foam were then removed from the tube and washed twice in 100% ethanol that had been dried with anhydrous sodium sulphate. The TEOS treated collagen slices were then freeze-dried and stored in a dessicator. A sample of the treated collagen, along with an untreated control piece, was taken for EDXA to determine whether silanol groups were present and if they were intimately associated with the collagen fibres.

4.5 Experimental results

4.5.1 Formaldehyde grafting experiments

A typical EDXA x-ray emission spectrum of one of the modified collagens is shown below in Figure 4.2, it can be seen that there is an absence of the peaks corresponding to the presence of calcium and phosphorus, indicating that mineralisation has not occurred. This was the case for all three of the compounds investigated.

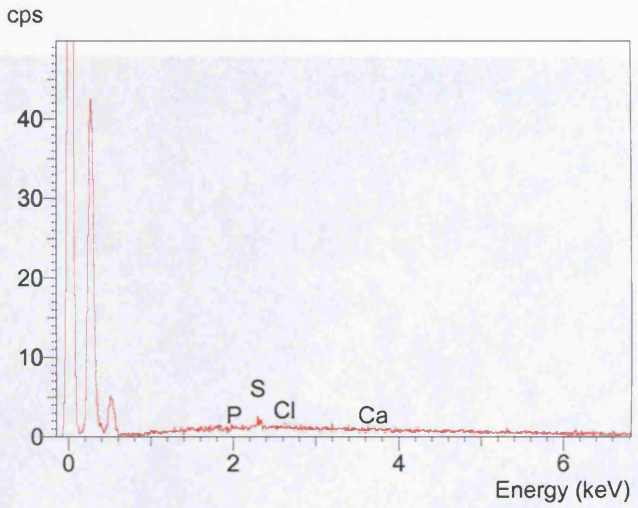

Figure 4.2 *EDXA x-ray emission spectrum of phosphoethanolamine grafted collagen foam after incubation in mineralisation solution for 28 days.*

The EDXA elemental maps confirmed the absence of mineral as no significant amounts of calcium or phosphorus could be observed within the substrate. A typical elemental map for the modified collagen foam is shown in Figure 4.3 below.

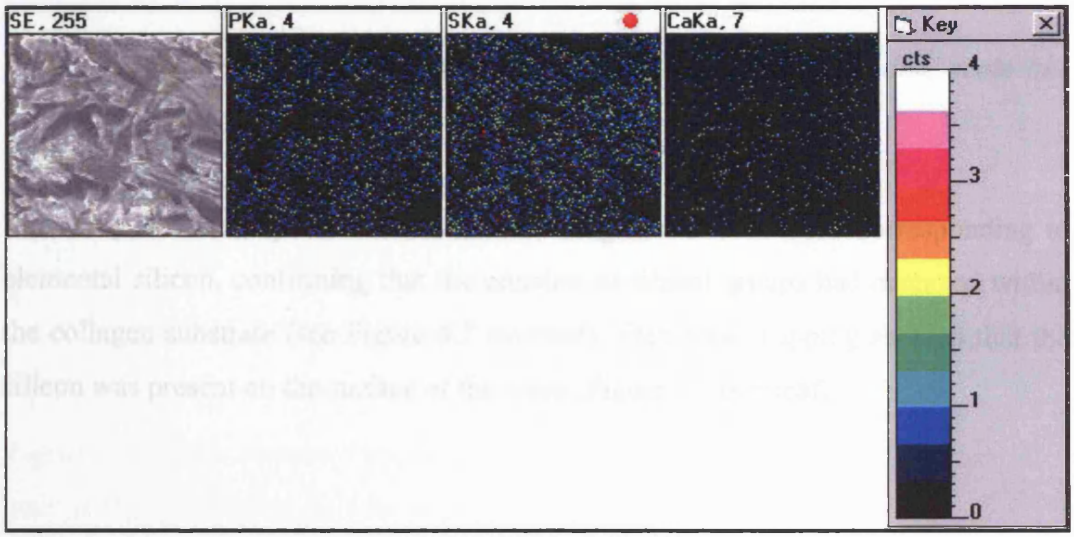

Figure 4.3 *EDXA elemental maps for phosphorus, sulphur and calcium for phosphoethanolamine modified collagen foam.*

4.5.2 Silation of collagen

The silated collagen substrates were imaged by SEM as in section 3.7, and analysed using EDXA for silicon as in section 3.8 to ascertain whether or not the silation step had been successful. No change in the structure of the collagen foam after the silation step was observed by SEM. A typical image of the silated collagen foam is shown below in Figure 4.4.

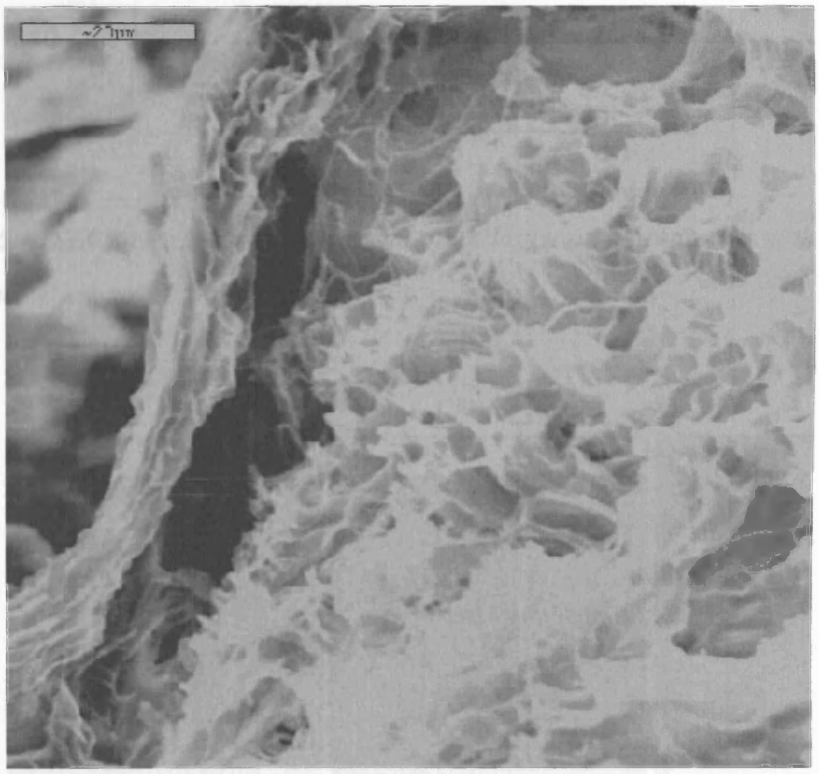

Figure 4.4 *SEM image of TEOS treated collagen (x1200 magnification, scale bar =20 μm)*

The x-ray emission spectra of the silated collagen showed a peak corresponding to elemental silicon, confirming that the creation of silanol groups had occurred within the collagen substrate (see Figure 4.5 overleaf). Elemental mapping showed that the silicon was present on the surface of the foam (Figure 4.6 overleaf).

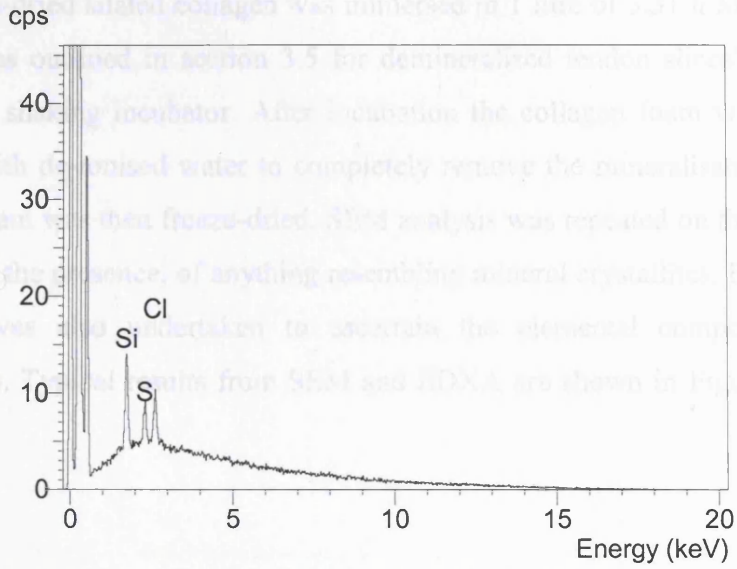

Figure 4.5 *EDXA x-ray emission spectrum of collagen after treatment with tetraethyl orthosilane.*

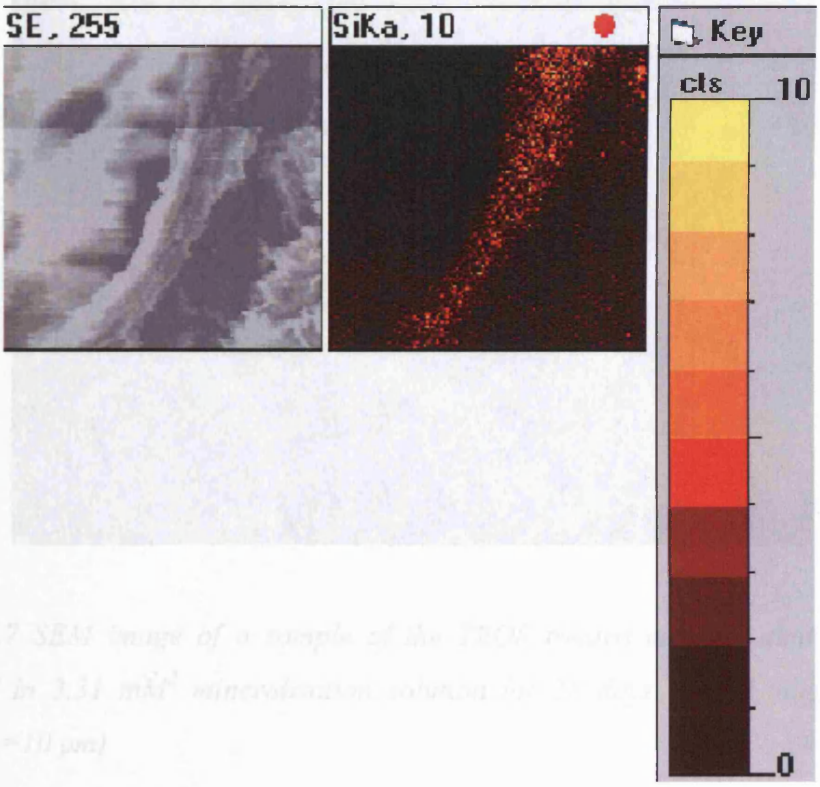

Figure 4.6 *EDXA elemental mapping of silicon for a section of tetraethyl orthosilane treated collagen silicon. (x2000 magnification)*

The freeze-dried silated collagen was immersed in 1 litre of 3.31 mM^2 mineralisation solution (as outlined in section 3.5 for demineralised tendon slices) for 28 days at 37°C in a shaking incubator. After incubation the collagen foam was removed and washed with de-ionised water to completely remove the mineralisation solution, the washed foam was then freeze-dried. SEM analysis was repeated on the collagen foam to identify the presence, of anything resembling mineral crystallites. EDXA elemental analysis was also undertaken to ascertain the elemental composition of these crystallites. Typical results from SEM and EDXA are shown in Figures 4.7, 4.8 and 4.9.

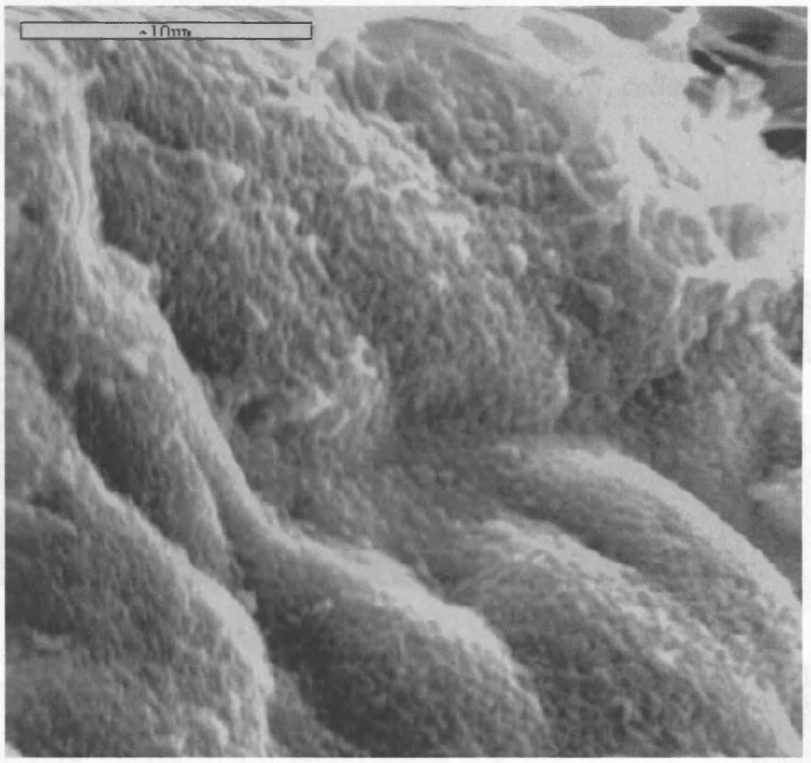

Figure 4.7 *SEM image of a sample of the TEOS treated collagen that had been immersed in 3.31 mM^2 mineralisation solution for 28 days (x4000 magnification, scale bar =10 μm)*

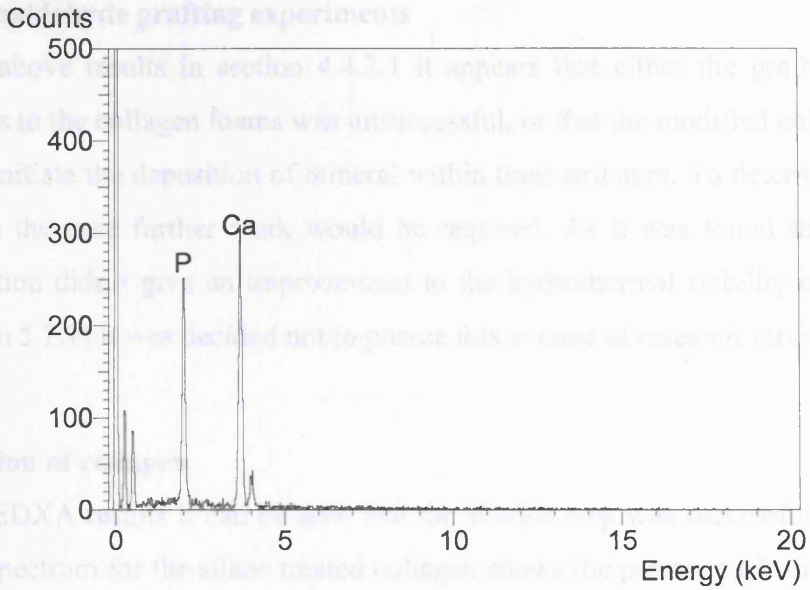

Figure 4.8 *EDXA x-ray emission spectrum for TEOS collagen that had been immersed in 3.31 mM^2 mineralisation solution for 28 days.*

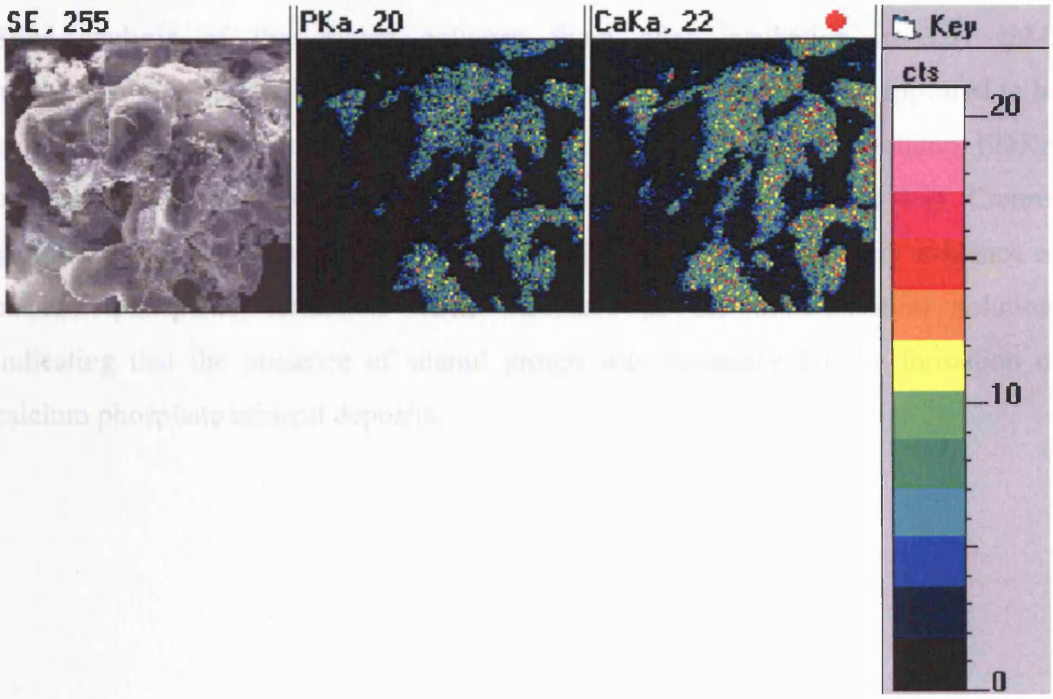

Figure 4.9 *EDXA elemental map for calcium and phosphorus of silated collagen foam that had been incubated for 28 days in 3.31 mM^2 mineralisation solution.*

4.6 Discussion of results

4.6.1 Formaldehyde grafting experiments

From the above results in section 4.4.3.1 it appears that either the grafting of the compounds to the collagen foams was unsuccessful, or that the modified collagens are unable to initiate the deposition of mineral within their structure. To determine which of these is the case further work would be required. As it was found that *in-vitro* mineralisation didn't give an improvement to the hydrothermal stability of collagen (see section 5.2.1) it was decided not to pursue this avenue of research further.

4.6.2 Silation of collagen

From the EDXA results it can be seen that the silation step was successful, the x-ray emission spectrum for the silane treated collagen shows the presence of silicon within the structure and the elemental map confirms that this is associated with the surface of the fibrils within the collagen foam. The silation reaction caused no visible changes to the structure of the collagen foam when viewed by SEM, the silated collagen being indistinguishable from the untreated collagen foam.

SEM analysis of the silated collagen foam after incubation in 3.31 mM^2 mineralisation solution for 28 days highlighted the appearance of what appeared to be mineral spherulites (Figure 3.7), similar to those seen in remineralised tendon. EDXA confirmed these deposits as calcium phosphate (see Figures 4.8 and 4.9). Control samples of collagen foam that had not been silated failed to show any evidence of calcium phosphate formation when incubated in the mineralisation solution, indicating that the presence of silanol groups was necessary for the formation of calcium phosphate mineral deposits.

Chapter 5

Hydrothermal stability studies of mineralised, demineralised, and remineralised collagen

5.1 Introduction

The thermal denaturation of collagen is important in the field of leather making, as the raising of the denaturation temperature by tanning agents allows the post-tanning processes, such as dyeing, to be carried out at higher temperatures. Collagen denaturation is also the intended effect in many surgical procedures such as treatment of joint laxity[151], as well as tissue welding and interstitial thermotherapy of cancer[152]. It is obvious then that a detailed understanding of the changes occurring within the hierarchical collagen structure upon denaturation is required for the optimisation of these areas of interest.

Many techniques have been used to investigate the denaturation of collagen triple helices in solution, such as circular dichroism[153], changes in intrinsic viscosity[154][155], optical rotation[156], dilatometry[57], measurement of sedimentation coefficient[154] and differential scanning calorimetry[156]. However the only one of these that can be used on fibrillar collagen is differential scanning calorimetry[157][158][159], although hydrothermal isometric tension has also been used to investigate the denaturation of fibrillar collagen[160].

Differential scanning calorimetry makes use of the fact that for a thermodynamic transition to occur energy must be either supplied to, or removed from the system under investigation. The DSC method involves the heating of two pans inside a calorimeter, one pan contains the sample under investigation, and the other is an empty pan used as a reference. Energy is supplied to raise the temperature of the pans at a constant rate. If a thermal transition occurs energy is given out, or absorbed by the sample and so a temperature difference occurs between the sample pan and the reference pan. Energy then has to be supplied to one of the pans in order for the temperature of the pans to be made equivalent once again, with this supplied energy being plotted as a peak in the thermal scan.

5.2 Investigation into the position of the denaturation endotherm for mineralised and demineralised turkey leg tendon.

5.2.1 Preliminary DSC studies

The position of the denaturation endotherm for naturally mineralised turkey leg tendon, acid demineralised turkey leg tendon, partially citrate demineralised turkey leg tendon, and *in-vitro* remineralised turkey leg tendon, all prepared as outlined in Chapter 2 were investigated using DSC. Samples of the material for testing were

soaked in pH 7.0 phosphate buffer for 24 hours, 10-20 mg samples of tendon were blotted dry and sealed into stainless steel DSC pans. The pans were heated from 25-195°C at 5°C min^{-1} in a DSC822e differential scanning calorimeter (Mettler Toledo, Leicester, UK.) fitted with a nitrogen gas intracooler, using a sealed empty pan as a reference. Prior to the experiments the DSC had been calibrated using both zinc (T_m = 419.6°C, ΔH_f = 3.2 J g^{-1}) and indium (T_m = 156.6°C, ΔH_f = 0.6 J g^{-1}) standards. The position of the peak maximum and onset temperature for each endotherm and also the area under the endothermic peaks, which corresponds to the enthalpy of the event, were calculated from the thermal scans using a spline type baseline using the STAR^e version 6.20 software (Mettler Toledo, Leicester, UK).

A typical thermal scan for naturally mineralised turkey leg tendon is shown below in Figure 5.1. The thermal scan displays a single broad endotherm with a peak maximum (T_{max}) at 148.9°C similar in shape and value of T_{max} previously reported for naturally mineralised turkey leg tendon and bone[108].

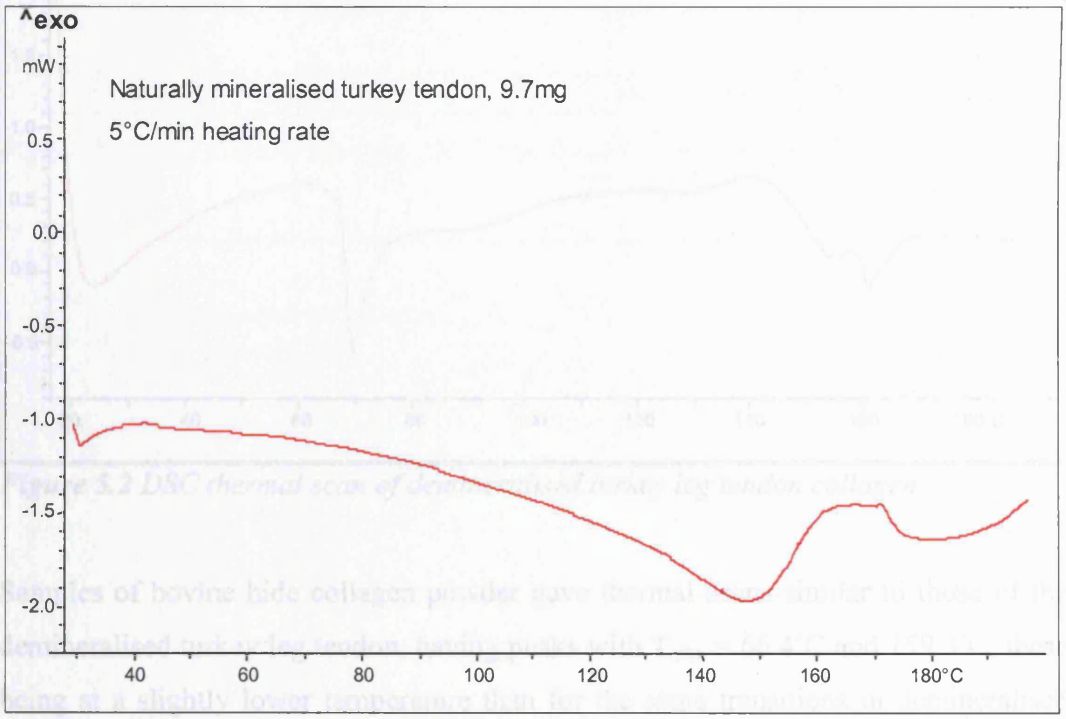

***Fig 5.1** DSC thermal scan of naturally mineralised turkey leg tendon collagen*

For acid demineralised turkey leg tendon a fairly sharp endotherm was observed with a T_{max} value of 69.3°C, as well as a second endotherm with a T_{max} of 161.1°C. It was thought that this second endotherm was due to some of the mineral phase still being present within the collagen structure, indicating that incomplete demineralisation of

the tendon had occurred. However chemical analysis and EDXA showed that no mineral remained within the collagen structure, suggesting that the second endotherm was in fact due to a thermal event in collagen hitherto unobserved. To confirm that the second endotherm was not associated with the mineralisation of the collagen, thermal scans were obtained of fully hydrated bovine hide powder collagen and these too showed the presence of a second endotherm. A typical thermal scan for demineralised turkey leg tendon is shown below in Figure 5.2 and that for bovine hide powder is shown in Figure 5.3 overleaf.

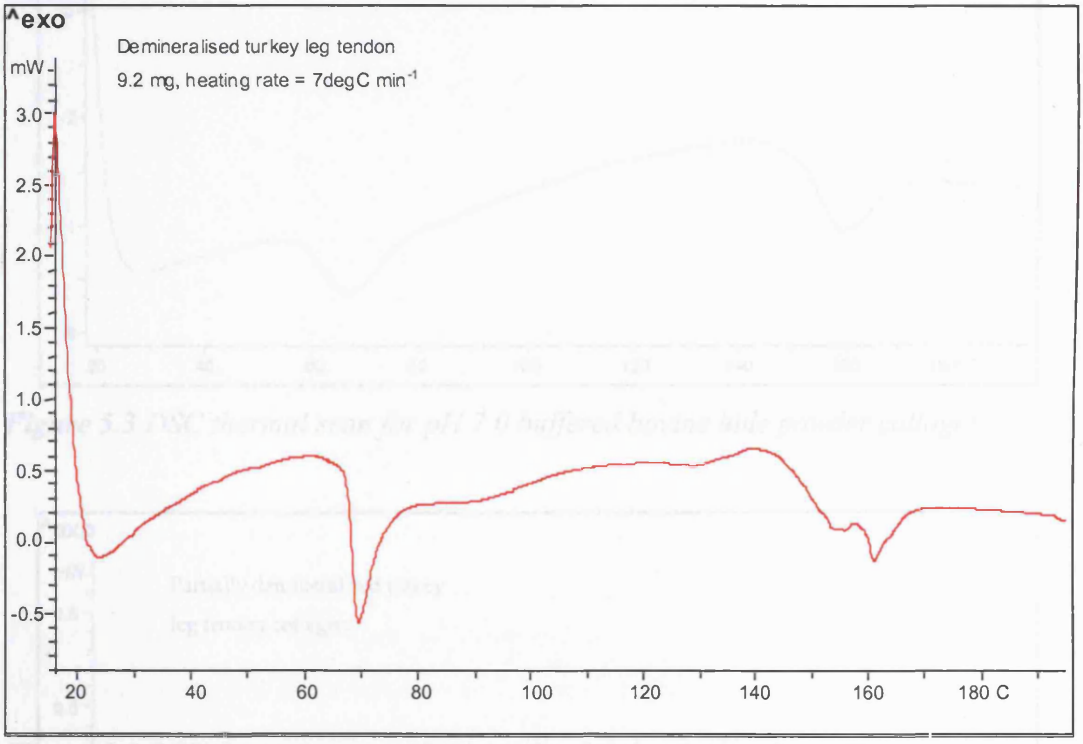

Figure 5.2 *DSC thermal scan of demineralised turkey leg tendon collagen.*

Samples of bovine hide collagen powder gave thermal scans similar to those of the demineralised turkey leg tendon, having peaks with T_{max} = 66.4°C and 159.3°C, these being at a slightly lower temperature than for the same transitions in demineralised turkey leg tendon.

For the samples of naturally mineralised turkey leg tendon that had been partially demineralised with citrate, a thermal scan similar to that seen for acid demineralised tendon was also observed, having an endothermic peak with the T_{max} value of 65.4°C due to the demineralised portion of the sample, and a broad endotherm between 130-170°C due to the collagen that had not been demineralised. No sign of an endotherm

at 113°C corresponding to that reported for partially citrate demineralised bone by Kronick and Cooke[108] was observed. A typical thermal scan for the partially demineralised tendon is shown in Figure 5.4 below.

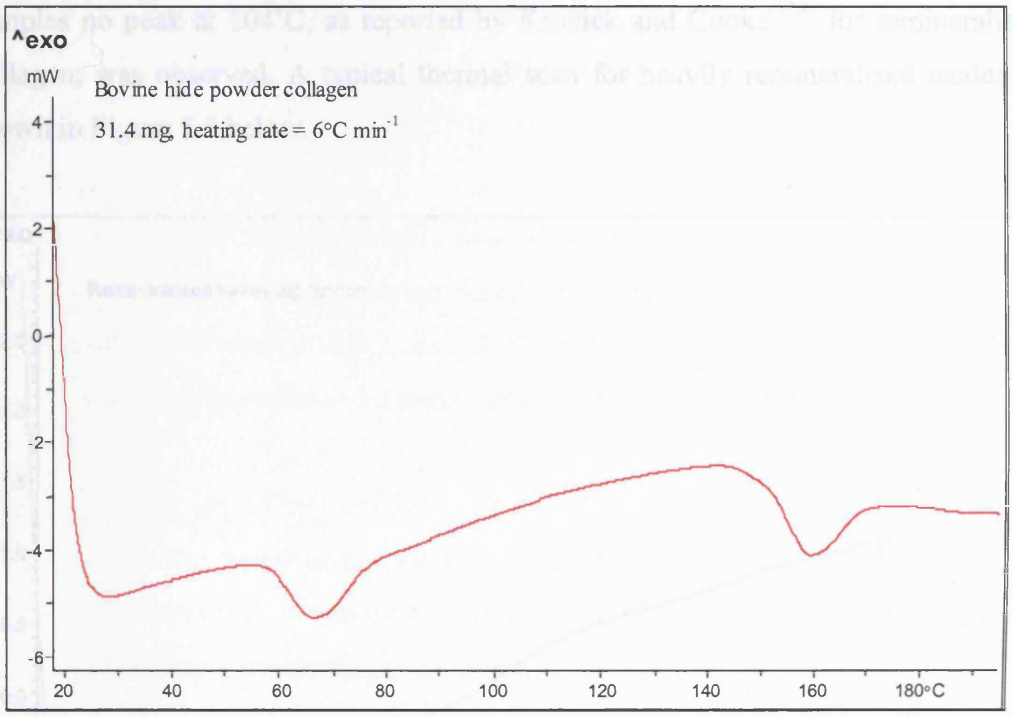

Figure 5.3 DSC thermal scan for pH 7.0 buffered bovine hide powder collagen.

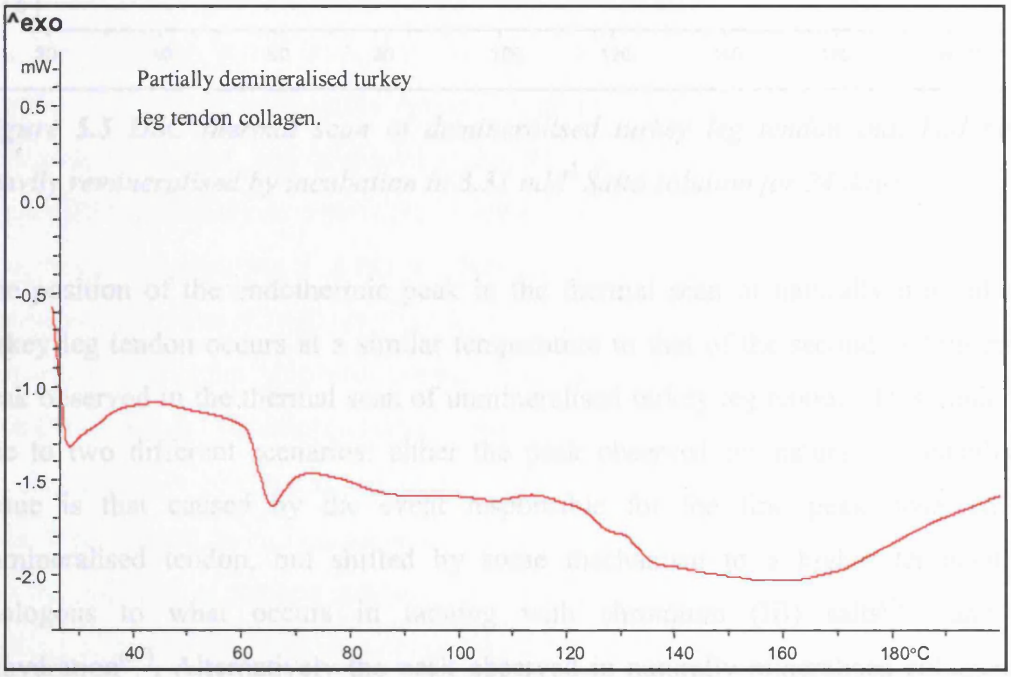

Figure 5.4 DSC thermal scan of turkey leg tendon partially demineralised with sodium citrate.

The thermal scan for samples of heavily remineralised turkey leg tendon again was similar to that of the acid demineralised tendon displaying two endothermic peaks with values of T_{max} of 69.4°C and 172.0°C. Again as with the partially demineralised samples no peak at 104°C, as reported by Kronick and Cooke[108] for remineralised collagen, was observed. A typical thermal scan for heavily remineralised tendon is shown in Figure 5.5 below.

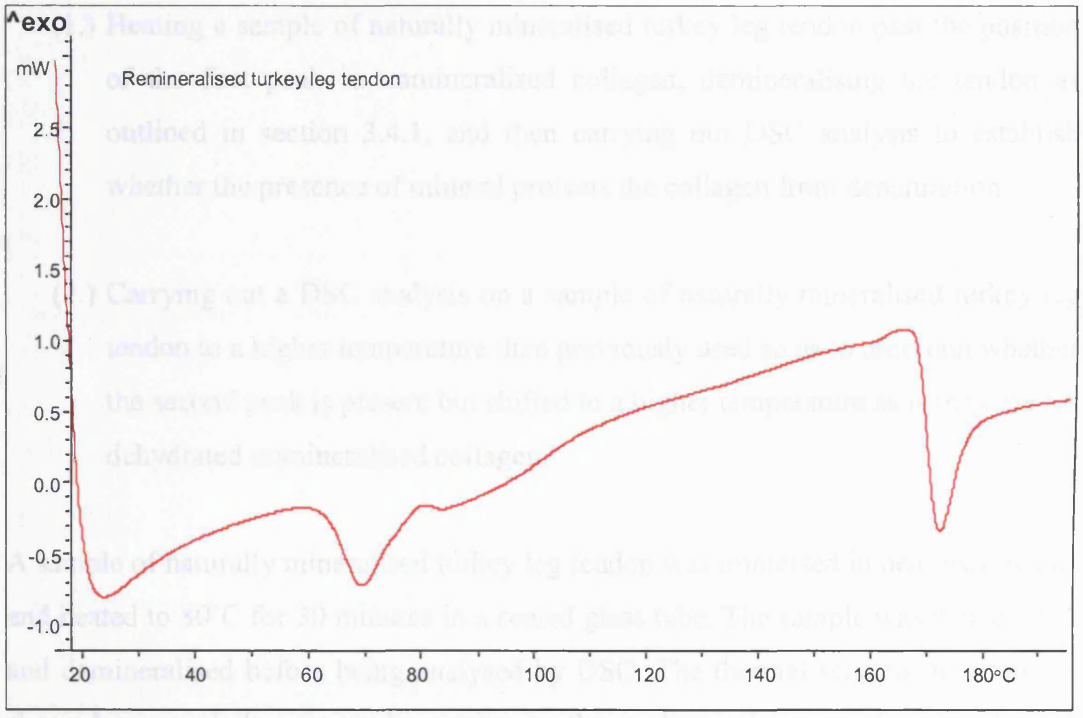

***Figure 5.5** DSC thermal scan of demineralised turkey leg tendon that had been heavily remineralised by incubation in 3.31 mM² Saito solution for 24 days.*

The position of the endothermic peak in the thermal scan of naturally mineralised turkey leg tendon occurs at a similar temperature to that of the second endothermic peak observed in the thermal scan of unmineralised turkey leg tendon. This could be due to two different scenarios: either the peak observed for naturally mineralised tissue is that caused by the event responsible for the first peak observed in unmineralised tendon, but shifted by some mechanism to a higher temperature analogous to what occurs in tanning with chromium (III) salts[161] and in dehydration[67]. Alternatively the peak observed in naturally mineralised collagen is due to the event responsible for the occurrence of the second peak that is observed in unmineralised collagen, and that the event leading to the occurrence of the first peak

is suppressed in some way so that no peak is observed in the thermal scan. Whatever the underlying mechanism the effect on the position of the peak in naturally mineralised tendon collagen indicates that there is a close association between the mineral phase and the collagen fibrils. In order to elucidate which of the above scenarios was occurring in naturally mineralised tendon collagen the following two experiments were carried out:

(1.) Heating a sample of naturally mineralised turkey leg tendon past the position of the first peak in unmineralised collagen, demineralising the tendon as outlined in section 3.4.1, and then carrying out DSC analysis to establish whether the presence of mineral protects the collagen from denaturation.

(2.) Carrying out a DSC analysis on a sample of naturally mineralised turkey leg tendon to a higher temperature than previously used so as to ascertain whether the second peak is present but shifted to a higher temperature as is the case for dehydrated unmineralised collagen.

A sample of naturally mineralised turkey leg tendon was immersed in deionised water and heated to 80°C for 30 minutes in a sealed glass tube. The sample was then cooled and demineralised before being analysed by DSC. The thermal scan for this sample showed two endothermic peaks similar to those observed in samples of unheated demineralised tendon and is shown in Figure 5.6 overleaf. The survival of the low temperature endothermic transition in mineralised collagen which has been heated prior to demineralisation to a temperature past that at which the transition occurs in unmineralised collagen indicates that the intimate association of mineral and collagen molecules within the hole and overlap regions of the fibril structure offers some protection against hydrothermal denaturation.

Heating a sample of mineralised tendon to 295°C did in fact show the presence of a second endotherm with T_{max} value of 259.0°C (as shown in Figure 5.7) confirming that the presence of mineral was shifting the endotherms to higher temperatures. The shifting of both peaks to higher temperatures was also observed for thermal scans of chrome tanned bovine hide powder collagen (Figure 5.8) and freeze-dried bovine hide powder collagen (Figure 5.9).

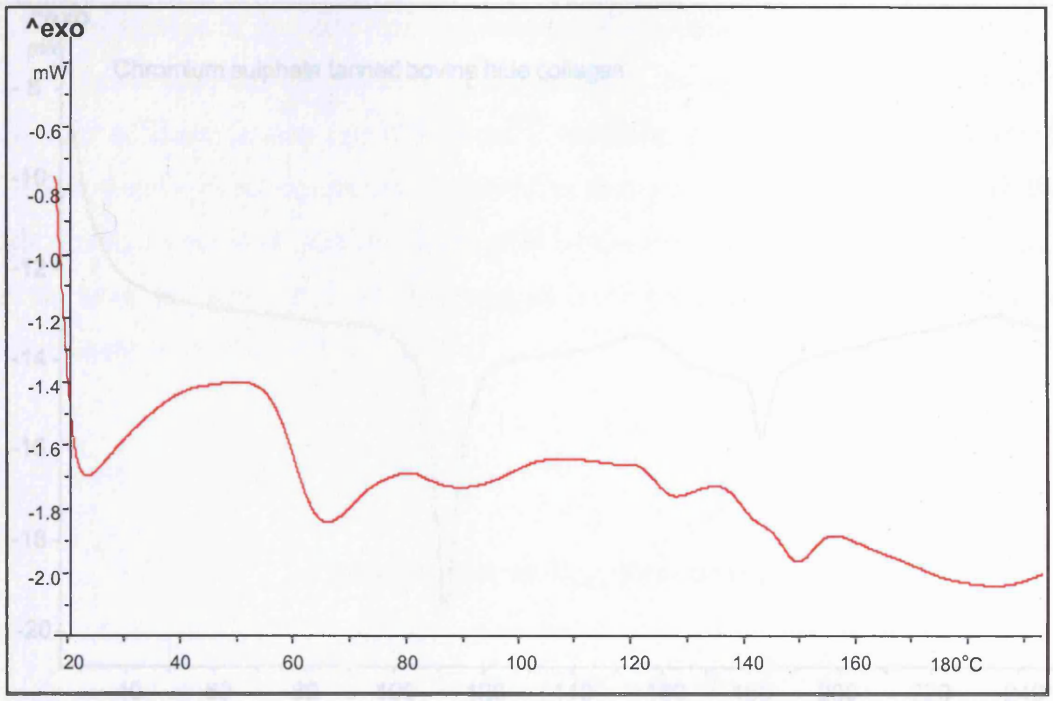

Figure 5.6 *DSC thermal scan of a sample of demineralised turkey leg tendon collagen that had been heated to 80°C prior to demineralisation showing the presence of the two transitions at temperatures similar to those of normally unmineralised collagen.*

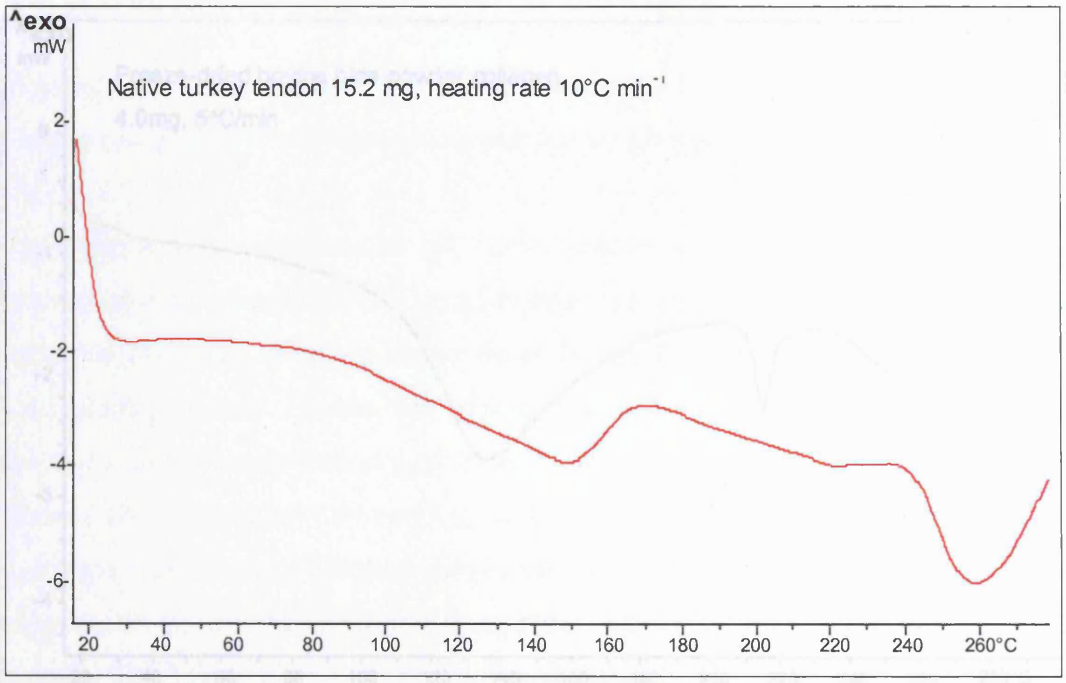

Figure 5.7 *DSC thermal scan of naturally mineralised turkey leg tendon collagen heated to 295°C showing the presence of the high temperature endotherm at 259°C.*

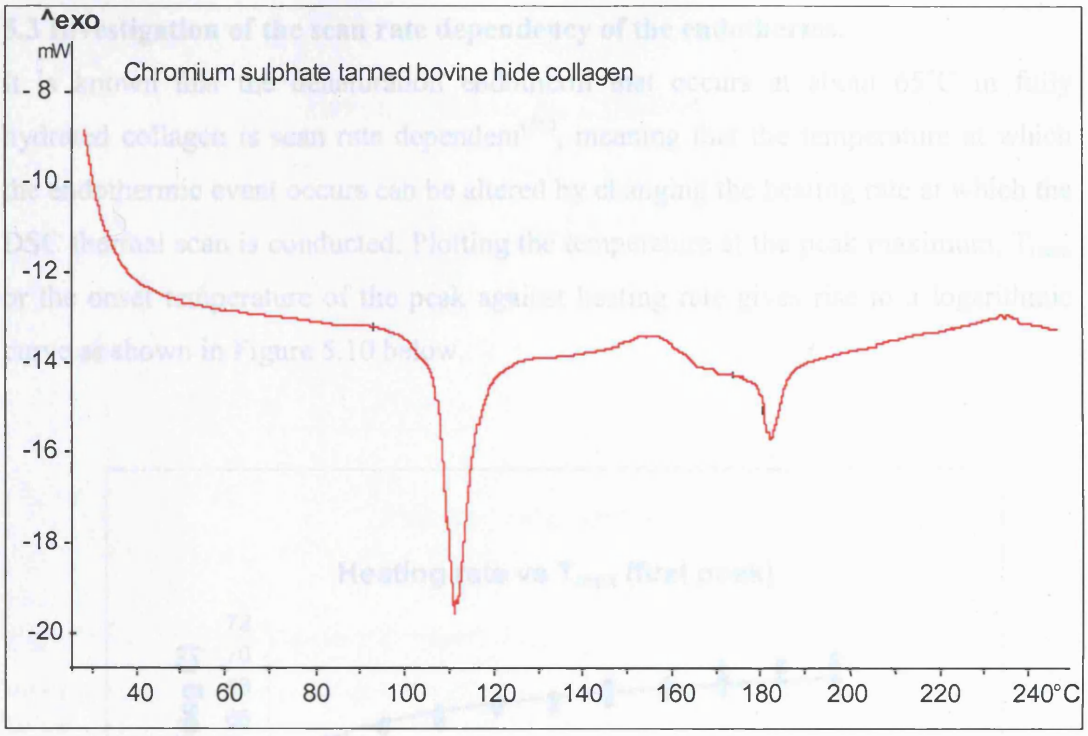

Figure 5.8 *DSC thermal scan of chromium sulphate tanned bovine hide powder collagen showing the shifting of the transitions to higher temperatures due to the tanning reaction.*

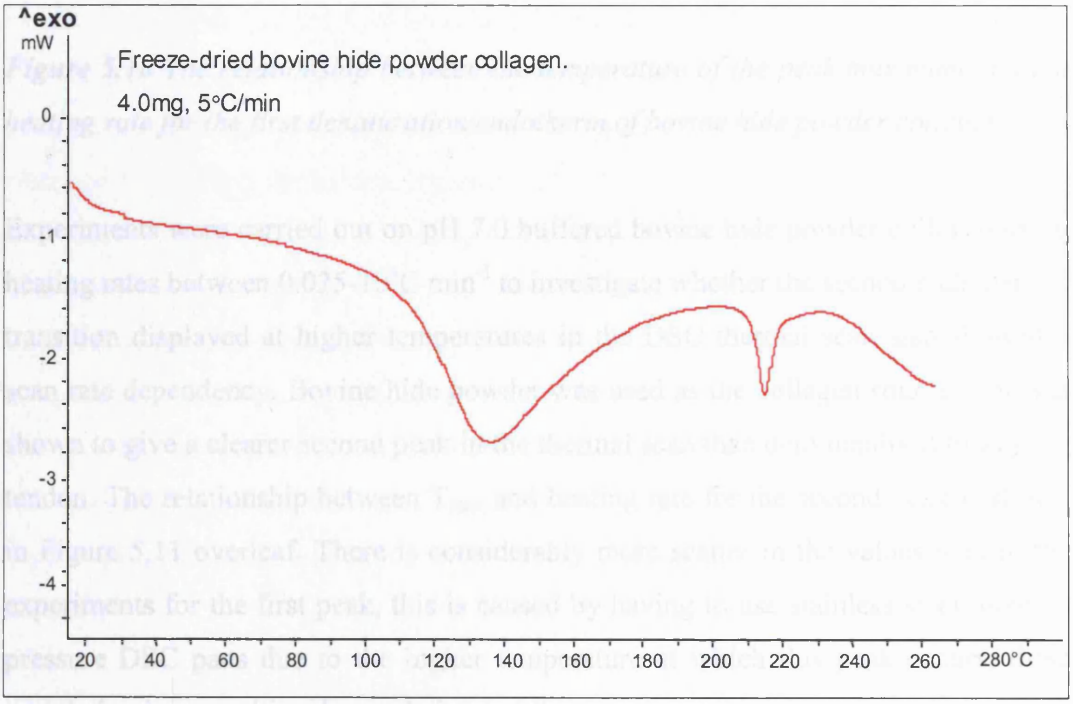

Figure 5.9 *DSC thermal scan for freeze-dried bovine hide powder collagen.*

5.3 Investigation of the scan rate dependency of the endotherms.

It is known that the denaturation endotherm that occurs at about 65°C in fully hydrated collagen is scan rate dependent[55], meaning that the temperature at which the endothermic event occurs can be altered by changing the heating rate at which the DSC thermal scan is conducted. Plotting the temperature at the peak maximum, T_{max}, or the onset temperature of the peak against heating rate gives rise to a logarithmic curve as shown in Figure 5.10 below.

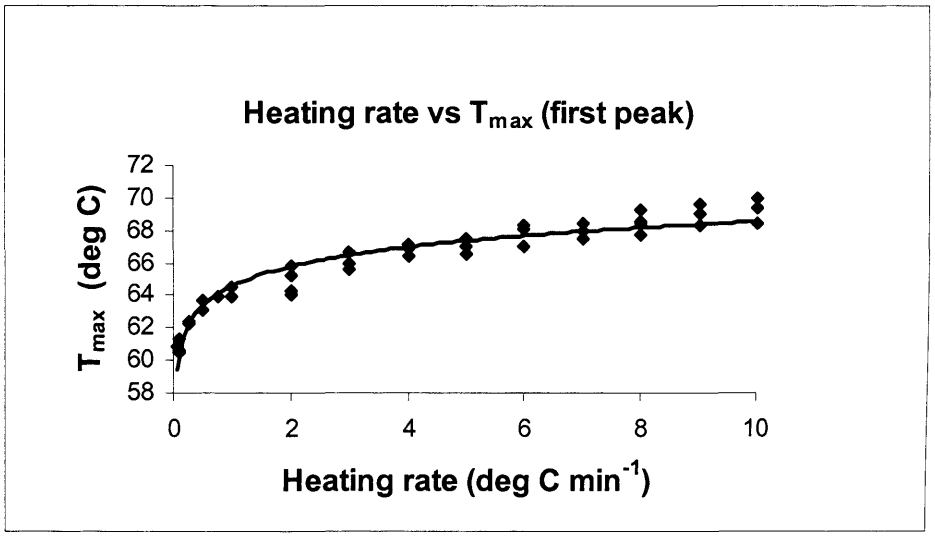

Figure 5.10 *The relationship between the temperature of the peak maximum and the heating rate for the first denaturation endotherm of bovine hide powder collagen.*

Experiments were carried out on pH 7.0 buffered bovine hide powder collagen using heating rates between 0.025-10°C min^{-1} to investigate whether the second endothermic transition displayed at higher temperatures in the DSC thermal scan also showed a scan rate dependency. Bovine hide powder was used as the collagen source as it was shown to give a clearer second peak in the thermal scan than demineralised turkey leg tendon. The relationship between T_{max} and heating rate for the second peak is shown in Figure 5.11 overleaf. There is considerably more scatter in the values than in the experiments for the first peak, this is caused by having to use stainless steel medium pressure DSC pans due to the higher temperature at which this peak occurs, these pans being less sensitive due to their greater mass.

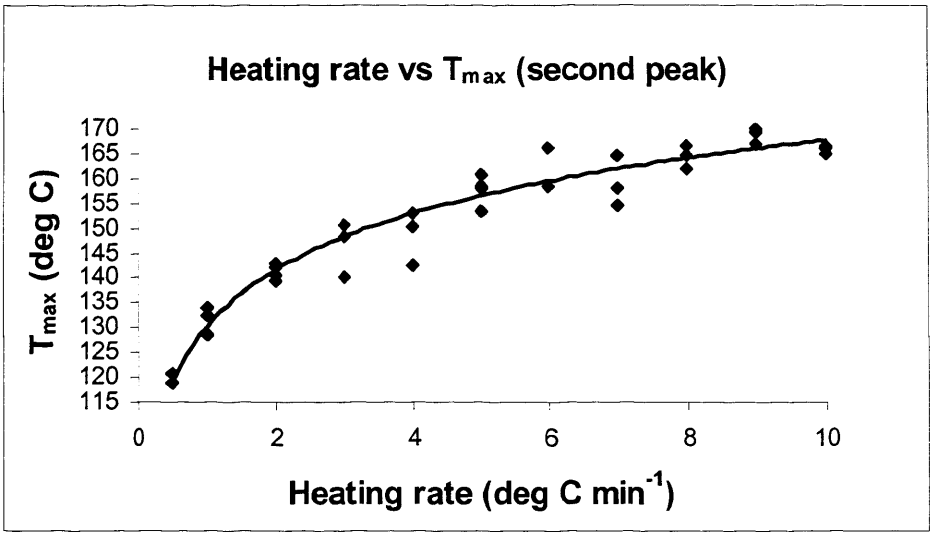

Figure 5.11 *The relationship between the temperature of the peak maximum and the heating rate for the second denaturation endotherm of bovine hide powder collagen.*

Reducing the heating rate used in the thermal scan gives rise to a decrease in the observed size of the endothermic peaks, this meant that heating rates lower than 0.5°C min^{-1} couldn't be used for experiments using stainless steel medium pressure pans, due to their reduced sensitivity compared to the light aluminium pans used in the experiments involving the first endothermic transition, as the peak size obtained was too small to evaluate.

A relative comparison of the scan rate dependency of each of the transitions can be obtained by plotting the natural logarithm of the heating rate against the reciprocal of the temperature at T_{max}, as is done in the making of an Arrhenius plot to determine activation energies. Such a plot gives a straight line, the slope of which is a measure of the relative scan rate dependency of the transition, the steeper the gradient of the line, the less scan rate dependent the transition. No information about the activation energies can be obtained in this case however as the heating rate is used and not a true rate of reaction for the denaturation transition. A comparison of the results for this type of plot for the data obtained from Figures 5.10 and 5.11 is shown in Figure 5.12 overleaf.

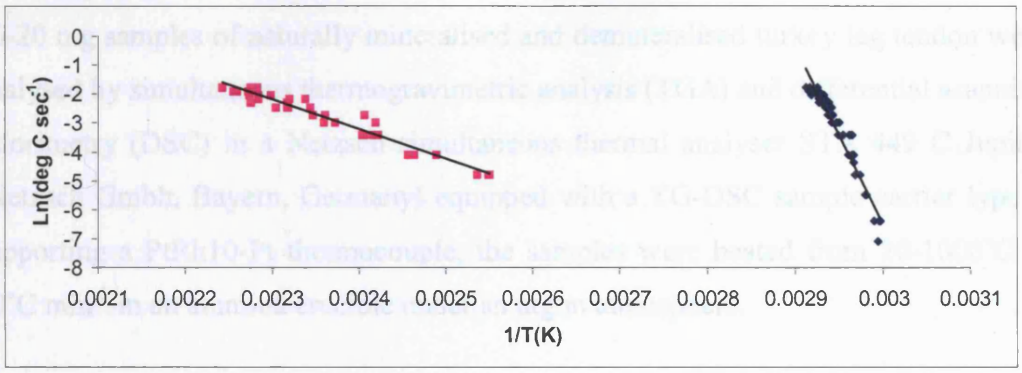

Figure 5.12 *Comparison of the scan rate dependencies of the two endothermic transitions that occur in the DSC thermal scan of collagen. From the results it can be seen that the second transition (pink squares) is much more scan rate dependent than the first transition (navy blue diamonds).*

5.4 Thermogravimetric analysis of mineralised turkey leg tendon

5.4.1 Introduction

Thermogravimetric analysis offers a convenient way of measuring mass changes within a material whilst it is subjected to a constant heating rate. Samples of naturally mineralised and acid demineralised turkey leg tendon were taken for thermogravimetric analysis (TGA) to determine the moisture contents and also to investigate the effect, if any, the mineral phase had on the stability of the collagen towards thermal decomposition as it has been reported[162] that the presence of mineral renders the collagen less stable towards this. Previous studies using TGA on mineralised collagen from bone have highlighted the presence of four peaks in the differentiated thermogravimetric scan when heated in air[163]. The temperature range and cause of each of these peaks is shown in Table 5.1 below.

Table 5.1 *Thermogravimetric events occurring in mineralised collagen heated in air between 20-1000°C (taken from Lim[163]).*

Peak temperature °C	Cause of peak
127	Removal of water
331	Protein combustion
403	Residual protein loss
747	Loss of H_2O from mineral

5.4.2 Experimental method

10-20 mg samples of naturally mineralised and demineralised turkey leg tendon were analysed by simultaneous thermogravimetric analysis (TGA) and differential scanning calorimetry (DSC) in a Netzsch simultaneous thermal analyser STA 449 C Jupiter (Netzsch Gmbh, Bayern, Germany) equipped with a TG-DSC sample carrier type S supporting a PtRh10-Pt thermocouple, the samples were heated from 20-1000°C at 10°C min^{-1} in an alumina crucible under an argon atmosphere.

5.4.3 Experimental results

The TGA/DSC thermal scan for a sample of naturally mineralised turkey leg tendon is shown in Figure 5.12 below.

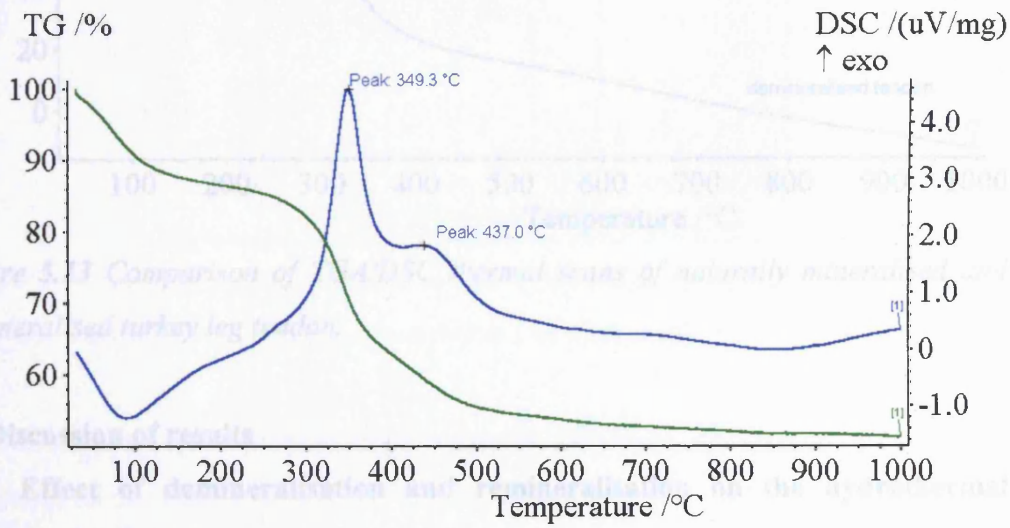

Figure 5.12 *Combined TGA/DSC thermal scan of naturally mineralised turkey leg tendon. The green curve is the TGA curve and the blue curve the DSC curve.*

From the above thermal scan of naturally mineralised turkey leg tendon it can be seen from the TGA curve that a mass change occurs between 20-200°C which corresponds with an endothermic transition in the DSC curve, this event being the driving off of water from the collagen sample. The endothermic transition associated with the first peak of collagen denaturation also occurs in this region but the peak from the vaporisation of water swamps its presence. A second large mass change occurs between 250-400°C in conjunction with a large exothermic peak, this being due to the

thermal decomposition of the organic material of the sample. The rate of mass change slows down between 400-500°C, at which point there is a shoulder in the DSC curve, this being attributed to the decomposition of residual protein. After heating the samples to 1000°C, the residue remaining in the sample pan is the hydroxyapatite mineral from which a rough indication of the amount of mineral within the sample can be gauged. A comparison of the TGA/DSC thermal scans for naturally mineralised and demineralised turkey leg tendon is shown in Figure 5.13 below.

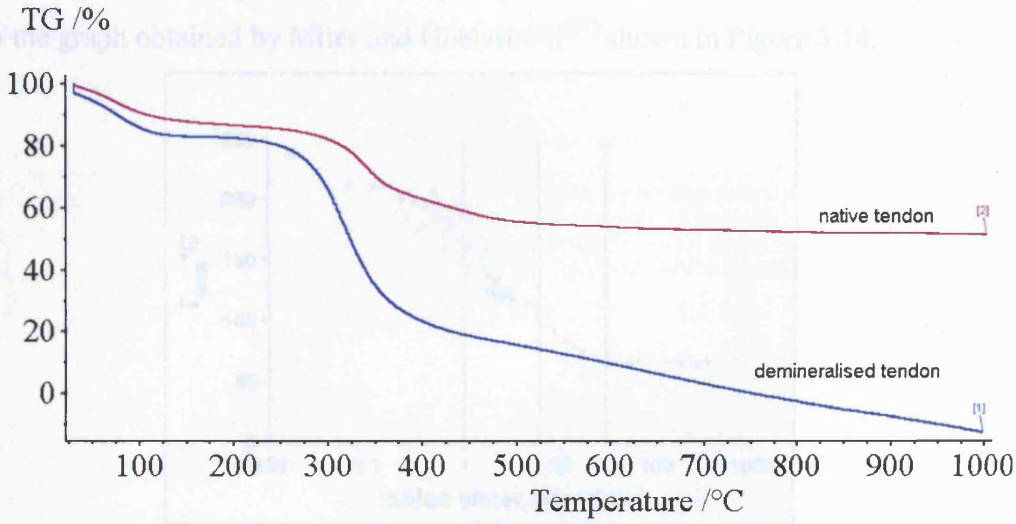

Figure 5.13 *Comparison of TGA/DSC thermal scans of naturally mineralised and demineralised turkey leg tendon.*

5.5 Discussion of results

5.5.1 Effect of demineralisation and remineralisation on the hydrothermal stability of collagen

Studies examining the influence of hydration on the denaturation temperature of collagen[67] have shown that there is a relationship between hydration and hydrothermal stability with the stability decreasing as the collagen becomes more hydrated. It is known that the formation of mineral crystals occurs within the gap region of the collagen fibrils[78] at the expense of the free water that is originally present within the structure here[164], therefore the growth of the mineral crystallites leads to a dehydrating of the collagen structure and thus a reduction in the intermolecular lateral d-spacing in this region. It is also in the gap region where the thermally labile domain of the collagen molecule is situated[67]. It follows that dehydrating this region by the exclusion of water caused by the growing crystallites

leads to a decrease in the available space in the thermally labile gap region in which the collagen molecules can denature into. This reduces the number of possible configurations, and thus the entropy of the uncoupled α-chains in the denatured state. Such a decrease in the entropy of the denatured state gives rise to an increase in the hydrothermal stability as predicted by the "polymer in a box" model of collagen denaturation[67]. By calculating the number of molecules of water present per triplet for a sample of naturally mineralised turkey leg tendon from its moisture content obtained by TGA, it is possible to interpolate its theoretical denaturation temperature from the graph obtained by Miles and Ghelashvili[67] shown in Figure 5.14.

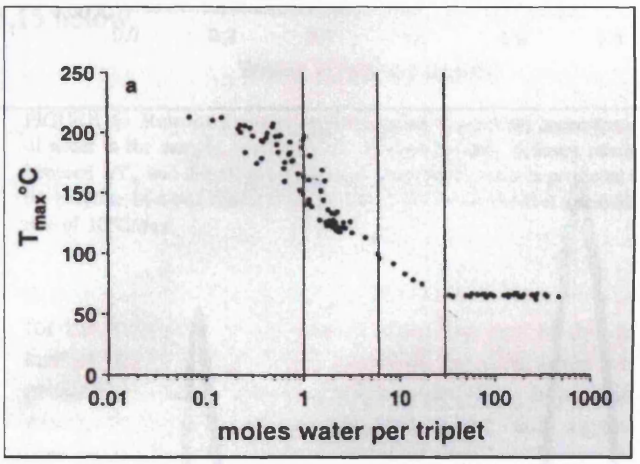

Figure 5.14 *The relationship between moisture content and denaturation temperature of rat tail tendon collagen. (Taken from Miles and Gelashvili[67])*

The moisture content obtained from a sample by thermogravimetric analysis was calculated to be approximately 7%, which corresponds to a figure of 1.14 molecules of water per collagen triplet. From the above graph we can see that this corresponds to a denaturation temperature of approximately 160°C, which is very close to the T_{max} value of 156°C observed from the DSC thermal scan of the same sample. The mineral crystallites in calcified tissue are located within the gap region of the collagen fibrils and it is also in this region that the fibril has its thermally labile domain. It appears that the presence of mineral within these regions stabilises the fibrils by reducing the space in which the collagen triple helix can uncoil into, thus reducing the size of the "box" and increasing the hydrothermal stability.

Previous studies[108] claimed that it was possible to partially remove the hydroxyapatite crystallites from mineralised tendon to produce a calcified collagenous matrix with a hydrothermal stability between that of the fully mineralised and non-

mineralised collagens. The mechanism was thought to involve the selective removal of mineral from the overlap regions of the collagen fibrillar structure, this being the most accessible, thus leaving the mineral in the thermally labile gap regions which is necessary for an increase in the hydrothermal stability. It was also claimed to be able to deposit mineral within the fibrillar structure of bovine hide collagen to give a matrix with an improved hydrothermal stability slightly lower than that of the partially demineralised collagen.

The DSC thermal scan obtained by Kronick and Cooke[108] for bovine hide collagen in which calcium phosphate mineral had been deposited within the fibril structure is shown in Figure 5.15 below.

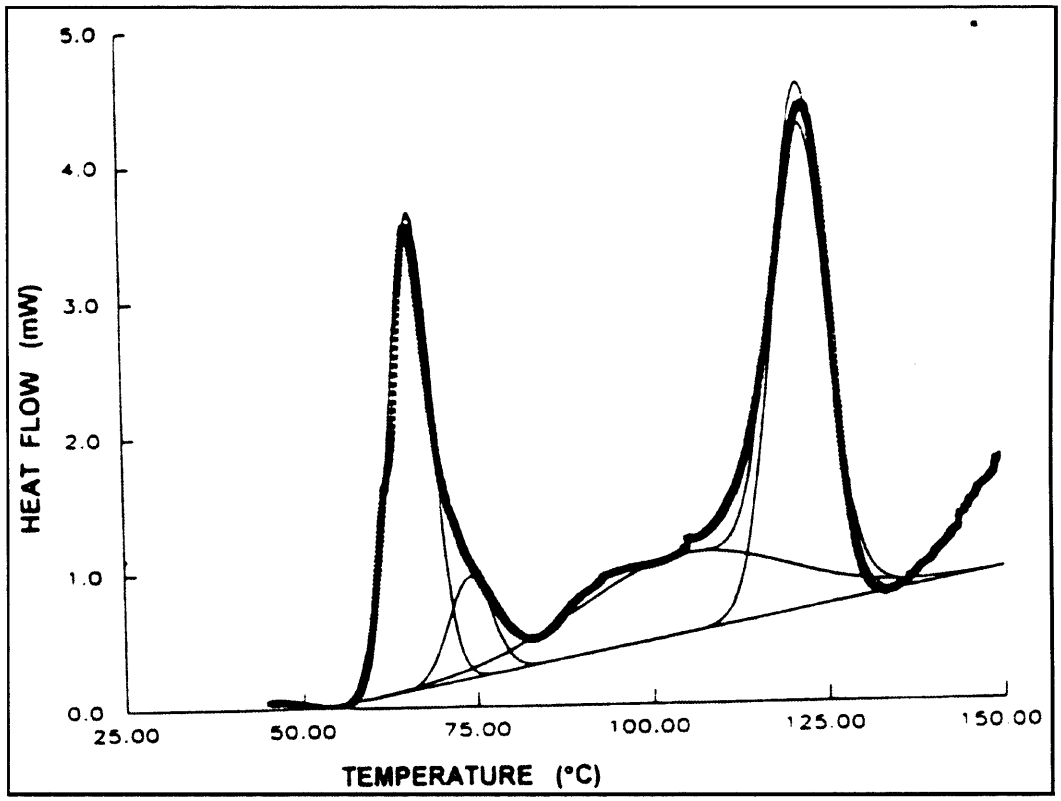

Figure 5.15 *DSC thermal scan for bovine hide powder collagen with calcium phosphate mineral deposited within the fibril structure. Note that the endotherms are presented pointing upwards as required for publication in some journals (taken from Kronick and Cooke[108]).*

It can be seen that the normally present endotherm of unmineralised collagen is present at ~65°C, along with an endothermic peak at ~120°C which was found to be due to a component of the reaction mixture. The peak attributed to the stabilisation of

the collagen by the deposited mineral is the small broad peak found at 104°C by deconvolution of the thermal scan. DSC thermal scans for complex substrates such as collagen are seldom without kinks and unevenness in the baselines, and as such deconvolution of these curves can lead to the identification of spurious peaks. A further query as to the validity of the partially mineralised peak obtained by Kronick for *in-vitro* mineralised collagen is due to the method of mineral formation. Altering the solubility of the mineral in solution would give rise to homogeneously nucleated mineral particles that would form within the solution. As very little solution would be contained in the hole regions of the collagen, it is unlikely that enough mineral formed in this way would be present to reduce the intermolecular spacing within this region to a level that would be necessary to bring about an increase in hydrothermal stability. During the course of these studies, many DSC thermal scans were carried out on partially demineralised and *in-vitro* remineralised turkey leg tendon collagen and in no case was an intermediate endothermic peak corresponding to that of the selective removal or deposition of mineral as postulated by Kronick observed. In the case of the partially demineralised samples no method could be found for producing testable quantities of collagen in which uniform levels of mineral were found only in the hole region. In the case of the remineralised tendon, the mineral crystallites were nucleated on the surface of the substrate, with these initially formed crystallites then bringing about the formation of other crystallites on their surface by secondary nucleation. Such a scenario leaves the majority of the collagen molecules within the substrate not having contact with the mineral crystallites. This was found to be the case for the remineralised samples as SAXS analysis showed that the mineral was not present in the hole region of the collagen substrate. This technique however averages the scattering over the bulk sample and since only a small percentage of the collagen molecules were in contact with the mineral crystallites. Mineral nucleation may have occurred in the hole regions of the fibrillar structure at the substrate surface, but the scattered SAXS intensity from such crystallites would be swamped from that of the majority of unmineralised gap regions. As the demineralised substrate was still able to induce the nucleation of mineral crystallites, and the polyanionic proteins required for this to occur are present in the hole zone, it seems sensible to speculate that the crystal nuclei formed on the substrate surface were formed within the hole regions.

5.5.2 Identification of a second endothermic denaturation transition

DSC thermal scans for demineralised turkey leg tendon still displayed an endothermic peak around 160°C, as shown in Figure 5.2. It was originally thought that this peak was due to some mineral remaining within the substrate as it occurred at roughly the same temperature as the peak observed in the DSC thermal scan of naturally mineralised turkey leg tendon. Chemical analysis as well as EDXA studies showed however that no mineral was present in such samples and so the second peak must be due to some event occurring within the collagen. DSC studies were carried out on bovine hide powder collagen, which does not undergo mineralisation, to confirm that the second peak was in fact a transition found in all Type I collagen. As the positions of the endotherm occurring in the DSC thermal scan of naturally mineralised turkey leg tendon and that of the second transition in unmineralised collagen occurred at a similar temperature, it was thought that the two peaks were caused by the same event. This could occur if the intimate relationship between the collagen fibrils and hydroxyapatite was such that the collagen molecules were encased in a shell of the mineral phase in such a way that the conformation of the individual α-chains of the triple helix were held in a fixed state. Breaking of the hydrogen bonds at the temperature of the first transition would still occur, but as the chain conformation is fixed by the mineral so that the triple helix could not uncoil, these hydrogen bonds could reform so that no net change in the enthalpy would be seen in the thermal scan. At the transition occurring at the temperature of the second endothermic peak some change in the collagen structure occurs that allows the conformation of the α-chains to vary. This in turn allows the rupture of interchain hydrogen bonds and hence uncoiling of the triple helix. Such a situation would arise if the second transition was due to a melting of the individual collagen molecules.

It is also possible that the similarity in the position of the endothermic peak for naturally mineralised turkey leg tendon collagen and that of the second endotherm in unmineralised collagen is just a coincidence, and that the peak in naturally mineralised tendon is due to the same transition as the first peak in unmineralised collagen, but is shifted by some mechanism to a higher temperature. To distinguish between the two possible scenarios, DSC thermal scans were conducted on naturally mineralised turkey leg tendon to a temperature just below that at which decomposition of the collagen occurs. These studies highlighted the presence of a second endothermic peak in the thermal scan of the naturally mineralised tendon, albeit at an

elevated temperature of 259°C. This result indicates that the peak observed at ~150°C in naturally mineralised turkey leg tendon is due to the same transition as that peak observed at ~65°C in unmineralised collagen.

Processes that increase the temperature at which the first endothermic peak occurs, such as crosslinking and dehydration, also had an effect on the temperature at which the second endothermic transition occurred. This is shown in the DSC thermal scans for chromium sulphate tanned (Figure 5.8) and freeze-dried (Figure 5.9) hide powder. In both such cases the temperature at which the first transition occurred was shifted by a greater amount than that of the temperature of the second transition. Values for the separation of the two transition temperatures for naturally mineralised (and hence partially dehydrated) turkey leg tendon, freeze-dried hide powder and chromium sulphate tanned hide powder are compared with those for demineralised tendon and fully hydrated bovine hide powder in Table 5.2.

Table 5.2 *Comparison of the T_{max} values of both peaks, and the difference between the two transitions for differently treated substrates.*

Substrate	1st transition °C	2nd transition °C	Peak separation °C
Demineralised tendon	69.3	161.1	91.8
Mineralised tendon	148.9	259.0	110.1
Freeze-dried hide powder	135.1	214.9	79.8
Chrome tanned hide	110.9	182.1	71.2
Bovine hide powder	66.4	159.3	92.9

From Table 5.2 it can also be seen that the peak separation is greatest in naturally mineralised turkey leg tendon. The fact that the peak separation changes during treatments such as crosslinking and freeze-drying suggest that the two transitions have different causes, a fact that is corroborated by the difference in scanning rate dependencies of the temperature of the transitions (Figure 5.12).

Another observation from Table 5.2 is that the naturally mineralised tendon collagen displays higher temperatures for the two transitions than that of the sample of freeze-dried hide powder despite the fact that it is hydrated to a higher degree than that of the dehydrated hide powder. This suggests that some other mechanism of hydrothermal stabilisation, as well as the reduction in intermolecular spacing of the collagen due to

dehydration is at work in naturally mineralised tissue. It is possible that the presence of mineral crystallites within the hole regions of the fibrillar structure of the collagen further increases the hydrothermal stability by reducing the space within this region that is available for the thermally labile domain of the collagen molecule to uncoil into. This would lead to a stabilising of the collagen by a further entropic effect distinct to that obtained by dehydration. Dehydration of the collagen only decreases the space between adjacent molecules, whereas the presence of mineral reduces the free volume of the hole regions, thus further reducing the size of the "box".

Chapter 6

Investigation into the nature of the 2nd endothermic transition

6.1 Investigation into the nature of the second endotherm

6.1.1 Effect of hydrogen bond breaking agents

To investigate whether the high temperature endotherm was a result of the breaking of hydrogen bonds within the collagen structure a sample of demineralised tendon was immersed in a solution of 8 mol dm^{-3} lithium bromide for 24 hours. This reagent would break the interchain hydrogen bonds that hold the α-chains together within the collagen structure, and so any denaturation endotherms produced by the breaking of these bonds during heating could be removed from the DSC thermogram by the prior treatment with lithium bromide solution. DSC analysis as in section 5.2.1 was carried out on this sample of tendon after the immersion. The thermal scan produced after lithium bromide treatment is shown in Figure 6.1 below.

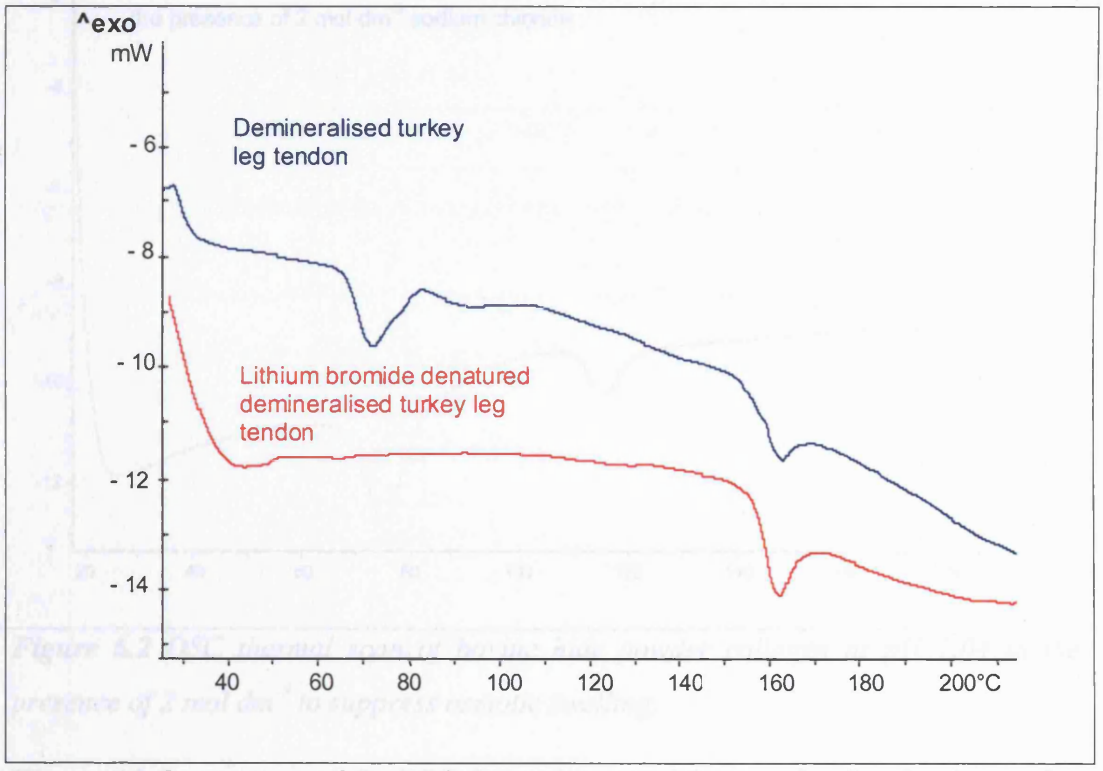

Figure 6.1 *Comparison of the DSC thermal scans of demineralised turkey leg tendon (black line) and demineralised turkey leg tendon treated with 8 mol dm^{-3} lithium bromide solution (red line).*

6.1.2 Electrostatic bond breaking conditions

As hydrogen bond breaking reagents had no effect on the position of the second endothermic peak it was thought that perhaps the second transition was due to the

rupture of electrostatic links within the fibril structure, as these bonds are important in the formation of collagen fibrils. In order to test this hypothesis, bovine hide powder was hydrated for 24 hours with a solution of hydrochloric acid at pH 1.04. The solution also contained 2 mol dm^{-3} sodium chloride to suppress osmotic swelling, as such swelling would affect the position of the endotherms. At this low pH the carboxyl groups of the collagen are fully protonated, leaving the collagen with a net positive charge (as shown in Figure 1.10 in section 1.2.1.) so that there is no electrostatic attraction between the triple helices. The acidified collagen was then taken for DSC analysis as outlined previously in section 5.2.1. The thermal scan obtained is shown in Figure 6.2 below.

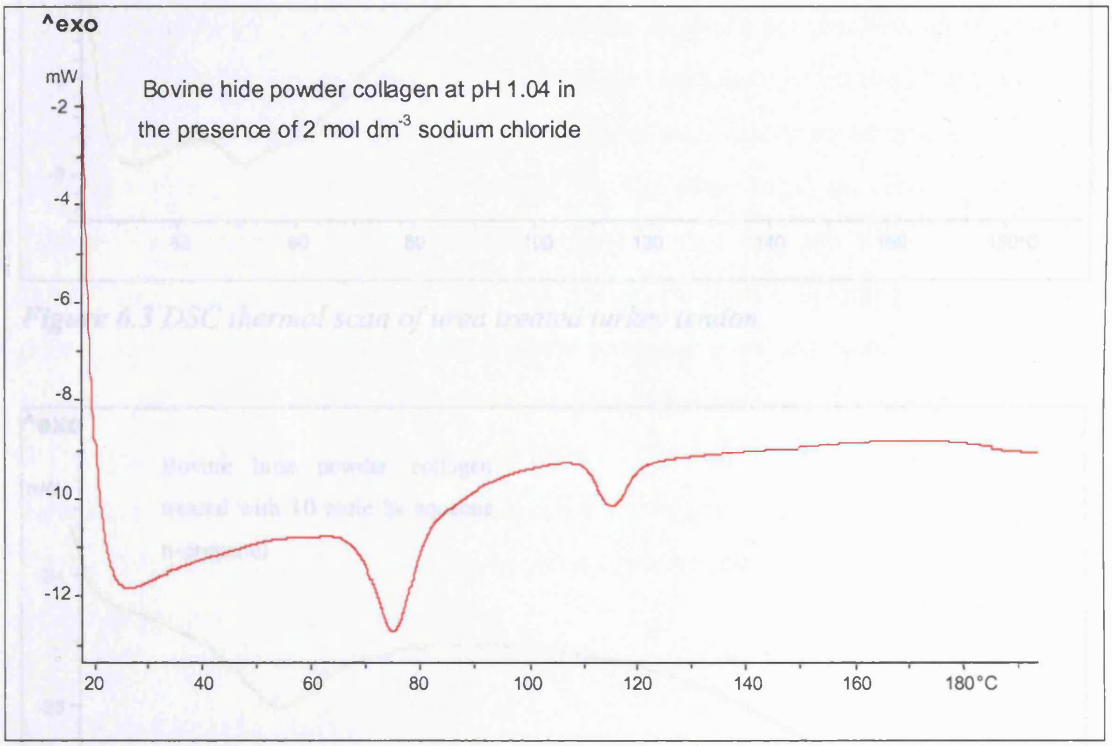

Figure 6.2 *DSC thermal scan of bovine hide powder collagen at pH 1.04 in the presence of 2 mol dm^{-3} to suppress osmotic swelling.*

6.1.3 Effect of hydrophobic bond breaking agents

To determine if reagents that disrupt the hydrophobic bonding within the collagen structure had any effect on the position of the second endotherm, thin sections of demineralised turkey tendon were immersed in an aqueous solution of 2 mol dm^{-3} urea for 24 hours. Urea is known to break hydrophobic bonds[165] as well as hydrogen bonds and so would be expected to have an effect on the position of both peaks if the second transition was due to the rupture of hydrophobic interactions. After treatment

with urea the samples were analysed by DSC as in section 5.2.1. Typical results are shown in Figure 6.3 below.

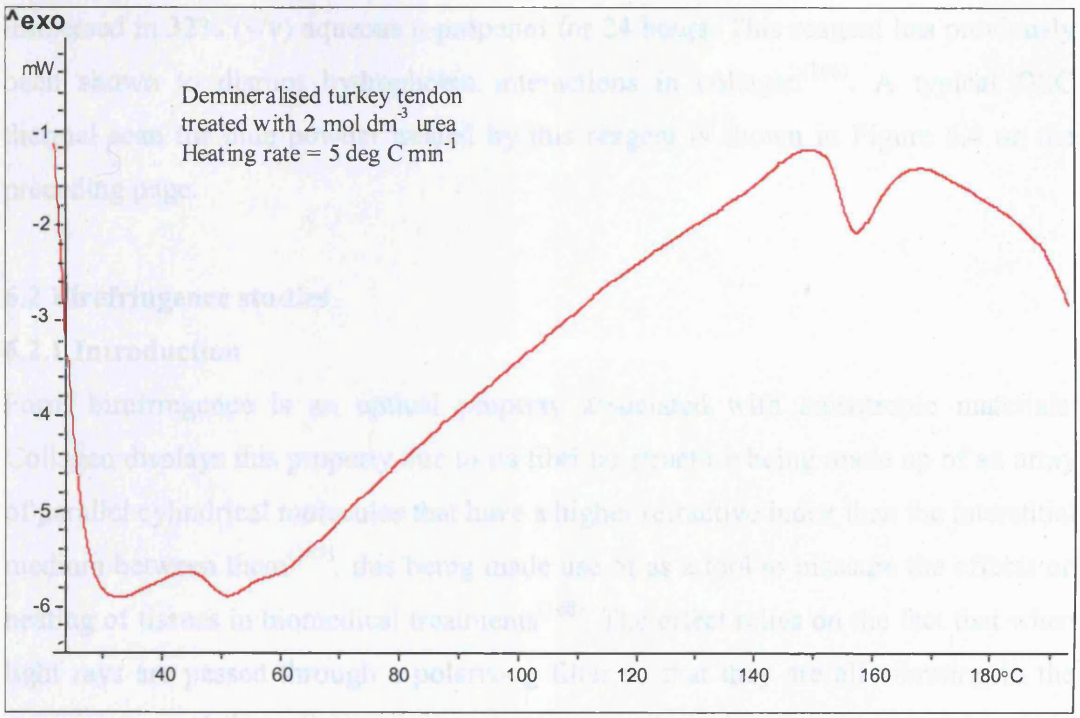

Figure 6.3 *DSC thermal scan of urea treated turkey tendon.*

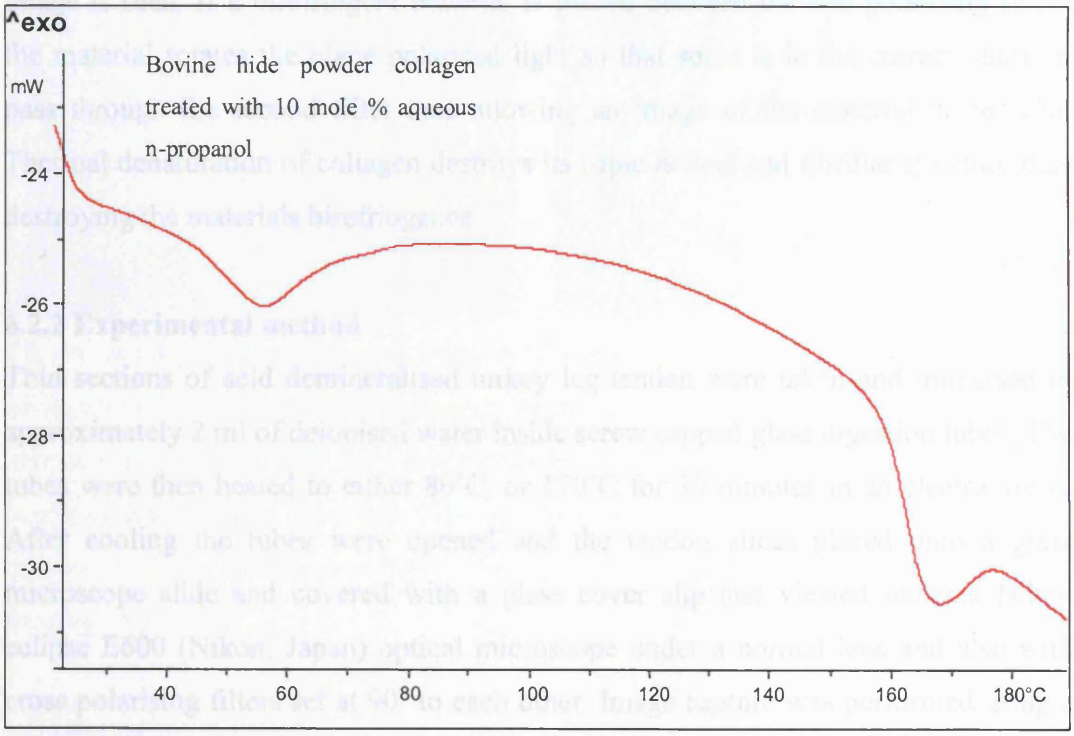

Figure 6.4 *DSC thermal scan of bovine hide powder soaked for 24 hours in 32% (v/v) aqueous n-propanol.*

In order to investigate the effect on the second transition of reagents, which only disrupt hydrophobic interactions, samples of bovine hide powder collagen were immersed in 32% (v/v) aqueous n-propanol for 24 hours. This reagent has previously been shown to disrupt hydrophobic interactions in collagen[166]. A typical DSC thermal scan for hide powder treated by this reagent is shown in Figure 6.4 on the preceding page.

6.2 Birefringence studies

6.2.1 Introduction

Form birefringence is an optical property associated with anisotropic materials. Collagen displays this property due to its fibrillar structure being made up of an array of parallel cylindrical molecules that have a higher refractive index than the interstitial medium between them[167], this being made use of as a tool to measure the effects on heating of tissues in biomedical treatments[168]. The effect relies on the fact that when light rays are passed through a polarising filter so that they are all vibrating in the same plane, and these light rays are then passed through a second polarising filter rotated at 90° to the first none of the plane polarised rays can pass through and no image is seen. If a birefringent material is placed between the two polarising filters the material rotates the plane polarised light so that some is in the correct phase to pass through the second filter thus allowing an image of the material to be seen. Thermal denaturation of collagen destroys its triple helical and fibrillar structure thus destroying the materials birefringence.

6.2.2 Experimental method

Thin sections of acid demineralised turkey leg tendon were taken and immersed in approximately 2 ml of deionised water inside screw capped glass digestion tubes. The tubes were then heated to either 80°C, or 170°C for 30 minutes in an electric oven. After cooling the tubes were opened and the tendon slices placed onto a glass microscope slide and covered with a glass cover slip and viewed under a Nikon eclipse E600 (Nikon, Japan) optical microscope under a normal lens and also with cross polarising filters set at 90° to each other. Image capture was performed using a Nikon coolpix 990 (Nikon, Japan) digital cameral mounted onto the eyepiece of the microscope. Unheated slices of demineralised tendon were used as a control. The images obtained are shown in Figure 6.5.

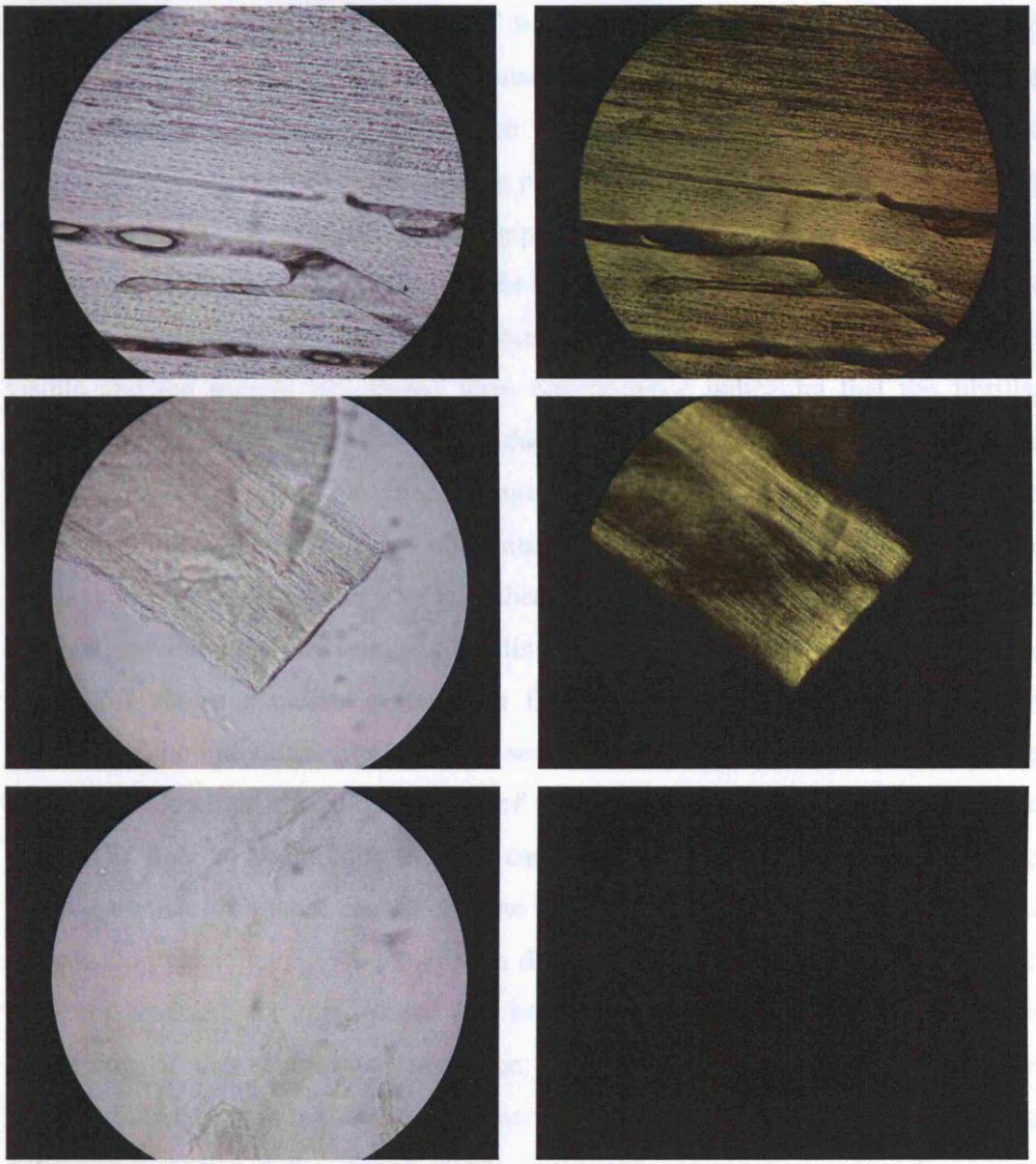

Figure 6.5 *Optical microscopy images of heated demineralised turkey leg tendon collagen samples. The left hand images are normal images and those on the right are images taken with the 90° cross-polarising filters in place to observe any birefringence effects. The top pair of images was taken of collagen at room temperature, the middle pair taken after heating to 80°C, and the bottom pair after heating to 170°C.*

6.3 Discussion of results

It is well known that the breaking of hydrogen bonds within the collagen triple helices causes the endothermic transition that occurs in collagen at around 65°C. What is

unknown however is the cause of the second endothermic transition observed in these studies. Visual observation of the state of the collagen before and after each of the two transitions helps to clarify the possible causes of the second endothermic event. In the case of demineralised turkey leg tendon collagen the original dimensions of the sample are altered somewhat after heating past the first endotherm, the sample having a shrunken appearance but still remaining physically intact in the form of an array of almost parallel fibres. A comparison of the light microscopy images in Figure 6.5 for the room temperature and 80°C heated samples shows that the fibre structure is still visible and the sample still shows form birefringence indicating that the fibrillar structure is still intact after the first endothermic transition. Imaging of the individual collagen fibrils by transmission electron microscopy (TEM) after this transition shows that a swelling of the fibrils takes place and the characteristic banding pattern of the fibrils is lost[169]. A TEM image of an unheated collagen fibril is shown in Figure 6.6 overleaf, in which the characteristic banding pattern of the fibril can clearly be seen. Figure 6.7 shows a cluster of collagen fibrils after heating to 80°C, the uneven swelling of the individual fibrils can be seen along with the absence of the banding pattern. It is thought that the breaking of the structural hydrogen bonds within the triple helix frees up hydrophilic sites that can now bind to water molecules by forming hydrogen bonds with them thus forcing the helical structure apart. This would explain the swelling phenomena that occur upon denaturation. Whether this swelling of the structure accounts for the loss of the banding pattern of the fibrils due to the weakening of the electrostatic attraction between triple helices caused by their increased separation is not known. Another possible cause of the loss of the banding pattern is a change in the charge profile of the collagen molecules. It is the lateral register of oppositely charged amino acid side chains that gives rise to the banding pattern[18] and so an alteration to the charge profile by the reaction of certain amino acid residues would disrupt the banding pattern. After the first endothermic transition at ~65° the asparagine residues in collagen start to undergo deamidation to aspartic acid[170], thus changing the charge profile by producing negatively charged groups from uncharged residues. Changing the balance of positively and negatively charged groups within the collagen structure would alter the isoelectric point of the collagen thus allowing the possibility of osmotic swelling to occur, which could also explain the swelling of the fibrils that occurs after this transition.

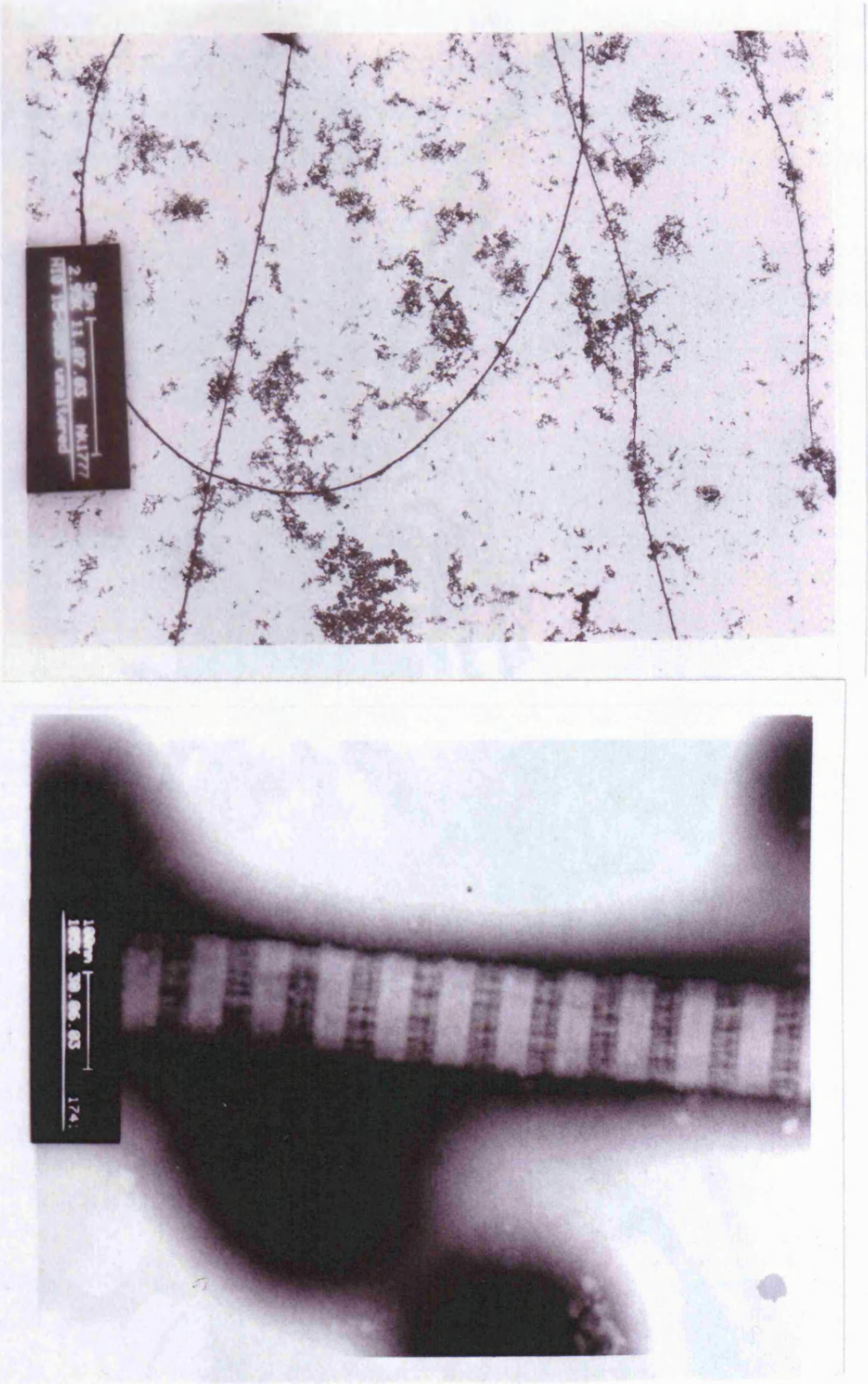

Figure 6.6 *TEM images of a single collagen fibril, the top image shows a single fibril at x2900 magnification, the bottom image is of the same fibril but at x100000 magnification in order to observe the banding pattern (TEM images courtesy of Hannah Koon[171]).*

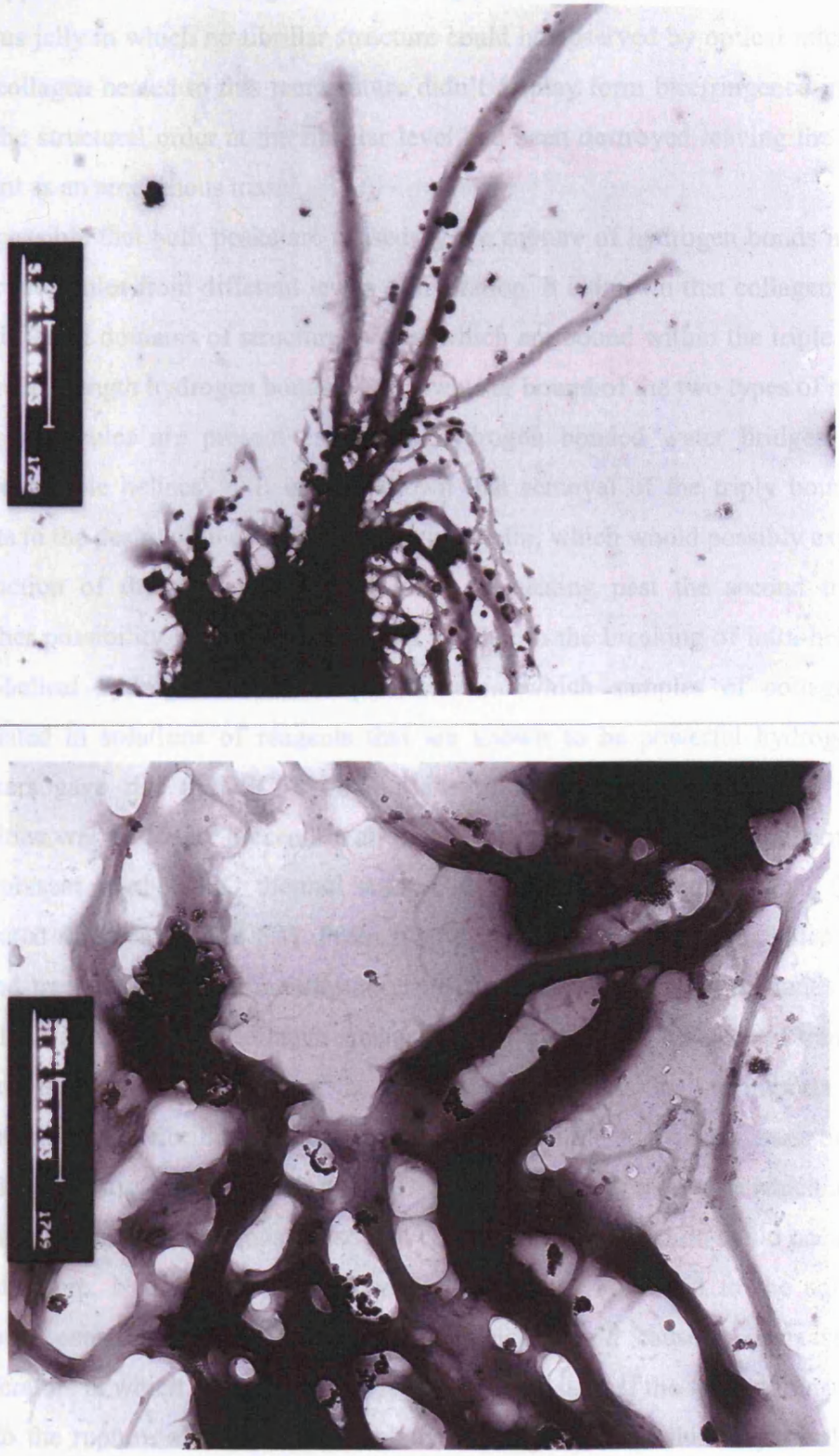

Figure 6.7 *TEM images of collagen fibrils that had been heated to 80°C. The top image shows the swollen appearance of the fibrils (x5200 magnification) and the bottom image shows the absence of the banding pattern (x21000 magnification) (TEM images courtesy of Hannah Koon[171]).*

The appearance of the collagen after heating past the second transition was that of a viscous jelly in which no fibrillar structure could be observed by optical microscopy. The collagen heated to this temperature didn't display form birefringence indicating that the structural order at the fibrillar level had been destroyed leaving the material present as an amorphous mass.

It is possible that both peaks are caused by the rupture of hydrogen bonds involving water molecules from different levels of hydration. It is known that collagen contains two different domains of structural water, which are bound within the triple helix by different strength hydrogen bonds[70]. The weaker bound of the two types of structural water molecules are present as double hydrogen bonded water bridges between adjacent triple helices[15]. It is also known that removal of the triply bound water results in the destruction of the collagen triple helix, which would possibly explain the production of the amorphous gel formed on heating past the second transition. Another possibility is that the two peaks are due to the breaking of intra-helical and inter-helical hydrogen bonds. Experiments in which samples of collagen were incubated in solutions of reagents that are known to be powerful hydrogen bond breakers gave rise to DSC thermal scans in which the endotherm for the first transition was no longer present. In all such experiments the second endothermic peak was present in the DSC thermal scan at the same temperature as that found in untreated samples (Figure 6.1). From such experiments it can be concluded that the second transition is not a manifestation of the breaking of hydrogen bonds. As the fibrillar structure of the collagen appeared to be lost during the second transition it was envisaged that disruption of the electrostatic salt links that are important in the formation of the fibrillar structure could be responsible for such a transition. This could be investigated by reducing the pH of the collagen to a level at which all of the carboxyl groups were protonated, so that no electrostatic attraction could occur within the structure. Neutral electrolyte would also have to be added to the solution to suppress osmotic swelling the effects of which would cause a decrease in the temperature at which the transitions occurred (Figure 6.8). If the second transition was due to the rupture of such interactions then collagen treated this way would fail to show the endothermic peak associated with this transition in its DSC thermal scan. The thermal scans of collagen treated this way (Figure 6.2) still displayed the presence of the second endotherm indicating that the transition was not due to the rupture of these electrostatic salt links. An interesting observation from this

experiment was the reduction in the temperature at which the second transition occurred, even in the presence of neutral electrolyte. The temperature of the first transition for samples soaked in acidic solutions containing high levels of neutral electrolyte was slightly higher than that for samples measured at pH 7.0 due to the slight improvement in hydrothermal stability gained in the presence of the 2 mol dm^{-3} sodium chloride[172].

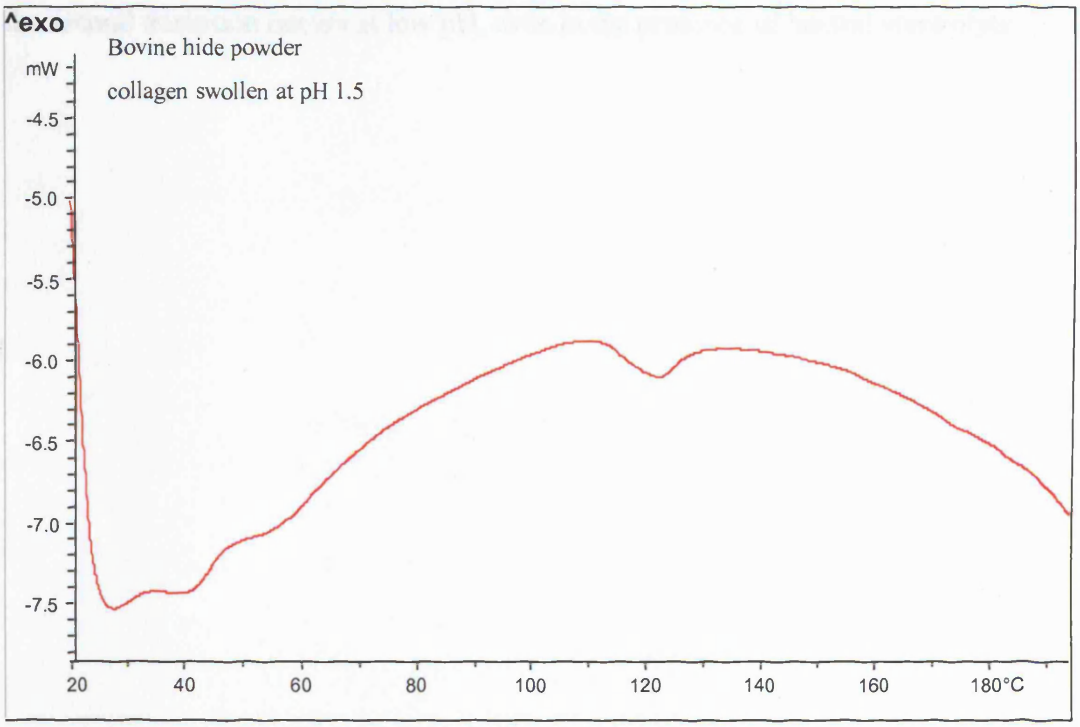

Figure 6.8 *DSC thermal scan of bovine hide collagen swollen in hydrochloric acid at pH 1.5 in the absence of neutral electrolyte, showing the reduction in transition temperatures caused by the osmotic swelling of the collagen structure.*

In investigations using reagents that disrupt hydrophobic interactions within the collagen structure no effect on the temperature at which the second transition occurs was observed (Figures 6.3 and 6.4). As the rupturing of hydrophobic bonds is an exothermic process[165] this phenomena could not be responsible for the second transition.

The only chemical interaction remaining that could be responsible was that of the breaking of covalent chemical bonds. The second transition occurs at a temperature lower than normally associated with the breaking of covalent bonds by thermal cleavage, however a chemical reaction in which certain bonds are broken is quite

feasible at these temperatures. It is known that the hydrolysis of peptide bonds between the individual amino acids of the α-chains can occur under certain conditions, and is catalysed by both acid and alkali[173]. This reaction breaks the peptide bond forming an amine and a carboxylic acid residue. The breaking of such bonds would lead to a fragmentation of the collagen molecules as is made use of in the acid hydrolysis of proteins for amino acid analysis[174]. The fact that the presence of acid catalyses this reaction would explain the reduction in the temperature at which the second transition occurs at low pH, even in the presence of neutral electrolyte.

Chapter 7

Conclusions and future work

7.1 Conclusions

From the studies outlined in this thesis the following conclusions can be drawn.

7.1.1 Demineralisation and the *in-vitro* remineralisation of turkey leg tendon

The complete removal of the mineral phase of naturally mineralised turkey leg tendon was found to be easily achieved using dilute acid. However, experiments to produce samples of uniformly partially demineralised turkey leg tendon, in which mineral remained within the gap regions of the fibrillar structure were found to be unsuccessful.

It was found that by using the 3.31 mM^2 Saito solution large quantities of hydroxyapatite crystallites could be grown on the demineralised tendon substrate. These crystallites were found to be different to those formed *in-vivo* in naturally mineralising Type I collagen. This is probably due to the absence of any biochemical control over the crystal growth in the experiments carried out *in-vitro*. It can be concluded that control over the nucleation of the mineral is a function of the substrate, whereas control over the crystal growth and morphology is a function of the solution.

7.1.2 Mineralisation of modified non-mineralising collagen

The chemical grafting experiments of non-mineralising collagen to produce a mineralisable substrate were unsuccessful. Silation of collagen using tetraethyl orthosilane however resulted in the formation of a collagen substrate that induced mineral crystallite formation when incubated in 3.31 mM^2 Saito solution.

7.1.3 Effect of the mineral phase on collagen hydrothermal stability

Naturally mineralised Type I collagen in turkey leg tendon and bone has a higher hydrothermal stability than that of unmineralised collagen. This is proposed to be due to the dehydration of the structure within the hole regions caused by the growth of crystallites within this region at the expense of water. It is also possible that a further increase in stability is obtained by the reduction in space within the hole region caused by the presence of mineral in this location. For collagen mineralised *in-vitro* the vast majority of the collagen molecules do not come into contact with the mineral crystallites, and so the hole regions are hydrated to a similar level as that found in unmineralised collagen. Consequently, the use partial remineralisation as a method for

improving the hydrothermal stability of collagen for the leather making process in this research was found to be unsuccessful.

7.1.4 The presence of a second endothermic transition in collagen denaturation and its possible cause

A second endothermic transition was observed to occur during collagen denaturation, this peak occurring at the higher temperature of approximately 160°C and has not previously been reported. The position of this second endotherm was dependant on the pH, hydration, and state of crosslinking of the collagen. The position of this transition was much more scan rate dependent than the lower temperature transition associated with the rupture of hydrogen bonds. DSC studies using reagents that break specific types of non-covalent interactions indicated that the rupture of hydrogen bonds, electrostatic interactions, or hydrophobic interactions did not cause this second transition. A possible cause of this transition is the hydrolysis of peptide bonds within the backbone of the protein chains of the triple helix. Collagen that has undergone this second transition displays an amorphous structure indicative of a total disruption of the fibrillar structure.

7.2 Future work

From the investigations carried out within this thesis the following experiments are suggested that may provide further useful information on the phenomena discussed.

In order to determine whether the presence of very small amounts of evenly distributed mineral within the fibrillar structure has any effect on the hydrothermal stability of collagen DSC studies need to be carried out on collagen that is just starting to mineralise, such as that found in embryonic bone. To investigate such an effect for *in-vitro* mineralised collagen some method of creating uniform levels of mineral formation throughout the substrate needs to be designed.

It is known that the extent of collagen hydration, and also collagen pH, has an effect on the temperature at which the first transition occurs in the DSC thermal scan. These studies indicate that this is also true for the transition occurring at the second transition. DSC studies need to be undertaken to determine the relationship between both the effect of hydration of the substrate, and the effect of substrate pH on the

temperature at which this transition occurs. Isothermal DSC studies also need to be carried out to elucidate the activation energy parameters for this transition, as this would give an indication of the mechanism involved.

To determine whether the second endotherm is caused by the hydrolysis of the peptide bonds within the polypeptide chain backbone, protein mass spectrometry and electrophoresis need to be carried out to determine whether any fragmentation occurs within these polypeptide chains upon heating to past the temperature of the second transition. Cleavage of peptide bonds would give rise to an increase in the content of free amino and carboxyl groups within the sample, which could be quantified to determine the extent, if any, of the peptide bond hydrolysis.

Finally, solid state Nuclear Magnetic Resonance (NMR) could also be used to determine whether hydrolysis of peptide bonds is indeed responsible for the presence of the second endothermic peak, as this technique would identify the differences in the chemical bonding that would occur when peptide bonds are broken.

References

1. Price, J.M., Corrado, M., Caterina, M. and Byers, P.H. "Identification, characterisation and expression analysis of a new fibrillar collagen gene, COL27A1" *Matrix Biology*, 2003, **22**, 3-14.

2. Friess, W. "Collagen-biomaterial for drug delivery" *European Journal of Pharmaceuticals and Biopharmaceuticals*, 1998, **45**, 113-136.

3. Fratzl, P. "Cellulose and collagen: from fibres to tissues" *Current Opinion in Colloid and Interface Sciences*, 2003, **8**, 32-39.

4. Fietzek, P.P. and Kuhn, K. "Information contained in the amino acid sequence of the α1(I)-chain of collagen and its consequences upon the formation of the triple helix, of fibrils and crosslinks" *Molecular and Cellular Biochemistry*, 1975, **8**, 141-157

5. Katz, E.P., Francois, C.J. and Glimcher, M.J. "The molecular weights of the α chains of chicken bone collagen by high speed sedimentation equilibrium" *Biochemistry*, 1969, **8**, 2609-2615.

6. Traub, W., Yonath, A. and Segal, D.M. "On the molecular structure of collagen" *Nature*, 1969, **221**, 914-917.

7. Kuhn, K. "Relationship between amino acid sequence and higher structures of collagen" *Connective Tissue research*, 1982, **10**, 5-10.

8. Schroeder, W.A., Kay, L.M., LeGette, J., Honnen, L. and Green, F.C. "The constitution of gelatin. Separation and estimation of peptides in partial hydrolysates" *Journal of the American Chemical Society*, 1954, **76**, 3556-3564.

9. Rich, A. and Crick, F.H.C. "The structure of collagen" *Nature*, 1955, **176**, 916-917.

10. Woodhead-Galloway, J. "Collagen: Anatomy of a protein", Edward Arnold, 1980.

11. Rich, A. and Crick, F.H.C. "The molecular structure of collagen" *Journal of Molecular Biology,* 1961, **3**, 483-506.

12. Okuyama, K., Tanaka, N., Ashida, T. and Kakudo, M. "A new structural model of collagen" *Polymer Journal*, 1977, **9**, 341-343.

13. Kramer, R.Z., Bella, J., Mayville, P., Brodsky, B. and Berman, H.M. "Sequence dependent conformational variations of collagen triple-helical structure" *Nature Structural Biology*, 1999, **6,** 454-457.

14. Ramachandran, G. N. and Kartha, G. "Structure of collagen" *Nature*, **176**, 593-595.

15. Ramachandran, G.N. and Chandrasekharan, R. "Interchain hydrogen bonds via bound water molecules in the collagen triple helix" *Biopolymers*, 1968, **6**, 1649-1958.

16. Ramachandran, G.N. "A hypothesis on the role of hydroxyproline in stabilizing collagen structure" *Biochimica et Biophysica Acta*, 1973, **322**, 166-171.

17. Bella, J., Brodsky, B., and Berman, H.M. "Hydration structure of a collagen peptide" *Structure*, 1995, **3**, 893-906.

18. Hodge, A.H., and Petruska, J.A. "Recent studies with the electron microscope on ordered aggregates of the tropocollagen macromolecule" in *Aspects of Protein Structure*, 289-300. Edited by Ramachandran, G.N., 1963, Academic Press.

19. Miller, A. and Wray, J.S. "Molecular packing in collagen" *Nature*, 1971, **230**, 437-439.

20. Hulmes, D.J.S. and miller, A. "Quasi-hexagonal molecular packing in collagen fibrils" *Nature*, 1979, **282**, 878-880.
21. Smith, J.W. "Molecular pattern in native collagen" *Nature*, 1968, **219**, 157-158.

22. Hulmes, D.J.S., Wess, T.J., Prockop, D.J. and Fratzl, P. "Radial packing, order, and disorder in collagen fibrils" *Biophysical Journal,* 1995, **68,** 1661-1670.

23. Hulmes, D.J.S., Miller, A., Parry, D.A.D., Piez, K.A. and Woodhead-Galloway, J. "Analysis of the primary structure of collagen for the origins of molecular packing" *Journal of Molecular Biology*, 1973, **79**, 137-148.

24. Fraser, R.D.B., MacRae, T.P., Miller, A. and Suzuki, E. "Molecular conformation and packing in collagen fibrils" *Journal of Molecular Biology*, 1983, **167**, 497-521.

25. Parry, D.A.D. and Craig, A.S. "Electron microscope evidence for an 80 A unit in collagen fibrils" *Nature,* 1979, **282**, 213-215.

26. Trus, B.L. and Piez, K.A. "Compressed microfibril models of the native collagen fibril" *Nature*, 1980, **286**, 300-301.

27. Orgel, J.P.R.O., Miller, A., Irving, T.C., Fischetti, R.F., Hammersley, A.P. and Wess. T.J. "The in-situ supermolecular structure of type I collagen" *Structure*, 2001, **9,** 1061-1069.

28. Woodhead-Galloway, J. and Machin, P.A. "X-ray scattering from a gas of uniform hard discs using the Percus-Yervick approximation: an application to a 'planar liquid'" *Molecular Physics*, 1976, **32**, 41-48.

29. Fratzl, P., Fratzl-Zelman, N. and Klaushofer, K. "Collagen packing and mineralisation: an x-ray scattering investigation of turkey leg tendon" *Biophysical Journal*, 1993, **64**, 260-266.

30. Heidemann, E. *Fundamentals of Leather Manufacture*, 1993, Eduard Roether.

31. Theis, E.R. and Steinhardt Jr, R.G. "Studies in animal skin proteins" *Journal of the American Leather Chemists Association*, 1942, **37**, 433-449.

32. Lim, J.J. "Transition temperature and enthalpy change dependence on stabilising and destabilising ions in the helix-coil transition of native collagen" *Biopolymers*, 1976, **15**, 2371-2383.

33. von Hippel, P.H. and Wong, K-Y. "Neutral salts: the generality of their effects on the stability of macromolecular conformations" *Science*, 1964, **145**, 577-580.

34. Bienkievicz, K. *Physical chemistry of Leather making*, 1983, Kreiger.

35. Pauling, L. "A theory of the structure and process formation in antibodies" *Journal of the American Chemical Society*, 1940, **62**, 2643-2657.

36. Bigi, A., Fichera, A.M., Roveri, N. and Koch, M.H.J. "Structural modifications of air dried tendon collagen on heating" *International Journal of Biological Macromolecules*, 1987, **9**, 176-180.

37. Engel, J. and Schwarz, G. "Cooperative conformational transitions of linear biopolymers" *Angewandte Chemie (International Edition)*, 1970, **9**, 389-400.

38. Miles, C.A. and Bailey, A.J. "Thermal denaturation of collagen revisited" *Proceedings of the Indian Academy of Sciences (Chemical Sciences)*, 1999, **111**, 71-80.

39. Burge, R.E. and Hynes, R.D. "The thermal denaturation of collagen in solution and its structural implications" *Journal of Molecular Biology*, 1959, **1**, 155-164.

40. Burjanadze, T.V. "Evidence for the role of 4-hydroxyproline localised in the third position of the triplet (Gly-X-Y) in adaptational changes to thermostability of a collagen molecule and collagen fibrils" *Biopolymers*, 1982, **21**, 1489-1501.

41. Berg, R.A. and Prockop, D.J. "The thermal transition of a non-hydroxylated form of collagen. Evidence for a role for hydroxyproline in stabilizing the triple helix of collagen" *Biochemical and Biophysical Research Communications*, 1973, **52**, 115-120.

42. Burjanadze, T.V. "Hydroxyproline content and location in relation to collagen thermal stability" *Biopolymers*, 1979, **18**, 931-938.

43. Gustavson, K.H., *The Chemistry and Reactivity of Collagen*, 1956, Academic Press.

44. Persikov, A.V., Ramshaw, J.A.M. and Brodsky, B. "Collagen Model Peptides: Dependence of Triple Helix Stability" *Biopolymers*, 2000, **55**, 436-450.

45. Chan, V. and Ramshaw, J.A.M. "Positional Preference of Ionisable Residues in Gly-X-Y- Triplets of the Collagen Triple Helix" *Journal of Biological Chemistry*, 1997, **272**, 31441-31446.

46. Shah, N.K, Ramshaw, J.A.M., Kirkpatrick, A., Shah, C. and Brodsky, B. "A host-guest set of triple helical peptides: Stability of Gly-X-Y triplets containing common non-polar residues" *Biochemistry*, 1996, **35**, 10262-10268.

47. Shah, N.K., Sharma, M., Kirkpatrick, A., Ramshaw, J.A.M. and Brodsky, B. "Gly-Gly- Containing Triplets of Low Stability Adjacent to a Type III Collagen Epitope" *Biochemistry*, 1997, **36**, 5878-5883.

48. Engel, J., Chen, H-T., Prockop, D.J. and Klump, H. "The Triple Helix ↔ Coil Conversion of Collagen-like Polytripeptides in Aqueous and Non-aqueous Solvents. Comparison of the Thermodynamic Parameters and the Binding of Water to (L-Pro-L-Pro-Gly)n and (L-Pro-L-Hyp-Gly)n" *Biopolymers* 1977, **16**, 601-622.

49. Holmgren, S.K., Bretscher, L.E., Taylor, K.M. and Raines, R. "A hyperstable collagen mimic" *Chemistry and Biology*, 1999, **6**, 63-70.

50. Okuyama, K., Nagarajan, V. and Kamitori, S. "7/2-helical model for collagen-Evidence from model peptides" *Proceedings of the Indian Academy of Sciences (Chemical Sciences)*, 1999, **111**, 19-34.

51. Cooper, A. "Thermodynamics of Protein Folding and Stability" in *Protein: A Comprehensive Treatise*, edited by Allen, G. 1997, JAI Press.

52. Hammond, G.S. "A correlation of reaction rates" *Journal of the American Chemical Society*, 1955, **77**, 334-338.

53. Weir, C.E. "Rate of shrinkage of tendon collagen-heat, entropy and free energy of activation of the shrinkage of untreated tendon: effect of acid, salt, pickle and tannage on the activation of tendon collagen" *Journal of the American Leather Chemists Association*, 1949, **44**, 108-138.

54. Miles, C. A. and Bailey, A.J. "Kinetics of collagen denaturation in mammalian lens capsule studied by differential scanning calorimetry" *International Journal of Biological Macromolecules*, 1993, **15**, 265-271.

55. Miles, C.A., Burjanadze, T.V. and Bailey, A.J. "The kinetics of the thermal denaturation of collagen in unrestrained rat tail tendon determined by differential scanning calorimetry" *Journal of Molecular Biology*, 1995, **245**, 437-446.

56. Van Hook, A. *Biodynamica*, 1947, **6,** 81

57. Flory, P.J. and Garrett, R.R. "Phase transition of collagen and gelatin systems" *Journal of the American Chemical Society*, 1958, **80**, 4836-4845.

58. Privalov, P.L., Tiktopulo, E.I. and Tischenko, V.M. "Stability and mobility of the collagen structure" *Journal of Molecular Biology*, 1979, **127,** 203-216.

59. Privalov, P.L. "Stability of proteins: Proteins which do not present a single cooperative system" *Advances in Protein Chemistry*, 1982, **35**, 1-104.

60. Fessler, L.I., Rudd, C. and Fessler, J.H. "Renaturation of disulphide-linked procollagen" *Journal of Supramolecular Structure*, 1974, **2**, 103-107.

61. Engel, J. "Folding and unfolding of collagen triple helices" *Advances in Meat Research*, 1987, **4**, 145-161.

62. Piez, K.A. and Sherman, M.R. "Equilibrium and kinetic studies of the helix-coil transition in α1-CB2, a small peptide from collagen" *Biochemistry,* 1970, **9**, 4134-4140.

63. Finch, A. and Ledward, D. "Shrinkage of collagen fibres: A differential scanning calorimetry study" *Biochimica et Biophysica Acta*, 1972, **278**, 433-439.

64. Luescher, M., Ruegg, M. and Schindler, P. "Effect of hydration on the thermal stability of tropocollagen and its dependence on the presence of neutral salts" *Biopolymers*, 1974, **13**, 2489-2503.

65. Kopp, J., Bonnet, M. and Renou, J.P. "Effect of collagen crosslinking on collagen-water interactions (A DSC study)" *Matrix* 1990, **9**, 443-450.

66. Komanowsky, W. "Thermal stability of hide and leather at different moisture contents" *Journal of the American Leather Chemists Association*, 1991, **86**, 269-278.

67. Miles, C.A. and Ghelashvili, M. "Polymer-in-a-box mechanism for the thermal stabilisation of collagen molecules in fibres" *Biophysical Journal*, 1999, **76**, 3243-3252.

68. Doi, M. and Edwards, S.F. "*The Theory of Polymer Dynamics*" 1986, Clarendon Press.

69. Eanes, E.D., Lundy, D.R. and Martin, G.N. "X-ray diffraction study of the mineralisation of turkey leg tendon" *Calcified Tissue Research*, 1970, **6**, 239-248.

70. Pineri, M.H., Escoubes, M. and Roche, G. "Water-collagen interactions: Calorimetric and mechanical experiments" *Biopolymers*, 1978, **17**, 2799-2815.

71. Cusack, S. and Lees, S. "Variation of longitudinal acoustic velocity at gigahertz frequencies with water content in rat tail tendon fibres" *Biopolymers*, 1984, **23**, 337-351.

72. Nomura, S., Hiltner, A., Lando, J.B. and Baer, E. "Interaction of water with collagen" *Biopolymers*, 1977, **16**, 231-246.

73. Haly, A.R. and Snaith, J.W. "Calorimetry of rat tail tendon collagen before and after denaturation: The heat of fusion of its absorbed water" *Biopolymers*, 1971, **10**, 1681-1699.

74. Eastoe, J.E. and Eastoe, B. "The organic constituents of mammalian compact bone" *Biochemical journal*, 1954, **57,** 453-459.

75. Cruess, R.L. and Clarke, I. "Alterations in lipids of bone caused by hypervitaminosis A and D" *Biochemical Journal*, 1965, **96,** 262-265.

76. Williams, P.A. and Peacock, A.R. "The physical properties of a glycoprotein from bovine cortical bone (bone sialoprotein)" *Biochimica et Biophysica Acta*, 1965, **101**, 327-335.

77. Arsenault, A.L. "Crystal-collagen relationships in calcified turkey leg tendons visualised by selected-area dark field electron microscopy" *Calcified Tissue International*, 1988, **43**, 202-212.

78. Glimcher, M.J. and Krane, S.M. "The organisation and structure of bone, and the mechanism of calcification" in *Treatise on Collagen, Volume 2: Biology of Collagen part B*, edited by Gould, B.S., 1968, Academic Press.

79. De Jong, W.F. "Le substance mineral dans les os" *Recueil des Travaux Chimiques des Pays-Bas*, 1926, **45,** 445.

80. Erts, D. Glathercole, L.J. and Atkins, E.D.T. "Scanning probe microscopy of interfibrillar crystallites in calcified collagen" *Journal of Materials Science: Materials in Medicine*, 1994, **5**, 200-206.

81. Weiner, S. and Traub, W. "Organisation of hydroxyapatite crystals within collagen fibrils" *FEBS Letters*, 1986, **206**, 262-266.

82. Wenk, H.R. and Heidelbach, F. "Crystal alignment of carbonated apatite in bone and calcified tendon: Results from Quantitative texture analysis" *Bone*, 1999, **24**, 361-369.

83. Fratzl, P., Fratzl-Zeman, N., Klaushofer, K., Vogl, G. and Koller, K. "Nucleation and growth of mineral crystals in bone studied by small angle x-ray scattering" *Calcified Tissue International*, 1991, **48**, 407-413.

84. Fratzl, P. "Mineral crystals in calcified tissues: A comparative study by SAXS" *Journal of Bone and Mineral Research*, 1992, **7**, 329-334.

85. Traub, W., Arad, T. and Weiner, S. "Origin of mineral crystal growth in collagen fibrils" *Matrix*, 1992, **12**, 251-255.

86. Nylen, M.U., Scott, D.B. and Mosley, V.M. in *Calcification in Biological Systems,* edited by Sognnaes, R.F., 1960. American Association for the Advancement of Science.

87. Hohling, H.J., Ashton, B.A. and Koster, H.D. "Quantitative electron microscopic investigations of mineral nucleation in collagen" *Cell and Tissue Research*, 1974, **148**, 11-26.

88. Bigi, A., Ripamonti, A., Cojazzi, G., Pizzuto, G., Roveri, N. and Koch, M.N.H. "Structural analysis of turkey tendon collagen upon removal of the inorganic phase" *International Journal of Biological Macromolecules*, 1991, **13**, 110-114.

89. Siperko, L.M. and Landis, W.J. "Aspects of mineral structure in normally calcifying avian tendon" *Journal of Structural Biology*, 2001, **135**, 313-320.

90. Landis, W.J., Song, M.J., Leith, A., McEwan, L. and McEwan, B.F. "Mineral and organic matrix interaction in the normally calcifying tendon visualised in three dimensions by high voltage electron microscopic tomography and graphic image reconstruction" *Journal of Structural biology*, 1993, **110**, 39-54.

91. Bigi, A., Ripamonti, A., Koch, M.H.J. and Roveri, N. "Calcified turkey leg tendon as structural model for bone" *International journal of Biological Macromolecules*, 1988, **10**, 282-286.

92. Landis, W.J., Hodgens, K. Song, M.J., Arena, J., Kiyonaga, S., Marko, M. Owen, C. and McEwan, B.F. "Mineralisation of collagen may occur on fibril surfaces: Evidence from conventional and high-voltage electron microscopy and three dimensional imaging" *Journal of Structural Biology,* 1996, **117**, 24-35.

93. Bonar, L.C., Lees, S. and Mook, H.A. "Neutron diffraction studies of collagen in fully mineralised bone" *Journal of Molecular Biology*, 1985, **181**, 265-270.

94. Landis, W.J., Arsenault, A.L. "Vesicle-mediated calcification in the turkey leg tendon" *Connective Tissue Research*, 1989, **22**, 35-42.

95. Glimcher, M.J. "Molecular biology of mineralised tissues with particular reference to bone" *Review in Modern Physics*, 1959, **31**, 359-393.

96. Glimcher, M.J., Brickley-Parsons, D. and Kossiva, D. "Phosphopeptides and γ-carboxyyglutamic acid containing peptides in calcified turkey tendon: their absence in uncalcified tendon" *Calcified Tissue International*, 1979, **27**, 281-284.

97. Ennever, J. Vogel, L.J. and Riggan, J.J. "Proteolipid and Collagen Calcification *in vitro*" *Cytobios*, 1984, **39**, 151-157.

98. Dahl, T., Sabsay, B. and Veis, A. "Type I collagen-phosphophoryn interactions: Specificity of the monomer-monomer binding" *Journal of Structural Biology*, 1998, **123**, 162-168.

99. Jager, I, and Fratzl, P. "Mineralised collagen fibrils: A mechanical model with a staggered arrangement of mineral particles" *Biophysical Journal,* 2000, **79**, 1737-1746.

100. Bonar, L.C, and Glimcher, M.J. "Thermal denaturation of mineralised and demineralised bone collagens" *Journal of Ultrastructural Research*, 1970, **32,** 545-557.

101. Wong, A.T.C, "Precipitation behaviour of calcium phosphate-A model for hard tissue mineralisation", PhD Thesis, 1993, Oxford University.

102. Koutsoukos, P.G. and Nancollas, G.H. "The mineralisation of collagen *in-vitro*" *Colloids and Surfaces*, 1987, **28**, 95-108.

103. Linde, A., Lussi, A. and Crenshaw, M.A. "Mineral induction by immobilised polyanionic proteins" *Calcified Tissue International*, 1989, **44**, 286-295.

104. Fleisch, H.A., Russell, R.G.G., Bisaz, S., Muelbauer, R.C. and Williams, D.A. "The inhibitory effect of phosphonates on the formation of calcium phosphate crystals *in-vitro* and on aortic and kidney calcification *in-vivo*" *European Journal of Clinical Investigation*, 1970, **1**, 12-18.

105. Robinson, R. "The possible significance of hexosephosphoric esters in ossification" *Biochemical Journal,* 1923, **17**, 286-293.

106. Banks, E., Nakajima, S., Shapiro, L.C. and Tilevitz, O. "Fibrous apatite grown on modified collagen" *Science*, 1977, **198**, 1164-1166.

107. Saito, T., Arsenault, A.L., Yamauchi, M., Kuboki, Y. and Crenshaw, M.A. "Mineral induction by immobilised phosphoproteins" *Bone*, 1997, **21**, 305-311.

108. Kronick, P.L. and Cooke, P. "Thermal stabilization of collagen fibres by calcification" *Connective Tissue Research*, 1996, **33**, 275-282.

109. Mucalo, M.R., Yokogawa, Y., Suzuki, T., Kawamoto, Y., Nagata, F. and Nishizawa, K. "Further studies of calcium phosphate growth on phosphorylated cotton fibres" *Journal of Materials Science: Materials in Medicine*, 1995, **6**, 658-669.

110. Li, S., Liu, Q., de Wijn, J., Wolke, J., Zhou, B. and de Groot, K. "*In-vitro* apatite formation on phosphorylated bamboo" *Journal of Materials Science: Materials in Medicine*, 1997, **8**, 543-549.

111. Yokogawa, Y., Paz Reyes, J. Mucalo, M.R., Toriyama, M., Kawamoto, Y., Suzuki, T., Nishizawa, K., Nagata, F. and Kamayama, T. "Growth of calcium phosphate on phosphorylated chitin fibres" *Journal of Materials Science: Materials in Medicine*, 1997, **8**, 407-412.

112. Walsh, W. R. and Christiansen, D. L. "Demineralised bone matrix as a template for mineral-organic composites" *Biomaterials*, 1995, **16**, 1363-1371.

113. Boyer, D. B. and Eirich, F. R. "Remineralisation of dentin *in vitro*" *Calcified Tissue International*, 1976, **21**, 17-28.

114. Bigi, A., Gandolfi, M. Koch, M.H.J. and Roveri, N. "X-ray diffraction study of *in-vitro* calcification of tendon collagen" *Biomaterials*, 1996, **17**, 1195-1201.

115. Bigi, A., Gandolfi, M., Roveri, N. and Valdre, G. "*In-vitro* calcified tendon collagen: an atomic force and scanning electron microscopy investigation" *Biomaterials*, 1997, **18**, 657-665.

116. Ennever, J., Vogel, J.J., Rigan, L.J. and Paoloski, S.B. "Proteolipid and calculus matrix calcification *in-vitro*" *Journal of Dental Research*, 1977, **56**, 140-142.

117. Lee, C.H., Vyavahare, N., Zand, R., Kruth, H., Schoen, F.J., Bianco, R. and Levy, R.J. "Inhibition of aortic wall calcification in bioprosthetic heart valves by ethanol pre-treatment: Biochemical and biophysical mechanisms" *Journal of Biomedical Materials Research*, 1998, **42**, 30-37.

118. Kirschvink, J.L. and Hagadorn, J.W. "A grand unified theory of biomineralisation" in *Biomineralisation: From Biology to Biotechnology and Medical Application*, edited by E. Baeuerlein, 2000, Wiley-VCH.

119. Lowenstam, H.A. and Weiner, S. *On Biomineralization*, 1989, Oxford University Press.

120. Mann, S., Webb, J. and Williams, R.J.P. *Biomineralization: Chemical and Biochemical Perspectives*, 1989, VCH.

121. Nielsen, A.E. "*Kinetics of Precipitation*" 1964, Pergammon Press.

122. Barone, J.P. and Nancollas, G.H. "The seeded growth of calcium phosphates, the effect of solid/solution ratio in controlling the nature of the growth phase" *Journal of Colloid and Interface Science*, 1977, **62**, 421-431.

123. Koutsoukos, P.G. and Nancollas, G.H. "Crystal growth of calcium phosphates: Epitaxial considerations" *journal of Crystal Growth*, 1981, **53**,10-19.

124. Kraus, B.L. and Crenshaw, M.A. "Phosphatidic acid liposomes as mineralising surfaces: kinetics and energetics" *Chemical Geology*, 1996, **132,** 193-189.

125. Addadi, L., Moradian, J., Shay, E., Maroudas, N.G. and Weiner, S. "A chemical model for the cooperation of sulphates and carboxylates in calcite crystal nucleation: Relevance to biomineralisation" *Proceedings of the National Academy of Sciences USA*, 1987, **84**, 2732-2736.

126. Simkiss, K. "Organic matrix of the oyster shell" *Comparative Biochemistry and Physiology*, 1985, **16**, 427-435.

127. Fisher, L.W., Termine, J.D., Dejter Jr, S.W., Whitson, S.W., Yanagishita, M., Kimura, J.H., Hascall, V.C., Kleinman, H.K., Hassell, J.R. and Nilsson, B. "Proteoglycans of developing bone" *Journal of Biological Chemistry*, 1983, **258**, 6588-6594.

128. Feng, Q.L., Pu, G., Pei, Y., Cui, F.Z., Li, H.D. and Kim, T.N. "Polymorph and morphology of calcium carbonate crystals induced by proteins extracted from mollusc shell" *Journal of Crystal Growth*, 2000, **216**, 459-465.

129. Robinson, K.L., Weaver, J.V.M., Armes, S.P., Diaz-Martin, E. and Meldrum, F.C. "Synthesis of controlled-structure sulphate-based copolymers via atom transfer radical polymerisation and their use as crystal habitat modifiers for $BaSO_4$" *Journal of Materials Chemistry*, 2002, **12**, 890-896.

130. Knott, L., Tarlton, J. F. and Bailey, A.J. "Chemistry of collagen crosslinking: Biochemical changes in collagen during the partial mineralisation of turkey leg tendon" *Biochemical Journal*, 1997, **321**,

131. Gadaleta, S.J., Camacho, N.P. Mendelsohn, and Boskey, A.L. "Fourier-transform infrared microscopy of calcified turkey leg tendon" *Calcified Tissue International*, 1996, **58**, 17-23.

132. Termine, J.D. and Posner, A.S. "Infra-red Analysis of Amorphous and Crystalline Mineral Fractions" *Science*, 1966, **153**, 1523-1525.

133. Weiner, S. and Bar-Josef, O. "States of preservation of bones from prehistoric sites in the near east: a survey" *Journal of Archaeological Science*, 1990, **17**, 187-196.

134. Gadaleta, S.J., Paschalis, E.P., Betts, F., Mendelsohn, R. and Boskey, A.L. "Fourier transform infrared spectroscopy of the solution mediated conversion of amorphous calcium phosphate to hydroxyapatite: New correlations between x-ray diffraction and infrared data" *Calcified Tissue International*, 1996, **58**, 9-16.

135. Matsushima, N., Akiyama, M. and Terayama, Y. "Quantitative analysis of mineral in bone from small angle x-ray scattering patterns" *Japanese Journal of Applied Physics*, 1984, **21**, 186-189.

136. Fratzl, P., Schreiber, S. and Klaushofer, K. "Bone mineralisation as studied by small angle x-ray scattering" *Connective Tissue research*, 1996, **34**, 247-254.

137. Wess, T.J., Drakopoulos, M., Smigirev, A., Wouters, J. Paris, O., Fratzl, P., Collins, M., Hiller, J. and Nielsen, K. "The use of small angle x-ray diffraction studies for the analysis of structural features in archaeological samples" *Archaeometry*, 2001, **43**, 117-129.

138. Kokubo, T., Kim, H-M., Miyaji, F., Takadama, H. and Miyazaki, T. "Ceramic-metal and ceramic-polymer composites prepared by a biomimetic process" *Composites: Part A*, 1999, **30**, 405-409.

139. Li, P., Ohtsuki, C., Kokubo, T., Nakanishi, K., Soga, N., Nakamura, T. and Yamamuro, T. "Process of formation of bone-like apatite layer on silica gel" *Journal of Materials science: Materials in Medicine*, 1993, **4**, 127-131.

140. White, S.W., Hulmes, D.J.S., Miller, A. and Timmins, P.A. "Collagen-mineral axial relationship in calcified turkey leg tendon by X-ray and neutron diffraction" *Nature*, 1977, **266**, 421-425.

141. Bunn, C.W. *Chemical Crystallography: An Introduction to Optical and X-ray Methods*, 1961, Clarendon Press.

142. Lihme, A., Schafer-Nielsen, C., Larsen, K.P., Muller, K.G. and Bog-Hansen, T.C. "Divinyl sulphone-activated agarose. Formation of stable and non-leaking affinity matrices by immobilisation of immunoglobulins and other proteins" *Journal of Chromatography*, 1986, **376**, 299-305.

143. Zeeman, R. Dijkstra, P.J., van Wachem, P. B., van Luyn, M.J.A., Hendriks, M., Cahalan, P.T. and Feijen, J. "Successive epoxy and carbodiimide cross-linking of dermal sheep collagen" *Biomaterials*, 1999, **20**, 921-931.

144. Silver, F.H. "*Biological Materials: Structure, Mechanical Properties, and Modelling of Soft Tissues*", 1987, New York University Press.

145. Bowes, J.H. and Elliot, R.G.H. "Tanning with formaldehyde in the presence of organic compounds" *Journal of the American Leather Chemists Association*, 1962, **57**, 374-391.

146. Fraenkel-Conrat, H. and Olcott, H.S. "Reaction of formaldehyde with proteins. II. Participation of the guanidyl groups and evidence of crosslinking" *Journal of the American Chemical Society*, 1946, **68**, 34-37.

147. Hauschka, P.V., Lian, J.B. and Gallop, P.M. "Direct identification of the calcium-binding amino acid, γ-carboxyglutamic acid, in mineralised tissue" *Proceedings of the National Academy of Sciences USA*, 1975, **72**, 3925-3929.

148. Cho, S.B., Miyaji, F., Kokubo, T., Nakanishi, K., Soga, N. and Nakamura, T. "Apatite formation on silica gel in simulated body fluid: Effects of structural modification with solvent exchange" *Journal of Materials Science: Materials in Medicine*, 1998, **9**, 279-284.

149. Mucalo, M.R., Yokogawa, Y., Toriyama, M., Suzuki, T., Kawamoto, Y., Nagata, F. and Nishizawa, K. "The growth of calcium phosphate on surface modified cotton" *Journal of Materials Science: Materials in Medicine*, 1995, **6,** 597-605.

150. Miyaji, F., Iwai, M, Kokubo, T. and Nakamura, T. "Chemical surface treatment of silicone for inducing its bioactivity" *Journal of Materials Science: Materials in Medicine*, 1998, **9**, 61-65.

151. Wall, M.S., Deng, X-H., Torzilli, P.A., Doty, S.B., O'Brien, S.J. and Warren, R.F. "Thermal modification of collagen" *Journal of Shoulder and Joint Surgery*, 1998, **8**, 339-344.

152. Beghuin, D., Schonenberger, K., Delacritaz, G. and Salathe, R.P. "Temperature-related reversible birefringence changes in rat tail tendon" *Applied Optics*, 2000, **39**, 3388-3395.

153. Hayashi, T., Curran-Patel, S. and Prockop, D.J. "Thermal stability of the triple helix of Type I procollagen and collagen. Precautions for minimising ultraviolet damage to proteins during circular dichroism studies" *Biochemistry*, 1979, **18**, 4182-4187.

154. Boedtker, H. and Doty, P. "The native and denatured states of soluble collagen" *Journal of the American Chemical Society*, 1956, **78**, 4267-4280.

155. Rose, C., Kumar, M. and Mandal, A.B. "A study of the hydration and thermodynamics of warm water and cold water fish" *Biochemical Journal*, 1988, **249**, 127-133.

156. Burjanadze, T.V. and Bezhitadze, M.O. "Presence of a thermostable domain in the helical part of the Type I collagen molecule and its role in the mechanism of triple helix folding" *Biopolymers*, 1992, **32**, 951-956.

157. Chahine, C. "Changes in hydrothermal stability of leather and parchment with deterioration: a DSC study" *Thermochimica Acta*, 2000, **365**, 101-110.

158. Flandin, F., Buffevant, C. and Herbage, D. "A Differential scanning calorimetry analysis of the age-related changes in the thermal stability of rat skin collagen" *Biochimica et Biophysica Acta*, 1984, **791**, 205-211.

159. Nielsen-Marsh, C. M., Hedges, R.E.M., Mann, T. and Collins, M.J. "A preliminary investigation of the applications of differential scanning calorimetry to the study of collagen degradation in archaeological bone" *Thermochimica Acta*, 2000, **365**, 129-139.

160. Le Lous, M., Flandin, F., Herbage, D. and Allain, J-C. "Influence of collagen denaturation on the chemorheological properties of skin, assessed by differential scanning calorimetry and hydrothermal isometric tension measurement" *Biochimica et Biophysica Acta*, 1982, **717**, 295-300.

161. Usha, R. and Ramasami, T. "Effect of crosslinking agents (basic chromium sulphate and formaldehyde) on the thermal and thermomechanical stability of rat tail tendon collagen fibre" *Thermochimica Acta*, 2000, **356**, 59-66.

162. Sakae, T., Mishima, H., Kozawa, Y. and LeGeros, R.Z. "Thermal stability of mineralised and demineralised dentin: A differential scanning calorimetric study" *Connective Tissue Research*, 1995, **33**, 193-196.

163. Lim, J.J. "Thermogravimetric analysis of human femur bone" *Journal of Biological physics*, 1975, **3**, 111-129.

164. Deakins, M. "Changes in the ash, water, and organic content of pig enamel during calcification" *Journal of Dental Research*, 1942, **21**, 429-435.

165. Finch, A., Gardner, P.J., Ledward, D.A. and Menashi, S. "The thermal denaturation of collagen fibres swollen in aqueous solutions of urea, hexamethylene tetramine, *p*-benzoquinone and tetra-alkylammonium salts" *Biochimica et Biophysica Acta*, 1974, **365**, 400-404.

166. Usha, R. and Ramasami, T. "Role of aliphatic alcohols on the stability of rat tail tendon (RTT) collagen fibre" *Journal of Polymer Science: Part B: Polymer Physics*, 1999, **37**, 1397-1405.

167. Sankaran, V. and Walsh Jr, J. "Birefringence measurement of rapid structural changes during collagen denaturation" *Photochemistry and Photobiology*, 1998, **68**, 846-851.

168. Thomsen, S., Pearce, J.A. and Cheong, W-F. "Changes in birefringence as markers of thermal damage in tissues", *IEEE Transactions on Biomedical Engineering*, 1989, **36**, 1174-1179.

169. Koon, H.E.C., Nicholson, R.A. and Collins, M.J. "A practical approach to the identification of low temperature heated bone using TEM" *Journal of Archaeological Science*, 2003, **30**, 1393-1399.

170. Menderes, O., Covington, A.D., Waite, A.E. and Collins, M.J. "The mechanism and effects of collagen amide group hydrolysis during liming" *Journal of the Society of Leather Technologists and Chemists*, 1999, **83**, 107-110.

171. Koon, H.E.C., Unpublished results.

172. Brown, E.M, Farrell Jr, H.M. and Wildermuth, R.J. "Influence of neutral salts on the hydrothermal stability of acid-soluble collagen" *Journal of Protein Chemistry*, 2000, **19**, 85-92.

173. Finar, I.L. *Organic Chemistry, Volume I,* 1981, Longman, page 263.

174. Woessner Jr, J.F. "The determination of hydroxyproline in tissue and protein samples containing small proportions of this amino acid" *Archives of Biochemistry and Biophysics*, 1961, **93**, 440-447.